

REMARKS

Applicants have amended claim 43. Upon entry of the proposed amendment, claims 43-71 will be under examination.

Support for amended claim 43 can be found as follows:

Claim 43: *see, e.g.*, page 44, lines 13-15 of the specification as filed (“Specification”).

No new matter has been introduced.

Reconsideration of the application is respectfully requested in view of the remarks set forth below.

Rejection under 35 U.S.C. § 112, First Paragraph

The Office Action rejects claims 43-71 as lacking enablement.

Independent Claim 43 is directed to a method of treating a disease or condition in a patient that results from the presence of neoplastic tissue, in which the treatment includes administering a compound of Formula 1.

The Examiner has maintained the rejection under 35 USC 112 (enablement). Applicants respectfully disagree with this conclusion; however Applicants have amended Claim 43 in order to recite one of the features of Applicants’ invention: methods of treating diseases arising from the recited forms of neoplastic tissue, all of which are supported by the present specification.

The compounds recited in the method of Claim 43 are metallotexaphyrins having novel apical ligands (*i.e.*, in the prior art, metallotexaphyrins had chloride, nitrate or acetate apical ligands, and novel the novel apical ligands disclosed in the present application). As noted in the specification, metallotexaphyrins are a class of compounds that act in synergy with other treatment modalities (*i.e.*, “a chemotherapeutic compound” or a “therapeutic energy means selected from photoirradiation and ionizing radiation”) to kill neoplastic tissue cells. *See* the Specification, page 2, lines 9-15; and page 52, lines 13-18. Methods for using the compounds of Formula I in combination with each of these other treatment modalities are described in detail in the Specification. *See* page 53, line 11 through page 59, line 14 and page 76, line 5 through page 78, line 10.

In addition, prior to the filing of the present application, other types of metallotexaphyrins had demonstrated effectiveness against tumor types, including the claimed tumor types. *See* Exhibit 1. For example, these studies showed that other metallotexaphyrins (having different apical ligands) accumulated in primary and secondary tumor types and therein acting as radiation sensitizers or photodynamic therapy enhancing agents. In addition, subsequent studies have demonstrated the

effectiveness of metallotexaphyrins in the claimed tumor types. *See, e.g.,* Exhibit 2. These studies include human clinical trials.

Thus, although the claimed novel metallotexaphyrins were not administered in the aforementioned references, one of skill in the art could utilize this art to avoid the sort of “fishing expedition” associated with undue experimentation. In other words, one of skill in the art, armed with the teachings disclosed in the present application could use (without undue experimentation, of course) the disclosed metallotexaphyrins for the treatment of neoplastic disease. As such, Applicant’s respectfully request withdrawal of the pending rejection under 35 USC 112 (enablement).

CONCLUSION

Based on the above arguments, it is respectfully requested that the rejection be withdrawn and the claims allowed. Applicants respectfully solicit the Examiner to expedite prosecution of this patent application to issuance. Should the Examiner have any questions, the Examiner is encouraged to telephone the undersigned.


The Commissioner is hereby authorized to charge any additional fees that may be required, or credit any overpayment to Deposit Account No. 23-2415 (Attorney Docket No. 25922.702.501).

Respectfully submitted,

WILSON SONSINI GOODRICH & ROSATI

Date: Jun 21, 2007

By: _____


Michael Hostetler, Ph.D., J.D.
Attorney for Applicants
Registration No. 47,664

650 Page Mill Road
Palo Alto, CA 94304
Direct Dial: (858) 350-2306
Customer No. 021971

Juliette Viala, MD
Daniel Variet, MD
Philippe Meingan, MD
Eric Lartigau, MD
Patrice Carde, MD
Markus Renschler, MD

Index terms:

Brain neoplasms, MR, 10.121412,
10.30
Brain neoplasms, secondary, 10.33
Brain neoplasms, therapeutic
radiology, 10.1299, 10.33
Contrast media, 10.12143, 10.1299
Texaphyrins, 10.33, 10.1299

Radiology 1999; 212:755-759

From the Departments of Radiology (J.V., D.V., P.M.) and Medicine (E.L., P.C.), Institut Gustave-Roussy, 39 rue Camille Desmoulins, 94805 Villejuif, France; and Pharmacocytics, Sunnyvale, Calif. (M.R.). From the 1997 RSNA scientific assembly. Received May 27, 1998; revision requested July 30; final revision received December 30; accepted March 26, 1999. Supported by Pharmacocytics. Address reprint requests to J.V. (e-mail: viala@igro.fr).

Dr. Carde and Dr. Renschler each has a financial interest through ownership of stock or stock options in the company developing gadolinium texaphyrin, Pharmacocytics. Dr. Carde also serves as a consultant to the company. Dr. Renschler is the senior director of clinical research and is an employee of the company.

© RSNA, 1999

Author contributions:

Guarantor of integrity of entire study, D.V.; study concepts, M.R.; study design, P.C.; definition of intellectual content, D.V.; literature research, J.V.; clinical studies, E.L.; data acquisition and analysis, P.M.; J.V. manuscript preparation and editing, J.V.; manuscript review, D.V.

Phases IB and II Multidose Trial of Gadolinium Texaphyrin, a Radiation Sensitizer Detectable at MR Imaging: Preliminary Results in Brain Metastases¹

PURPOSE: To evaluate magnetic resonance (MR) imaging results after administration of gadolinium texaphyrin, a tumor-selective radiation sensitizer that is detectable at MR imaging, and to determine an appropriate intravenous dose of gadolinium texaphyrin for repeated injections during radiation therapy, the dose-limiting toxicity of reiterated doses of gadolinium texaphyrin, the maximal tolerated dose, the biolocalization of gadolinium texaphyrin (as assessed at MR examinations), and the response to treatment.

MATERIALS AND METHODS: Ten daily intravenous injections of gadolinium texaphyrin, each followed by whole-brain radiation therapy (total of 10 fractions, 30 Gy), were administered to patients with brain metastases in a multicenter study. At the study institution, 11 patients underwent MR imaging before and after the first injection, after the 10th injection, and 8 weeks after entry into the study.

RESULTS: MR imaging revealed selective drug uptake in metastases, without enhancement of normal brain tissue. In 10 patients, tumor uptake was higher after the 10th injection than after the first injection, which indicated accumulation of gadolinium texaphyrin in metastases. One lesion was visible only after the 10th injection and not at the pretherapeutic MR examination with injection of conventional gadolinium-based contrast material. Response to treatment was defined as a reduction in the size of the metastases between the preinjection MR study and the last MR study; seven patients achieved partial remission with tumor regression exceeding 50% of the initial size, and four achieved a minor response with less than 50% tumor regression.

CONCLUSION: These preliminary results indicate that gadolinium texaphyrin is tumor selective and that brain metastases can be depicted at MR imaging long after the administration of gadolinium texaphyrin.

Radiation therapy is an important treatment for localized cancers. Unfortunately, the radiation dose is often too limited because of injury to normal surrounding tissue. A radiation-sensitizing agent capable of maximizing the cytotoxic effect of radiation delivered to the tumor while minimizing exposure of surrounding tissue would improve the chances of achieving local control.

Gadolinium texaphyrin is the prototype of a new class of compounds, the texaphyrins, which are expanded porphyrins. Several models have been used to demonstrate the radiation-sensitizing effect of gadolinium texaphyrin in studies carried out with HT29 cells in vitro and experimentally in single and multifraction irradiation studies with a murine model (mammary carcinoma) in vivo (1). Findings from a phase IA study, in which 38

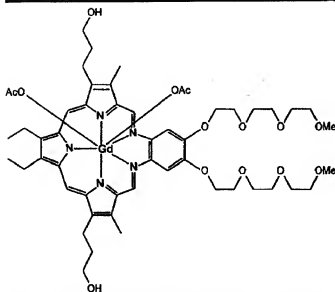


Figure 1. Diagram of the gadolinium texaphyrin molecule. Ac = acetyl, Gd = gadolinium, H = hydrogen, Me = methyl, N = nitrogen, O = oxygen.

patients were enrolled, demonstrated very good tolerance and a maximal tolerated dose of 19.4 μmol per kilogram of body weight in a single bolus (2).

The present study is part of a multicenter phase IB study (establishment of the maximal tolerated dose in patients with brain metastases requiring palliative therapy) in which gadolinium texaphyrin and standard radiation therapy are being used in patients with brain metastases. Magnetic resonance (MR) imaging was used exclusively for the follow-up of these patients in our institution, Institut Gustave-Roussy. We report the preliminary results of our participation in the phase IB study in which MR imaging is being used.

The primary objectives of the multicenter phase IB study were to determine an appropriate intravenous dose of gadolinium texaphyrin for repeated injections during radiation therapy, the dose-limiting toxicity of reiterated doses of gadolinium texaphyrin, the maximal tolerated dose, the biocalculation of gadolinium texaphyrin (as assessed at MR examinations), and the response to treatment.

Texaphyrins are expanded porphyrins that are capable of binding lanthanide metals such as lutetium or gadolinium (Fig 1) (3). Gadolinium texaphyrin captures x rays that are delivered in radiation treatment and can be activated by radio-frequency pulses, such as those used in MR imaging (Fig 2) (4).

Gadolinium texaphyrin is water soluble and kinetically stable and is not depen-

dent on tumor oxygenation or on cell-cycle phases. The radiation-sensitizing property of texaphyrins is not dependent on the inserted metal and is exclusively a function of the ligand. Porphyrins localize selectively in tumors; this prompted the simultaneous use of gadolinium texaphyrin as a selective radiosensitizer and as a contrast agent for MR imaging.

MATERIALS AND METHODS

This phase IB and II study, initiated in September 1996 and ended in May 1998, is a multidose trial. The study protocol was approved by the institutional review board of the University of Bicelle, Paris, France.

All patients older than 18 years with brain metastases requiring palliative radiation therapy were eligible, providing the following other criteria were met: a baseline World Health Organization (5) performance status of 0-2 (ambulatory and capable of all self-care but unable to carry out any work activities, ambulatory more than 50% of waking hours); neurologic function less than 2 (able to carry out normal activities with minimal difficulties, neurologic impairment does not require nursing care or hospitalization); and a life expectancy of at least 2 months.

Patients had a hematologic profile with a white blood cell count greater than 3,000 per cubic millimeter (0.003×10^9 per liter), an absolute granulocyte count greater than 1,500 per cubic millimeter

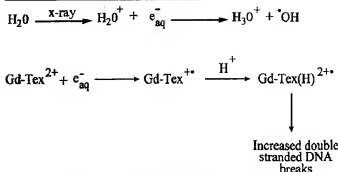


Figure 2. Diagram demonstrates the mechanism of action of gadolinium texaphyrin (Gd-TeX).

(0.0015×10^9 per liter), platelets greater than 100,000 per cubic millimeter (0.1×10^9 per liter); hepatic and renal functions with bilirubin level less than 2 mg/dL (34.2 $\mu\text{mol/L}$); aspartate aminotransferase, alanine aminotransferase, and alkaline phosphatase levels less than 2 times the upper normal limit; prothrombin time and activated partial thromboplastin time less than 1.5 times the upper normal limit; and serum creatinine level less than 1.5 mg/dL (132.6 $\mu\text{mol/L}$).

Patients had no concomitant chemotherapy during the 14-day follow-up observation period after the end of treatment; no prior surgical resection of metastases; and no medical or psychiatric condition likely to compromise their ability to give informed consent. They were fully informed of the type of disease diagnosed, the objectives, and the experimental nature of the study and were able to return to the study site for treatment and follow-up visits, as defined in the protocol.

Eleven patients (six women, five men), aged 41-82 years, were enrolled in this study. Ten patients had already undergone treatment for a tumor: three for breast cancer, five for lung cancer, one for thyroid cancer, and one for skin cancer (melanoma). One patient had brain metastases, which revealed a lung cancer.

Each patient received 10 daily intravenous injections of gadolinium texaphyrin (Xcytrin; Pharmacyclis, Sunnyvale, Calif), except during weekends and on public holidays, followed within 2-5 hours with whole-brain radiation therapy. Radiation therapy was delivered in 10 fractions of 3 Gy, for a total of 30 Gy.

The gadolinium texaphyrin doses injected were as follows: 0.25 $\mu\text{mol/kg}$ (one patient), 0.50 $\mu\text{mol/kg}$ (one patient), 0.80 $\mu\text{mol/kg}$ (one patient), 1.30 $\mu\text{mol/kg}$ (two patients), 1.80 $\mu\text{mol/kg}$ (one patient), 2.30 $\mu\text{mol/kg}$ (one patient), 3.10 $\mu\text{mol/kg}$

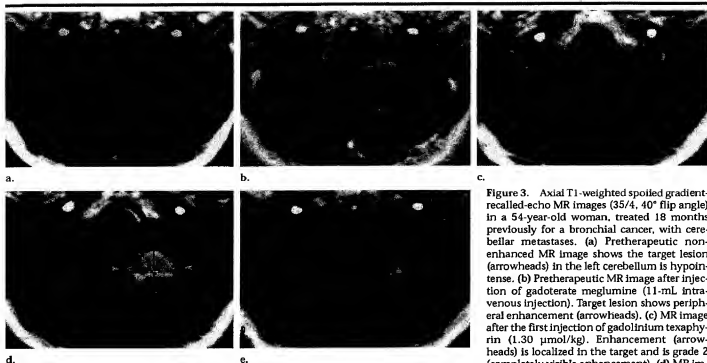


Figure 3. Axial T1-weighted spoiled gradient-recalled-echo MR images (35/4, 40° flip angle) in a 54-year-old woman, treated 18 months previously for a bronchial cancer, with cerebellar metastases. (a) Pretherapeutic non-enhanced MR image shows the target lesion (arrowheads) in the left cerebellum is hypointense. (b) Pretherapeutic MR image after injection of gadoterate meglumine (11-mL intravenous injection). Target lesion shows peripheral enhancement (arrowheads). (c) MR image after the first injection of gadolinium texaphyrin (1.30 $\mu\text{mol/kg}$). Enhancement (arrowheads) is localized in the target and is grade 2 (completely visible enhancement). (d) MR image after the 10th injection of gadolinium texaphyrin. Enhancement (arrowheads) is higher and is grade 3 (high enhancement). 1 and 2 are the two largest perpendicular diameters of the lesion. (e) MR image 56 days after the first gadolinium texaphyrin injection, without injection of contrast agent. Enhancement (arrowheads) is still well visible and is grade 2. Tumor decreased to 65% of initial size.

Dose of Gadolinium Texaphyrin Injection

Group	Dose	Increase above Preceding Dose (%)	Actual Dose ($\mu\text{mol/kg}$)
1	0.25
2	2.0 \times group 1 dose	100	0.50
3	3.3 \times group 1 dose	67	0.80
4	5.0 \times group 1 dose	50	1.30
5	7.0 \times group 1 dose	40	1.80
6	9.3 \times group 1 dose	33	2.30
7	12.4 \times group 1 dose	33	3.10
8	16.5 \times group 1 dose	33	4.10

(three patients), and 4.10 $\mu\text{mol/kg}$ (two patients).

A modified Fibonacci system (with modifications imposed by the manufacturer) was used for dose escalation of gadolinium texaphyrin injections in subsequent cohorts of treated patients (Table).

Three patients were evaluated at each nontoxic dose. The second patient in a cohort must have completed a 7-day follow-up period (after the last injection and irradiation), and the third patient in a cohort must have completed at least the 10-day therapy course before the next cohort was initiated.

If the maximal tolerated dose was not reached by group 8, additional cohorts of three patients were to have been enrolled and were to have received incremental increases of 33% in relation to the previous dose level until the maximal toler-

ated dose was reached. Three patients were required per cohort, which could have been increased to five patients if grade 3 or 4 toxic reactions had been observed. Data in patients with toxic reactions attributable to radiation therapy were excluded from the determination of the maximal tolerated dose (no patients in our institution, Institut Gustave-Roussy).

Timing of MR Studies

In our institution, Institut Gustave-Roussy, each patient underwent at least four brain MR imaging examinations. The first MR study was performed before the first injection (pretherapeutic) without or with intravenous injection of gadoterate meglumine (0.1 mmol per kilogram of body weight; Dotarem; Guerbet, Roissy, France). The second study was performed after the first injection of gado-

linium texaphyrin and before radiation therapy. The third study was performed after the last injection of gadolinium texaphyrin and before the last radiation therapy session, and the fourth was performed 56 days after the beginning of the treatment. Two patients underwent an extra MR examination 3–4 months after the beginning of the treatment. One patient underwent two additional MR examinations 6 and 9 months after the beginning of the treatment.

A 1.5-T magnet (Signa; GE Medical Systems, Milwaukee, Wis) and a T1-weighted spoiled gradient-recalled-echo pulse sequence (35/4 [repetition time msec/echo time msec], 40° flip angle) were used. Images were acquired in axial, coronal, and sagittal planes. A maximum of three studies were graded for each patient per target lesion. Two radiologists (J.V., D.V.) evaluated together, by consensus, enhancement of signal intensity after the first and last injections and 56 days later. This enhancement was graded 0–3, where 0 was no enhancement, 1 was moderate enhancement, 2 was fully visible enhancement, and 3 was high enhancement.

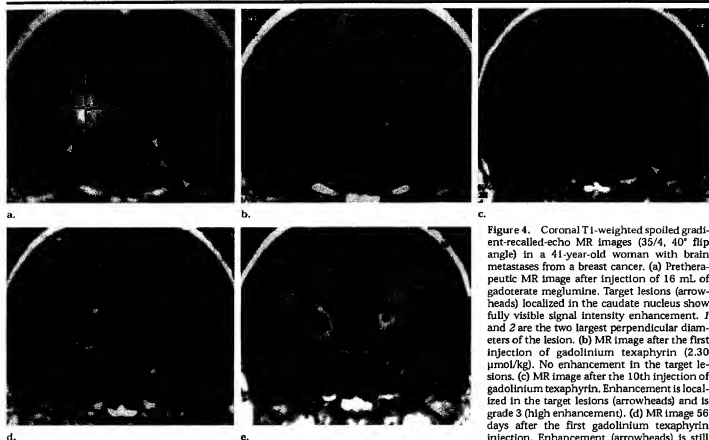


Figure 4. Coronal T1-weighted spoiled gradient-recalled-echo MR images (35/4, 40° flip angle) in a 41-year-old woman with brain metastases from a breast cancer. (a) Pretherapeutic MR image after injection of 16 mL of gadoterate meglumine. Target lesions (arrowheads) localized in the caudate nucleus show fully visible signal intensity enhancement. 1 and 2 are the two largest perpendicular diameters of the lesion. (b) MR image after the first injection of gadolinium texaphyrin (2.30 $\mu\text{mol/kg}$). No enhancement in the target lesions. (c) MR image after the 10th injection of gadolinium texaphyrin. Enhancement is localized in the target lesions (arrowheads) and is grade 3 (high enhancement). (d) MR image 56 days after the first gadolinium texaphyrin injection. Enhancement (arrowheads) is still visible and is grade 3. Tumor decreased to 68% of initial size. (e) MR image 16 weeks after the first gadolinium texaphyrin injection. Enhancement (arrowheads) is still visible and is grade 1 (moderate enhancement).

Evaluation of Response

Response to the treatment was assessed between the pretherapeutic MR study and the MR study performed 56 days after the beginning of the treatment. Response was based on World Health Organization criteria (the product of the two largest perpendicular diameters of measurable lesions).

RESULTS

Treatment was very well tolerated. There was no nausea or vomiting after administration of gadolinium texaphyrin. A single incident of considerably increased intracranial pressure occurred in one patient on the day of the first injection and treatment. Gradual yellow-green discoloration of urine was noted from the fourth dose level (1.30 $\mu\text{mol/kg}$) upward, and discoloration of skin was noted by the seventh level (3.10 $\mu\text{mol/kg}$). Biologic functions, in particular, liver or kidney functions, were normal.

During the months following treatment, five patients died; one died of massive pulmonary embolism, one died of septic shock (which was probably pul-

monary in origin), and three died of tumor progression. The maximal tolerated dose had not been reached in our center.

Results of Brain MR Examinations

Enhancement of signal intensity.—In the patient with a melanoma, signal intensity was high in brain metastases before injection of any contrast agent; this patient was excluded from the evaluation of enhancement. Therefore, signal intensity was evaluated in 10 patients (Figs 3, 4).

On MR images acquired after the first injection, enhanced signal intensity was visible in five patients. No enhancement was observed when the dose injected was below or equal to 0.80 $\mu\text{mol/kg}$. On MR images obtained after the last injection, enhanced signal intensity was visible in nine patients. The patient with no enhancement had received a dose of 0.80 $\mu\text{mol/kg}$. The patient who had received a dose of 0.50 $\mu\text{mol/kg}$ per injection had no enhancement of signal intensity in the target lesion on the MR image obtained after the first injection of gadolinium texaphyrin. However, after the 10th injection, there was enhanced signal in-

tensity, which was grade 2. One lesion was visible on the MR study acquired after the 10th injection of gadolinium texaphyrin (1.80 $\mu\text{mol/kg}$ per injection), but it had not been visible on the first MR image obtained after injection with conventional gadolinium-based contrast material.

MR images obtained 56 days after the beginning of treatment showed persistent enhancement of signal intensity in seven patients. The patient who had received the dose of 0.80 $\mu\text{mol/kg}$ per injection had images that showed enhanced signal intensity in the three grade 1 target lesions that had become visible only on the fourth MR study.

Additional MR studies were obtained in two patients 3–4 months after the beginning of treatment; the high level of signal intensity was still visible and was of a magnitude comparable to that of the fourth MR studies.

In a patient who received a dose of 1.30 $\mu\text{mol/kg}$ per injection, the MR images acquired after the beginning of treatment

showed enhancement of signal intensity, which had been grade 3 on the fourth MR image and was still fully visible at 6 months (grade 2) and moderate at 9 months (grade 1).

Localization of enhanced signal intensity.—Enhancement of signal intensity was noted only in target lesions, never in normal brain tissue or the mucous membrane.

Appearance of enhanced signal intensity.—There was no remarkable modification in the appearance of the signal intensity noted on successive MR images, which means enhancement was not due to hemorrhage in metastases.

Response to Treatment

Response was evaluated according to World Health Organization criteria. Seven patients achieved a partial remission, with tumor regression greater than or equal to 50%. One patient achieved a minor response with a tumor regression of 25%–49% of the initial size, and in three patients the disease stabilized, with tumor regression of 1%–24% of the initial size. One patient had new brain metastases 2 months after the end of the treatment.

DISCUSSION

Radiation therapy is an important treatment for localized cancers. Unfortunately, the radiation dose is often too limited because of injury to normal surrounding tissue. An ideal radiosensitizer would exert its effect only when administered in the appropriate sequence with radiation therapy, with no direct toxic reaction.

Metronidazole, which was used as a radiation sensitizer in the treatment of supratentorial glioblastomas 20 years ago, achieved a notable positive effect (6). A few years later, nimorazole was used as a hypoxic radiation sensitizer in the treatment of supraglottic laryngeal and pha-

ryngeal carcinoma; the study findings (7) revealed an apparent independent and additive relationship between the hemoglobin concentration and the use of the hypoxic radiosensitizer, and the tumor response was better in patients randomly assigned to the nimorazole group than in patients in the placebo group.

Unfortunately, most radiation sensitizers do not show any differential therapeutic index between tumor and surrounding normal tissues. The use of a tumor-selective radiation sensitizer could help maximize tumor exposure to ionizing radiation and could help improve the chances of obtaining tumor control. Furthermore, a tumor-selective radiation sensitizer that is detectable at MR imaging could help in the appreciation of response to radiation therapy. Such was the case with gadolinium texaphyrin, the prototype of a new class of compounds.

These preliminary results based on limited findings in 11 patients indicate that gadolinium texaphyrin is safe and tumor selective, since enhancement of signal intensity was detected only in target lesions and never in normal brain tissue. Uptake in target lesions was higher after 10 daily injections of gadolinium texaphyrin than after the first one, which indicated the accumulation of gadolinium texaphyrin in brain metastases and its persistence several months later in metastases, as revealed at additional MR examinations. The lesion that was visible only after the 10th injection of gadolinium texaphyrin was either a new metastasis or a lesion that was undetectable with conventional gadolinium-based contrast material.

It is possible not only to depict brain metastases at MR imaging with gadolinium texaphyrin but also to evaluate response to treatment at successive MR imaging examinations, since gadolinium texaphyrin remains in tumors for several months. Injection of a paramagnetic contrast agent for the follow-up MR examinations would be redundant.

These preliminary results do not reflect the radiation-sensitizing effect of gadolinium texaphyrin, which requires further investigation.

Findings of this phase IB and phase II study indicate that gadolinium texaphyrin is tumor selective. The accumulation of gadolinium texaphyrin in metastases over several months as revealed at brain MR studies should permit imaging of brain metastases after radiation therapy and, therefore, evaluation of response to the treatment. A further study in more patients is necessary to appreciate the radiation-sensitizing effect of gadolinium texaphyrin.

References

1. Young S, Qing F, Harriman A, et al. Gadolinium(III) texaphyrin: a tumor selective radiation sensitizer that is detectable by MRI. *Proc Natl Acad Sci USA* 1996; 93:6610–6615.
2. Rosenthal DI, Nurenberg P, Becerra CR, et al. A phase I single-dose trial of gadolinium texaphyrin (Gd-TeX), a tumor selective radiation sensitizer detectable by magnetic resonance imaging. *Clin Cancer Res* 1999; 5:739–745.
3. Young SW, Sidhu MK, Qing F, et al. Preclinical evaluation of gadolinium (III) texaphyrin complex: a new paramagnetic contrast agent for magnetic resonance imaging. *Invest Radiol* 1994; 29:330–338.
4. Sessler JL, Hemmi G, Mody TD, Mural T, Burrell A, Young SA. Texaphyrins: synthesis and applications. *Accounts Chem Res* 1994; 27:43–50.
5. Borgelt B, Gelber R, Kramer S, et al. The palliation of brain metastases: final results of the first two studies by the Radiation Therapy Oncology Group. *Int J Rad Oncol Biol Phys* 1980; 6:1–9.
6. Urtasun R, Band F, Chapman JD, Feldstein ML, Mielke B, Fryer C. Radiation and high-dose metronidazole in supratentorial glioblastomas. *N Engl J Med* 1976; 294:1364–1367.
7. Overgaard J, Sand Hansen H, Lindelov B, et al. Nimorazole as a hypoxic radiosensitizer in the treatment of supraglottic larynx and pharynx carcinoma: first report from the Danish Head and Neck Cancer Study (DAHANCA) protocol 5-85. *Radiation Oncol* 1991; (suppl 1):143–149.

A Phase I Single-Dose Trial of Gadolinium Texaphyrin (Gd-Tex), a Tumor Selective Radiation Sensitizer Detectable by Magnetic Resonance Imaging¹

David I. Rosenthal,² Pamela Nurenberg, Carlos R. Becerra, Eugene P. Frenkel, David P. Carbone, Bert L. Lum, Richard Miller, Julie Engel, Stuart Young, Dale Miles, and Markus F. Renschler

Department of Radiation Oncology, University of Pennsylvania Medical Center, Philadelphia, Pennsylvania 19104-4283 [D. I. R.]; Departments of Radiology [P. N.] and Internal Medicine [C. R. B., E. P. F.], University of Texas Southwestern Medical Center at Dallas, Dallas, Texas 75235; Department of Internal Medicine, Vanderbilt University Medical Center, Nashville, Tennessee 37232 [D. P. C.]; Division of Oncology, Stanford University, Stanford, California 94305 [B. L. L.]; and Pharmacia, Inc., Sunnyvale, California 94086 [R. M., J. E., S. Y., D. M., J. F. R.]

ABSTRACT

Gadolinium Texaphyrin (Gd-Tex) is a radiation sensitizer with a novel mechanism of action that sensitizes both oxic and hypoxic cells, localizes selectively in tumors, and is detectable by magnetic resonance imaging (MRI). This Phase I single-dose trial of Gd-Tex administered concurrently with radiation therapy was carried out to determine the maximally tolerated dose (MTD), dose-limiting toxicities, pharmacokinetics, and biolocalization of Gd-Tex as determined by MRI. Adults with incurable cancers of any histology requiring radiation therapy were eligible. A single i.v. dose of Gd-Tex was followed at least 2 h later by radiation therapy. The Gd-Tex dose was escalated in cohorts of 3 to 5 patients. Thirty-eight patients (median age, 58 years; range, 35-77 years) with incurable cancers of the lung (26), cervix (3), or other solid tumors (9) received a total of 41 single administrations of Gd-Tex. The Gd-Tex dose was escalated from 0.6 to 29.6 mg/kg. Irradiated sites included the thorax, brain, pelvis, bone, soft tissue, and sites of nodal metastases. The MTD was 22.3 mg/kg, determined by reversible acute tubular necrosis as the dose-limiting toxicities. Gd-Tex selectively accumulated in primary and metastatic tumors as demonstrated by MRI. No increase in radiation

toxicity to normal tissues was seen. The median half-life of Gd-Tex after single-dose administration is 7.4 h. This study demonstrates that Gd-Tex is well tolerated in doses below the MTD, and that there is selective biolocalization in tumors. The maximum recommended dose for single administrations is 16.7 mg/kg.

INTRODUCTION

Local control continues to be a major therapeutic challenge for locally advanced, nonmetastatic solid tumors. These tumors are often not amenable to surgical resection, and are poorly controlled by XRT.³ Radiation dosage is limited by normal tissue tolerance rather than being directed by the higher dose that would more likely improve tumor control. For example, studies indicate that local control is achieved in fewer than 30% of patients with locally advanced but nonmetastatic head and neck and non-small cell lung cancers despite treatment with maximally tolerated doses of XRT (1-3). Higher radiation doses would increase the probability of tumor control but would also increase the risk for normal tissue complications (4). The use of radiation sensitizers is one strategy that might help to overcome treatment resistance.

Gd-Tex (NSC 695238) is a pentadentate aromatic metalloporphyrin developed as a sensitizer for radiation and chemotherapy (5). Like many naturally occurring porphyrins, it has selective biolocalization in tumor and the ability to form long lived radicals by accepting solvated electrons generated by ionizing radiation in oxic or anoxic conditions (6). *In vitro* studies have demonstrated dose-dependent radiation sensitization of human cancer cell lines. *In vivo* studies in single fraction and multifraction experiments of a variety of tumor models demonstrated dose-dependent radiation sensitization resulting in improved survival of tumor-bearing animals (6).

Gd-Tex accumulates in tumor tissue with selective sparing of normal surrounding tissue. Animal studies using [⁵¹Gd] or [¹⁴C]Gd-Tex injected into tumor-bearing animals demonstrated rapid clearance of the drug from blood and normal tissues, with delayed clearance from tumors, which resulted in up to 8-fold greater concentrations in tumors compared with surrounding tissues (7). Because Gd-Tex contains the paramagnetic metal ion gadolinium, its selectivity has been demonstrated by MRI of tumor-bearing animals. These studies show enhancement of tumors but not normal surrounding tissues. This persists for up

Received 8/17/98; revised 12/29/98; accepted 12/29/98.

The costs of publication of this article were defrayed in part by the payment of page charges. This article must therefore be hereby marked advertisement in accordance with 18 U.S.C. Section 1734 solely to indicate this fact.

¹ Supported by a research Grant from Pharmacia, Inc., Sunnyvale, CA.

² To whom requests for reprints should be addressed, at Department of Radiation Oncology-2 Donner, University of Pennsylvania Medical Center, 3400 Spruce Street, Philadelphia, PA 19104-4283. Phone: (215) 662-4204; Fax: (215) 349-5445.

EXHIBIT 1

PAGE 6

³ The abbreviations used are: XRT, radiation therapy; Gd-Tex, gadolinium texaphyrin; MRI, magnetic resonance imaging; MTD, maximum tolerated dose; DLT, dose-limiting toxicity; ICP-AES, Inductively Coupled Plasma Atomic Emission Spectroscopy; AUC, area under curve; G6PD, glucose 6 phosphate dehydrogenase.

to 48 h after single-dose administration (8) and is attributed to the hepatic and renal clearance of the drug. Because of the hepatic and renal clearance of the drug, liver and kidney enhancement has been observed as well. DLT in animals is hepatotoxicity. Gd-Tex has the potential to be a clinical tumor-selective radiation sensitizer. We report here the results of the Phase I clinical trial.

PATIENTS AND METHODS

Eligibility. This study was approved by the Institutional Review Board at the University of Texas Southwestern Medical Center at Dallas, where all of the patients were treated. Informed consent was obtained from every patient enrolled. Patients with incurable primary or metastatic cancer requiring palliative radiotherapy were eligible. Pretreatment evaluation included a complete history and physical examination, posteroanterior and lateral chest X-ray, an electrocardiogram, a complete blood count, and serum chemistries.

Eligibility criteria included: (a) Eastern Cooperative Oncology Group (ECOG) performance status, 0–2; (b) age, ≥ 18 years; (c) serum creatinine, ≤ 1.5 mg/dl; (d) aspartate transaminase and alanine transferase, \leq twice the upper limit of institutional normal; (e) serum bilirubin, ≤ 2 mg/dl; (f) absolute granulocyte count, $\geq 1500/\text{mm}^3$; (g) the ability to complete a 14-day posttreatment follow-up; and (h) an expected survival of 3 weeks. Patients were not eligible if their radiotherapy fields involved entry-exit through the liver or kidneys, if they had received prior involved field XRT, if they were lactating or pregnant women, if they had received other investigational agents within 30 days, or if they had a medical or psychiatric illnesses that would preclude informed consent. No chemotherapy was allowed for 2 weeks before or 2 weeks after Gd-Tex administration.

Gd-Tex Dosage and Administration. A single i.v. dose of Gd-Tex (Xcyrin, Pharmacia, Inc., Sunnyvale, CA), formulated in an aqueous solution of 5% (isotonic) mannitol at a concentration of 2.3 mg/kg, was administered at a rate of 1–32 ml/min during the 1st week of palliative radiation. Before Gd-Tex administration, patients were hydrated p.o. with 240 ml of clear liquids/h for each of 4 h and then with 500 ml D5W i.v. immediately before Gd-Tex infusion.

The starting dose of Gd-Tex was one-tenth of the human equivalent of the lethal-dose for 10% (LD_{10}) for mice, or 0.6 mg/kg. The dose was increased in cohorts of 3–5 patients according to the following modified Fibonacci system: 0.9, 1.1, 2.0, 2.9, 4.0, 5.4, 7.1, 9.5, 12.6, 16.7, 22.3, and 29.6 mg/kg. Dose escalation progressed if none of 3 patients had any treatment-related grade 3 or grade 4 toxicity, using the Cancer Therapy Evaluation Program/National Cancer Institute (CTEP/NCI) Common Toxicity Criteria to score adverse events. If one patient experienced grade 3 or 4 toxicity, two additional patients were enrolled in the same cohort, and the dose was escalated if no additional patient had grade 3 or grade 4 toxicity. If two patients in a cohort experienced treatment-related grade 3 or grade 4 toxicity, the MTD would have been exceeded, and the dose below that cohort would have been declared the MTD. Thus the MTD was defined as the dose level below which 2 patients developed grade 3 or 4 toxicity and at which 3 of 3

or 4 of 5 patients completed the cohort without treatment-related grade 3 or grade 4 adverse events. The serious toxicity-limiting dose escalation was defined as the DLT. Patients returning for all scheduled follow-up visits including the final 14-day follow-up visit were considered to have successfully completed the study. All of the patients were included in the safety analysis.

XRT. One of the first five fractions of palliative XRT was delivered between 2 and 5 h after the completion of the Gd-Tex infusion. At least two parallel opposed or wedge pair X-ray beams were used to deliver 2, 2.5, or 3 Gy once daily to the planning target volume. Computerized dosimetry was performed for all patients. Dose gradient was maintained below 5%. Total doses ranged between 30 Gy in 10 fractions and 60 Gy in 30 fractions. The kidneys and liver were excluded from the irradiated volume. The spinal cord dose was limited to 40 Gy at 2 Gy/day or 30 Gy at 3 Gy/day. No X-ray entry-exit through the liver or kidneys was allowed.

MRI. Axial MRI scans of the brain, upper abdomen, and the site to be irradiated were obtained on all of the patients who could be scheduled and who could complete the study. Imaging was performed with a 1.5 Tesla device using the body or head coil. Axial T1 weighted spin echo, turbo spin echo, or fast field echo images were obtained of the site to be irradiated, the liver, and the kidneys before and after the administration of Gd-Tex. The slice thickness ranged from 6 to 15 mm. Images were obtained before, and within one h after, the administration of Gd-Tex. Additional delayed images were obtained in some patients up to 14 h after injection. The same MRI equipment and identical parameters were used for the pre- and post-Gd-Tex scans for each patient. Regions of interest were created in the tumors imaged as well as in the normal hepatic and renal parenchyma. Enhancement was scored if there was a $\geq 20\%$ increase in signal intensity in the images obtained post-Gd-Tex administration as compared with the pre-Gd-Tex images.

Pharmacokinetics. Plasma samples were obtained at baseline and over the first 1.5 h after dosing in patients treated with 0.6–2.0 mg/kg, and at 1, 4, and 24 h after drug infusion in the remainder of the patients. Additional time points were obtained from some patients. All of the blood samples were anticoagulated with K_2EDTA . The plasma layer was separated by centrifugation and stored frozen until the time of analysis. The concentration of gadolinium was determined in each plasma sample by ICP-AES using a validated method. The ICP-AES analysis was performed by MDS Harris Laboratories in Lincoln, Nebraska. Gadolinium concentrations in plasma were converted to units of $\mu\text{g-equiv/ml}$ before pharmacokinetic analysis. A $\mu\text{g-equiv}$ was defined as the quantity of Gd-Tex (intact parent compound) in μg that would contain an amount of gadolinium metal equivalent to what was measured by ICP-AES. The lower limit of quantitation for this assay was determined to be 3.7 $\mu\text{g-equiv/ml}$. The interday relative error and precision of the assay were determined to be ≤ 7.4 and $\leq 7.5\%$, respectively, during the validation.

For the patients with early sampling time points, plasma concentration *versus* time profiles were fit to a 1-compartment, open, linear pharmacokinetic model with zero order input and first order elimination. Pharmacokinetic parameter estimates were obtained using nonlinear weighted least squares regression analysis using WinNonlin Version 2.0 (Pharsight Corporation,

Mountain View, CA), with the regression weighted to $1/C_p$, where C_p equals the measured plasma concentration of Gd-Tex.

For patients sampled at 1, 4, and 24 h, it was not considered appropriate to use a compartment model because contributions from α , β , and γ elimination phases could contribute to the Gd-Tex concentrations measured at these time points. Therefore, noncompartmental analysis was used to determine the area under the plasma concentration versus time curve between 1 and 24 h ($AUC_{1-24\text{ h}}$) using the logarithmic trapezoidal method of integration. Because plasma samples for several patients were not obtained at exactly 1 h or 24 h, the logarithm of the plasma concentration at these time points was extrapolated/interpolated for some patients. The percentage of extrapolated area for each patient was less than 9%.

To test for a nonlinear relationship between $AUC_{1-24\text{ h}}$ and dose, the data were fitted to a power function described as $AUC_{1-24\text{ h}} = A(\text{dose})^B$, and the function was transformed by taking logarithms of both sides to yield $\ln(AUC_{1-24\text{ h}}) = \ln(A) + B\ln(\text{dose})$. After calculating the value of B , Student's t test was used to see whether B was significantly different from 1.0.

Follow-up Evaluation. Patients were followed for 4 h after infusion, then seen again at 24 h, 48 h, 72 h, 7 days, and 14 days after infusion. Follow-up safety information was obtained through day 30 after infusion.

RESULTS

Patient Characteristics

Thirty-eight patients (19 men, 19 women, ages 35–77; median age, 58 years) entered the study. Three patients developed second areas of metastases requiring additional palliative irradiation and entered the trial twice. A total of 41 single-doses of Gd-Tex were administered. The patient characteristics are shown in Table 1. The most common tumor was lung cancer. The most frequently irradiated sites were the thorax and the brain. The majority of patients had a good performance status at baseline evaluation. All but three of the patients were ambulatory and capable of total self care.

Study Completion

All of the patients received the fully planned dose of Gd-Tex and XRT, and were included in the trial for toxicity analysis. All but one patient were followed for 30 days. One patient in the 12.6-mg/kg cohort who received palliative XRT for brain metastases from small cell lung cancer died from progressive systemic disease 11 days postdose. There was no evidence to suggest any relationship to the administration of Gd-Tex.

Dose Escalation

The Gd-Tex dose was escalated in 13 cohorts from 0.6 mg/kg to 29.6 mg/kg. The number of patients and doses of Gd-Tex administered in each cohort is shown in Table 2. The 10th cohort was expanded to four patients because the patient who died did not complete the 30-day follow-up. The 11th cohort was expanded to five patients per protocol because one patient experienced a treatment-related grade 3 rise in bilirubin. No further grade 3 or 4 toxicity was observed in the additional patients enrolled at that dose. Dose escalation continued accord-

Table 1 Patient characteristics

Total Number	39
Sex	
Female	19
Male	19
Age	
Range	33–77
Median	58
No. of Gd-Tex administrations	
1	35
2	3
Total	41
Performance status (ECOG)*	
0	16
1	10
2	10
3	3
Not done	2
Primary cancer	
Lung	26
Cervical	3
Soft tissue sarcoma	2
Breast cancer	1
Glioblastoma multiforme	1
Head and neck cancer	1
Multiple myeloma	1
Ovarian cancer	1
Renal cell carcinoma	1
Uterine cancer	1
Radiation treatment site	
Thorax	15
Brain	9
Pelvis	7
Spine/Bone	5
Lymph nodes	4
Head and neck	1

* ECOG, Eastern Cooperative Oncology Group.

ing to the escalation rules. Dose escalation was discontinued after the 13th cohort when a pattern of dose-related renal toxicity became apparent. The MTD defined per protocol was 22.3 mg/kg.

Adverse Events

The i.v. administration of Gd-Tex followed by XRT was well tolerated at doses up to 22.3 mg/kg. Grade 3 and 4 toxicities that were treatment-related are shown in Table 3. A total of four patients experienced serious adverse events. At 9.5 mg/kg, one patient experienced grade 3 nausea and vomiting. At 16.7 mg/kg, one patient developed hemolytic anemia. Above the MTD, at 29.6 mg/kg, one patient developed serious dyspnea, myalgia, photophobia, asthenia, and grade 3 acute renal failure. Another patient developed grade 2 acute renal failure. There were no serious hepatic, pulmonary, or cardiovascular toxicities observed. Adverse events are discussed by body system.

Renal Toxicity. The DLT for single i.v. administration of Gd-Tex followed by XRT was dose-dependent reversible acute renal failure. No significant renal toxicity was observed at Gd-Tex doses of 0.6–12.6 mg/kg. One of five patients treated at 16.7 mg/kg experienced a transient grade 2 rise in creatinine to 2.0 mg/dl 24 h post Gd-Tex administration that normalized by 72 h. At the 22.3 mg/kg dose level, two of three patients developed transient grade 2 renal toxicity, one with a peak rise

Table 2 Gd-Tex doses administered and number of patients per cohort

Cohort	1	2	3	4	5	6	7	8	9	10	11	12	13
Dose (mg/kg)	0.6	0.9	1.1	2.0	2.9	4.0	5.4	7.1	9.5	12.6	16.7	22.3	29.6
Patients	3	3	3	3	3	3	3	3	3	4	5	3	2

Table 3 Treatment-related grade 3 or 4 or serious adverse events

	Cohort												
	1	2	3	4	5	6	7	8	9	10	11	12	13
Dose (mg/kg)	0.6	0.9	1.1	2.0	2.9	4.0	5.4	7.1	9.5	12.6	16.7	22.3	29.6
Asthenia													1
Nausea									1				
Vomiting									1				
Hemolytic anemia											1		
Renal failure													2
Dyspnea													1
Myalgia													1
Photophobia													1
Patients with serious adverse events									1		1		2

in creatinine to 2.4 at 24 h and the other with a peak rise in creatinine to 3.4 mg/dl at 72 h after Gd-Tex administration. The creatinine returned to normal in both patients. Both patients treated at 29.6 mg/kg developed nonoliguric acute renal failure. Creatinine levels rose to 2.7 mg/dl (grade 2) and 4.8 mg/dl (grade 3), peaking at 24 and 72 h after infusion, and returning to normal by 7 and 14 days after Gd-Tex administration, respectively. Both patients were hospitalized for observation and treated conservatively with a renal diet and reduced fluid intake, and both recovered completely. A renal biopsy in the patient with grade 3 renal toxicity demonstrated acute tubular necrosis. The toxicities experienced by the four patients who received 22.3 mg/kg and 29.6 mg/kg Gd-Tex led to a decision to discontinue dose escalation and declare the previous dose level of 22.3 mg/kg as the MTD, although expansion of the dose cohort would have been acceptable by the dose escalation rules. Transient albuminuria was seen on urine dip-stick in one patient treated at 12.6 mg/kg and in two patients each treated at 22.3 and 29.6 mg/kg.

Dermatological Toxicity. The most frequently reported adverse event was transient green discoloration of skin, mucosa, feces, and urine in all of the patients receiving Gd-Tex doses ≥ 7.1 mg/kg. The discoloration was attributed to the dark green color of the study drug and resolved completely over 72–96 h. Patients accepted this well as long as they and their families were prepared for it. One patient treated at the 22.3 mg/kg dose level developed a vesicular rash on the palms of his hands after administration of Gd-Tex. A biopsy was consistent with pseudoporphyria or porphyria cutanea tarda. However, a quantitative urine porphyrin analysis was not consistent with porphyria cutanea tarda. The rash was self-limited. Two patients reported pruritus—one at the MTD and the other at a dose above the MTD.

Gastrointestinal Toxicity. Treatment-related dose-dependent nausea and vomiting, the second most frequently reported adverse event, was observed in 28% of the patients,

including all of the patients in the 7.1- and 9.5-mg/kg dose groups. All of the patients treated at 12.6 mg/kg or higher were premedicated with oral antiemetics (dexamethasone, 10 mg, and prochlorperazine, 10 mg), which prevented the nausea until the MTD was exceeded. Above the MTD, grade 2 nausea and vomiting were seen again in one patient. Diarrhea was observed after eight treatments but was not dose-dependent. Although one patient each in the 1.1-, 2.0-, 4.0-mg/kg cohorts, two patients in the 9.5-mg/kg cohort, and three patients in the 12.6-mg/kg cohort reported possibly treatment-related diarrhea, no patients in cohorts receiving above 12.6 mg/kg reported diarrhea.

Hematological Toxicity. One patient with a previously unknown history of G6PD deficiency treated at 16.7 mg/kg developed hemolytic anemia, manifested by a drop in hemocrit and a grade 3 rise in total bilirubin. There was no treatment-related neutropenia, thrombocytopenia, or anemia.

Hepatic Toxicity. Transient grade 1 and grade 2 rises in transaminases peaking at 48 h after dose was observed in fewer than five patients and resolved within 7 days in all of the cases.

Radiation Toxicity All in-field XRT toxicities were mild, expected, and commensurate with dose. There was no increase in normal tissue toxicity within the XRT treatment volume. There were no grade 3 or 4 toxicities within the radiation ports. All of the unusual or potentially serious toxicities seen in this trial and described above were systemic.

MRI Results

MRI images were used to document the biodistribution of Gd-Tex. Tumor and normal tissue enhancement was measured in the irradiated sites as well as in the brain, liver, kidneys, muscle, and lungs. Fig. 1 shows the contrast enhancement as a percent increase from baseline, averaged per cohort. At doses up to 4.0 mg/kg, some but not all of the tumors enhanced after Gd-Tex administration, with signal intensities increasing up to 31%. At doses above 4.0 mg/kg, every tumor that was evaluable-enhanced significantly, with signal intensities increasing

Fig. 1 MRI contrast enhancement per cohort. Percent change in MRI signal intensity of the tumor after Gd-Tex administration, averaged per cohort.

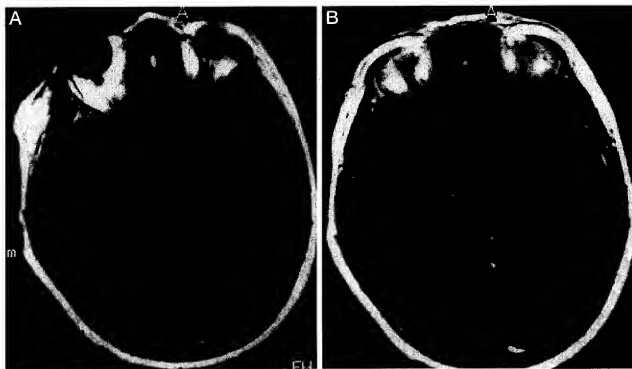
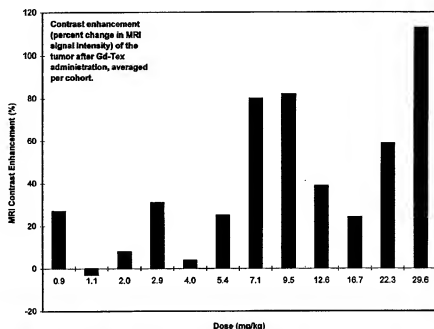


Fig. 2 Head MRI of a patient with a brain metastasis (A) before Gd-Tex administration and (B) after Gd-Tex administration. Both images represent T1 weighted noncontrast MRI images obtained without administration of conventional gadolinium-containing contrast reagents.

from 24 to 113%. Other sites demonstrating increased enhancement were the kidney and the liver, the two organs in which Gd-Tex is cleared. There was no significant enhancement of the normal brain at any of the doses (<3 to 12% contrast enhancement). There was no significant contrast enhancement in muscle at doses up to 12.6 mg/kg. At and above the MTD, there was

moderate contrast enhancement in muscle (25–28% contrast enhancement). The lungs did not enhance visibly, although the percent change in very low signal intensities at 0.9 and 29.6 mg/kg calculated to be 35% and 70% respectively. Fig. 2 shows an MRI scan of the brain of a patient with a brain metastasis from non-small cell lung cancer on study before (A) and after

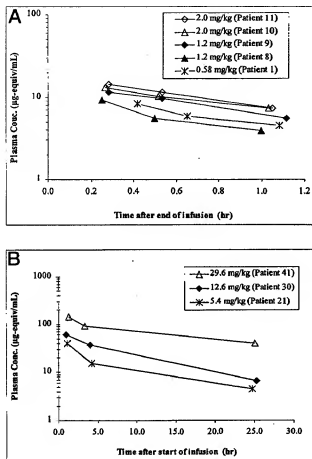


Fig. 3 Semilog plot of plasma concentration versus time (A) for the five patients treated with low doses of Gd-Tex and sampled at early time points after drug administration and (B) for three representative patients sampled at later time points after Gd-Tex administration.

(B) the injection of Gd-Tex. Enhancement of the tumor but not the normal brain is seen, indicating that Gd-Tex is selectively taken up and retained by the metastasis. Signal enhancement of tumors was seen as late as 14 h after a single Gd-Tex administration.

Pharmacokinetic Results

A total of 23 patients had a sufficient number of blood draws to allow pharmacokinetic analysis. The first five patients were dosed from 0.58 to 2.0 mg/kg of Gd-Tex at a rate of 9.5 ± 6.7 mg/min (mean \pm SD), and 3 blood samples were obtained over the first 1.5 h after dosing. The remaining 18 patients received doses ranging from 5.4 to 29.6 mg/kg of Gd-Tex at a rate of 47.6 ± 15.0 mg/min (mean \pm SD). Blood from these patients was sampled at baseline and at 1, 4, and 24 h after drug infusion, and additional time points were sampled for some patients.

The plasma concentration versus time profiles for five patients sampled at early time points are shown in Fig. 3(A). The pharmacokinetic data from these patients were fit to a 1-compartment, open, linear model and a median (interquartile range)

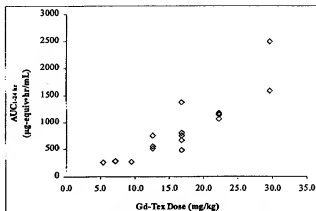


Fig. 4 $AUC_{0-24 h}$ plotted versus dose for patients administered 5.4–29.6 mg/kg Gd-Tex.

value for the plasma elimination half-life was determined as 0.78 h (0.74–0.79 h). Although the sampling scheme was not sufficiently detailed to resolve an α distribution and a β elimination phase, 0.78 h still represents a reasonable estimate of an upper limit for the α half-life because any β phase contribution would increase the 1-compartment model-derived value of the elimination half-life.

In Fig. 3B, representative plasma concentration versus time profiles have been plotted for three individuals selected from the second group of 18 patients. Patients in this group received doses ranging from 5.4 to 29.6 mg/kg. Blood samples were drawn at 1, 4, and 24 h after administration of Gd-Tex. The area under the plasma concentration versus time curve ($AUC_{0-24 h}$) for each patient was compared with the estimated value of $AUC_{0-24 h}$ for an efficacious dose of Gd-Tex in mice (23 mg/kg). For each patient, $AUC_{0-24 h}$ was greater than the corresponding value in mice. Thus, the Gd-Tex levels achieved in humans exceed those achieved in mice at an efficacious dose.

$AUC_{0-24 h}$ was plotted versus dose for each patient to determine whether a nonlinear relationship existed between these two variables. As shown in Fig. 4, a trend toward nonlinearity (concave up) was observed between $AUC_{0-24 h}$ and dose. However, a fit of the data to a power function revealed that this trend was not statistically significant.

DISCUSSION

This clinical trial demonstrates tumor enhancement uniformly in every patient imaged at doses ≥ 4.0 mg/kg, independent of tumor type. A general dose-response relationship between signal intensity and drug concentration was observed; however, the heterogeneity of tumors examined and sites imaged precluded the description of a quantitative relationship. A dose-response relationship was also seen with respect to the percent of patients with tumor enhancement at a given dose. Enhancement was noted in primary as well as in metastatic tumors alike. Unlike conventional MRI contrast agents, the signal enhancement after Gd-Tex administration persisted for up to 14 h after single i.v. injection, despite rapidly falling plasma levels with a median half-life of 7.4 h. This is thought to be caused by the

intracellular uptake and retention of Gd-Tex in tumor cells, demonstrated in preclinical studies. Gd-Tex could, thus, allow for selective radiosensitization of tumors in patients based on its selective localization in tumors. Gd-Tex also has the potential to be studied in the context of an initial and follow-up diagnostic tumor imaging agent and to delineate the tumor for MRI-based three-dimensional treatment planning, including stereotactic radiosurgery.

We recommend the use of 16.7 mg/kg as the maximum single dose of Gd-Tex, although this is not the MTD to obviate the grade 2 renal toxicity seen at the MTD. The dose-limiting nonoliguric acute tubular necrosis responded to renal diet and fluid restriction in both patients. Because texaphyrins are highly lipoprotein-bound, dialysis was not indicated to increase the elimination of Gd-Tex.

Patients with differing tumor histologies and irradiated sites were included in this trial, which was adequate to assess the intended systemic and preliminary loco-regional Phase I end points. Future radiation site-specific Phase I trials will be necessary to fully evaluate potential toxicities within irradiated volumes in different body areas. Enhancement demonstrated in normal renal and hepatic parenchyma confirms the initial impression that the liver and kidneys should be excluded from the irradiated volume. We recommend that the drug not be used in patients with G6PD deficiency, and that it be used selectively and with great care in those with porphyrias. Adequate initial renal function is essential.

In conclusion, Gd-Tex plasma concentrations exceeding that reported for radiosensitization can be achieved at well-tolerated doses below the MTD. Using MRI, Gd-Tex selectively biolocalizes in tumors. These results are also consistent with the finding that normal tissue radiation toxicity was not increased. The nonlinear character of tumor enhancement, however, did not permit a reliable correlation with plasma concentration in this study, and continues as a subject of ongoing research.

Multiple dose administration of Gd-Tex will be necessary to realize its potential as a useful clinical radiation sensitizer. Radiation site-specific Phase I trials with multiple dosing of Gd-Tex are ongoing under the sponsorship of the Cancer Therapy Evaluation Program (CTEP) at the National Cancer Insti-

tute. The optimal dose and schedule of Gd-Tex and integration with XRT will be determined by the MRI, pharmacokinetic, and clinical data derived from these trials as well as this one. Ultimately, a Phase III trial randomizing patients to site-specific XRT with or without Gd-Tex will be necessary to determine the clinical efficacy of this new drug as a clinical radiation sensitizer.

ACKNOWLEDGMENTS

We thank Rosemarie Mick for statistical support and review of the article and Jennifer Stanford, RN and Laurie Benanti, RN of Medtrials for research assistance.

REFERENCES

1. Arriagada, R., Le Chevalier, T., Quoix, E., Ruffie, P., de Cremoux, H., Douillard, J. Y., Tarayre, M., Pignon, J. P., and Lapiance, A. Effect of chemotherapy on locally advanced non-small lung carcinoma: a randomized study of 353 patients. *Int. J. Radiat. Oncol. Biol. Phys.*, 20: 1183-1190, 1991.
2. Vokes, E. E., Weichselbaum, R. R., Lippman, S. M., and Hong, W. K. Head and neck cancer. *N. Engl. J. Med.*, 328: 184-194, 1993.
3. Merlano, M., Vitale, V., Rosso, R., Benasso, M., Corvo, R., Cavallari, M., Sanguineti, G., Bacigalupo, A., Badellino, F., and Margarin, G. Treatment of advanced squamous cell carcinoma with alternating chemotherapy and radiotherapy. *N. Engl. J. Med.*, 327: 1115-1121, 1992.
4. Perez, C. A., Brady, L. W., and Roti Roti, J. L. Overview. In: C. A. Perez and L. W. Brady (eds.), *Principles and Practice of Radiation Oncology*, Ed. 3, pp 3-34. Philadelphia: Lippincott-Raven Publishers, 1997.
5. Sessler, J. L., Mody, T. D., Hemmi, G. W., and Lynch, V. Synthesis and structural characterization of lanthanide (III) texaphyrins. *Inorganic Chem.*, 32: 3175-3187, 1993.
6. Young, S. W., Qing, F., Harriman, A., Sessler, J. L., Mody, T. D., Hemmi, G. W., Hao, Y., and Miller, R. A. Gadolinium (III) texaphyrin: a tumor selective radiation sensitizer that is detectable by MRI. *Proc. Natl. Acad. Sci. USA*, 93: 6610-6615, 1996.
7. Gadolinium Texaphyrin Investigator's Brochure. Sunnyvale, CA: Pharmacocycles, Inc., 1995.
8. Young, S. W., Sidhu, M. K., Qing, F., Miller, H. H., Neuder, M., Zanassi, G., Mody, T. D., Hemmi, G., Dow, W., and Mutch, J. D. Preclinical evaluation of gadolinium (III) texaphyrin complex: a new paramagnetic contrast agent for magnetic resonance imaging. *Invest. Radiol.*, 29: 330-338, 1994.

Gadolinium(III) texaphyrin: A tumor selective radiation sensitizer that is detectable by MRI

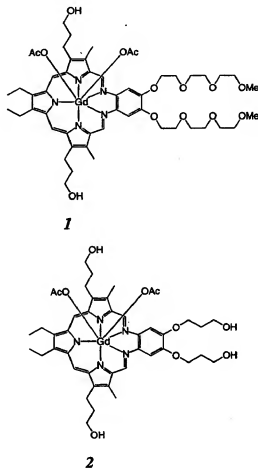
STUART W. YOUNG^{†*}, FAN QING^{*}, ANTHONY HARRIMAN^{‡§}, JONATHAN L. SESSLER^{||}, WILLIAM C. DOW^{*},
TARAK D. MODY^{*}, GREGORY W. HEMMI^{*}, YUNFENG HAOL^{||}, AND RICHARD A. MILLER^{*}

^{*}Pharmaceuticals, Inc., 995 East Arques Avenue, Sunnyvale, CA 94086; [†]Center for Fast Kinetics Research, University of Texas, Austin, TX 78712; [‡]Department of Chemistry and Biochemistry, University of Texas, Austin, TX 78712; and [§]Department of Radiology, Stanford University, Stanford, CA 94305

Communicated by Jack Halpern, University of Chicago, Chicago, IL February 27, 1996 (received for review October 17, 1995)

ABSTRACT Gadolinium(III) texaphyrin (Gd-tex³⁺) is representative of a new class of radiation sensitizers detectable by magnetic resonance imaging (MRI). This porphyrin-like complex has a high electron affinity [$E_{1/2}$ (red.) \sim 0.08 V versus normal hydrogen electrode] and forms a long-lived π -radical cation upon exposure to hydrated electrons, reducing ketyl radicals, or superoxide ions. Consistent with these chemical findings, Gd-tex³⁺ was found to be an efficient radiation sensitizer in studies carried out with HT29 cells *in vitro* as well as *in vivo* single and multifraction irradiation studies with a murine mammary carcinoma model. Selective localization of Gd-tex³⁺ in tumors was confirmed by MRI scanning.

Radiation therapy is a well established and important cancer treatment modality that is widely used (1, 2). Unfortunately, the therapeutic benefit of radiation therapy is limited by normal tissue tolerance and by tumor cell resistance to ionizing radiation (3, 4). Also limiting the efficacy of radiation therapy, often by a factor of 2.5–3 (5, 6), are the low levels of oxygen present in some portions of the tumor because the presence of oxygen may prolong the lifetime of cytotoxic free radicals generated upon exposure to ionizing radiation (7, 8). Previous attempts to overcome these limitations have included the use of radiation dose fractionation (1, 2, 7, 9) and the use of radiation sensitizers—drugs that potentiate the efficacy of the delivered radiation (7, 8, 10–13). Agents that have been explored extensively in this latter context include the halogenated pyrimidines (14–18) and hypoxic cell sensitizers (e.g., nitroimidazoles) (19–21). However, to date, these compounds have had some associated toxicity and do not adequately sensitize the entire tumor cell population (8). They also lack the preferential localization in tumors required to increase the therapeutic index (14), although the radiation therapy itself can to some extent be localized. With halogenated pyrimidines, a mechanistic dependence on incorporation of the drug into replicating DNA also has limited efficacy since many tumors contain a low fraction of cells in S phase (22, 23). There remains a need for improved radiation sensitizers. Ideally, these should (i) potentiate the activity of the administered radiation in the tumor but not in the surrounding tissues, (ii) operate via a mechanism that is active against oxygenated and hypoxic cells and is independent of DNA incorporation, and (iii) have low inherent toxicity. We have developed a new radiation sensitizer [i.e., gadolinium(III) texaphyrin (Gd-tex³⁺)] that, due to its novel mechanism of action, and tumor-selective localizing ability, meets these criteria. An additional benefit of this radiation sensitizer that has not been available with previous sensitizers is that it is detectable *in vivo* by magnetic resonance imaging (MRI) methods (24, 25). Monitoring the selective accumulation of gadolinium(III) texaphyrin in neoplasms by MRI enables the possibility of treatment planning and subsequent monitoring of the response



of cancers to the radiation therapy. Gadolinium(III) texaphyrin is representative of a new class of compounds known as the texaphyrins (e.g., structures 1 and 2) (25–27).

Texaphyrins are large planar porphyrin-like macrocycles that are capable of coordinating a range of relatively large cations, including Gd(III) and other members of the trivalent lanthanide series (26, 27). In general, the complexes formed are stable and of a 1:1 metal-to-ligand stoichiometry (27). However, the complexes are also easily reduced [E (red.) \sim 0.08 V versus normal hydrogen electrode for both compounds 1 and 2] and this facile reduction process, coupled with a demonstrated ability to localize selectively in certain animal tumor models (24), led to a consideration that these species

Abbreviation: Gd-tex³⁺, gadolinium(III) texaphyrin.
To whom reprint requests should be addressed.

^{||}Present address: Faculté 130 de Chimie Université 130 Louis Pasteur, 1, rue Blaise Pascal, B. P. 296, 67008 Strasbourg Cedex, France.

^{*}The redox potential of Gd-tex³⁺ is well above the upper threshold proposed for electron-affinic hypoxic cell sensitizers.

The publication costs of this article were defrayed in part by page charge payment. This article must therefore be hereby marked "advertisement" in accordance with 18 U.S.C. §1734 solely to indicate this fact.

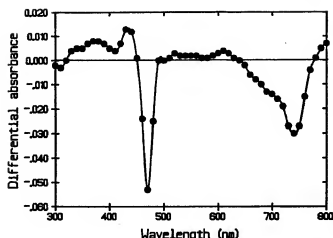


FIG. 1. Differential absorption spectrum of the π -radical cation obtained from complex 2 via pulse radiolytic reduction. The spectrum was recorded 25 μ s after the pulse. Identical results were obtained using complex 1.

could function as effective radiation sensitizers (28).** Our hypothesis was that, like molecular oxygen, the easy-to-reduce metallotetraphyrins would be able to "capture" hydrated electrons (e_{aq}^-) and thus increase the concentration of hydroxyl radicals available after exposure to a given dose of ionizing radiation. In addition, it was recognized that certain paramagnetic tetraphyrin complexes, including the Gd(III)-containing species 1 and 2, are detectable by MRI (24) and that this ready visualization would provide a means for determining directly the biolocalization properties (both temporal and spatial) of this new class of putative radiation sensitizer.

MATERIALS AND METHODS

Synthesis. Gadolinium tetraphyrins 1 and 2 were prepared in accord with the procedure described earlier (26).

Cyclic Voltammetry. The quoted redox potentials were determined by cyclic voltammetry in 2 mM aqueous phosphate solution. Under these conditions, the one-electron reduction potential of both compounds 1 and 2 is independent of pH (4 < pH < 10). However, the electrode process is quasi-reversible, with at least two other, more cathodic, reduction waves being apparent in the voltammograms.

Pulse Radiolytic Studies. All pulse radiolysis studies were made using a 4-MeV van der Graaff electron beam accelerator (Center For Fast Kinetics Research, University of Texas; 1



FIG. 3. (a) Precontrast: Axial MRI scan obtained through an SMT-F tumor in the right leg (arrow) of a DBA/2N mouse. Pulsing sequence: 0.5 T, TR/TE 350/15/FR (3-mm slice thickness 256 \times 256, 2 NEX, variable band width). (b) MRI at same level as a 10 min after the injection of Gd-tex $^{2+}$ (40 μ mol/kg) as a 2 mM solution in 5% aqueous mannitol. Pulsing sequence: 0.5 T, TR/TE 350/15/FR (3-mm slice thickness 256 \times 256, 2 NEX, variable band width).

eV = 1.602×10^{-19} J). Solutions of the gadolinium(III) tetraphyrin complex in question (1×10^{-4} M) were made up in 2 mM sodium phosphate (pH 7) and studied in the presence of 0.1 M 2-propanol. The solutions were purged thoroughly with oxygen-free N_2 prior to irradiation and a fresh aliquot was used for each pulse (100-ns duration). The course of reaction (if any) was followed by transient absorption spectroscopy. Differential absorption spectra were recorded point-by-point with three individual shots being averaged at each time base. Data analysis was made by computer nonlinear least-squares iteration. Dosimetry was made with the thiocyanate dosimeter

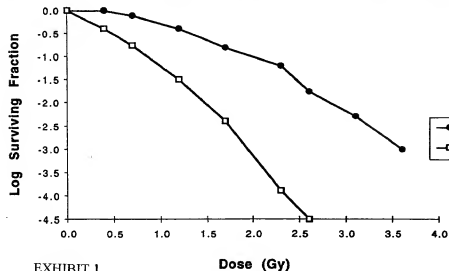


FIG. 2. Effect of radiolysis on cell survival for HT29 cells. Control experiments were carried out with HT29 cells not exposed to Gd-tex $^{2+}$ but irradiated under identical conditions (all standard deviations were less than $\pm 10\%$).

(29, 30). For kinetic analyses, the concentration of the material under investigation was varied systematically and the rate of formation (or decay) of the relevant transient species was measured at each concentration.

Cells and Tumor Models. Murine leukemia L1210 and HT29 human colon cancer cells were obtained from the American Type Culture Collection. L1210 cells, a suspension cell line, were grown in RPMI 1640 medium (GIBCO) supplemented with 10% fetal bovine serum and gentamycin ($5 \mu\text{g/ml}$). HT29 cells, an adherent cell line, were maintained in minimal essential medium (MEM) (GIBCO/BRL) supplemented with 10% fetal bovine serum and gentamycin ($5 \mu\text{g/ml}$). *In vitro* studies were performed in growth medium with 25 mM Hepes (pH 7.2).

The SMT-F, fast-growing spontaneous mouse mammary tumor, and the EMT-6 tumor cell line, murine mammary sarcoma, were obtained from J. Martin Brown (Stanford School of Medicine). The SMT-F tumors were maintained in DBA/2N mice according to Pavelic *et al.* (31). EMT-6 cells are syngeneic to BALB/c mice and were propagated according to the protocol of Rockwell *et al.* (32). Female mice weighing 18–22 g, 10–12 weeks old, were obtained from Simonsen Laboratories (Gilroy, CA). The tumor cells (5×10^5 cells) were implanted into the right hind gastrocnemius of recipient mice. The tumor-bearing animals were studied when the tumor size was 40–70 mm² (5–7 days after implantation). Tumor size was based on two orthogonal cross-sectional diameter measurements from the tumor-bearing leg and were measured biweekly.

Radiation Sensitization of Cancer Cells *in vitro*. The *in vitro* radiosensitization experiments were adapted from a procedure utilized by Miller *et al.* (33) and involved both L1210 and HT29 cells. Briefly, for the HT29 adherent cell line, the cells were incubated for 24 h with a fixed amount of gadolinium(III) texaphrin (either compounds 1 or 2; 10^{-7} M to 10^{-2} M), washed thoroughly with PBS, trypsinized, and resuspended in fresh medium (5 ml) at a density of 2×10^5 cells per ml. The cells were exposed to radiolysis for fixed times. Irradiation was made with doses of 250-kV x-rays generated by a Philips TR 250 orthovoltage x-ray machine at a dose rate of 1.25 Gy/min. Three dishes were plated for each dose, which were left to incubate for 10 days at 37°C. The numbers of surviving

colonies (>50 individual cells) were counted after staining with crystal violet and compared with the value obtained for unirradiated cells to estimate the sensitizer enhancement ratio.

L1210 cells were treated in the same manner as above with some experimental modifications to allow for differences between adherent versus suspension cell lines and also growth kinetics. Briefly, the L1210 cells were suspended at a density of 5×10^5 cells per ml (5 ml) prior to exposure to radiation. The cells were then resuspended at a density of 1×10^5 cells per dish and incubated for 7 days. Cell viability was assessed using the trypan blue exclusion method. Radiosensitization efficacy was expressed as the amount of cell killing achieved without and with a particular concentration of sensitizer after exposure to 2 Gy. The actual values were extrapolated from cell survival versus dose curves using a nonlinear least-squares iterative procedure to fit the data points.

MRI Studies. To assess the biodistribution of compound 1 MRI scans in SMT-F mice were performed. A solution of Gd-tex²⁺ (complex 1, $2 \mu\text{mol/ml}$ in sterile 5% aqueous mannitol) was administered i.v. via the tail vein at a dose of 40 $\mu\text{mol/kg}$. Axial MRI scans of the SMT-F tumors were obtained at 0.5 T, with the mouse ($n = 4$) in the prone position, using a spin-echo T1 weighted pulsing sequence (TR/TE, 350/15). MRI scans were performed before the dose and at 10 min and 1, 2, 3, 4, 5, 12, and 24 h after Gd-tex²⁺ i.v. injection. Contrast enhancement (CE) was determined by obtaining the signal intensity (SI) readings from a cursor placed over the SMT-F tumors by using the following formula: CE = (SI post - SI pre/SI pre) \times 100.

Radiation Sensitization *in vivo*. After pilot studies,^{††} the following protocol was initiated: Gd-tex²⁺ at a dose of 40 $\mu\text{mol/kg}$ was administered i.v. to SMT-F-bearing mice. The mannitol solution was administered i.v. to SMT-F bearing mice

^{††}Pilot studies were conducted using SMT-F-tumor-bearing animals as follows: Animals were studied after a single dose of 10–50 Gy of radiation, at 30 min to 24 h after Gd-tex²⁺, and after Gd-tex²⁺ at 40 $\mu\text{mol/kg}$ i.v. (50% of the LD₅₀ of 80 $\mu\text{mol/kg}$). Irradiation at 1 h or earlier produced morbidity and mortality and the optimal time window of irradiation appeared to be between 2 and 5 h after injection of Gd-tex²⁺ at 40 $\mu\text{mol/kg}$ i.v. In addition, the maximal beneficial effect of Gd-tex²⁺ appeared to be associated with a single 30-Gy dose of radiation.

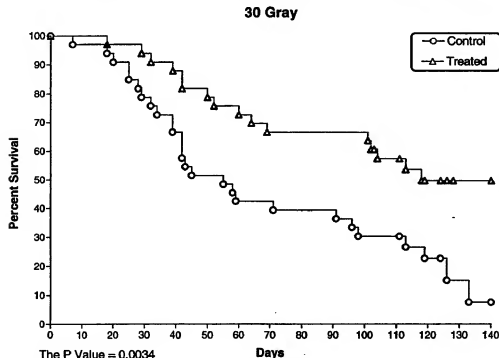


FIG. 4. Kaplan-Meier survival curves of DBA/2N mice with SMT-F neoplasms after 30-Gy single dose irradiation and i.v. administration of Gd-tex²⁺ at 40 $\mu\text{mol/kg}$ (treated) and a matched set of control animals treated with 30-Gy of irradiation only. Also note that 16 of 33 animals were cured (no evidence of disease). Note the significant difference in survival ($P = 0.0034$) for those animals receiving Gd-tex²⁺ ($n = 66$).

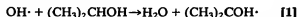
and they served as a control group ($n = 33$ mice per group). The test group was divided and irradiated at 2 and 5 h after drug administration (single fraction of 30 Gy). A special leg jig (lead shield) was used during the treatment. Each mouse was positioned prone inside a leg individually such that only the right leg was exposed to the x-ray. The tumor response and animal survival were evaluated for 140 days.

EMT6 tumors were found to be more resistant to radiation than the SMT-F tumors so the EMT6 tumor line became the tumor line used subsequently in the multidose fractionation studies. The sensitizer was equally effective when radiation was given at 2–5 h after Gd-tex^{2+} i.v., so radiation was given at 2 h in these studies. Gadolinium texaphyrin complex I (2 $\mu\text{M}/\text{ml}$ in 5% mannitol) or 5% mannitol was administered i.v. for five consecutive days to EMT6-bearing mice in the designated test and control groups, respectively ($n = 6$ mice per group). Two hours after each i.v. injection, x-ray treatment (five fractions of 1, 2, or 4 Gy) was administered. The study duration was 45 days and consisted of 78 mice. Mice in the 4-Gy protocol were treated in two study groups [i.e., (i) control and 5 and 20 $\mu\text{M}/\text{kg}$ and (ii) control and 40 $\mu\text{M}/\text{kg}$].

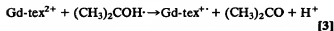
In all of the studies described above, an additional set of animals was injected with comparable amounts of gadolinium texaphyrin i.v. in the absence of radiation. No difference in tumor growth or host survival was found between the control animals and those animals which received gadolinium texaphyrin i.v. in the absence of radiation.

RESULTS AND DISCUSSION

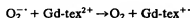
Pulse Radiolysis Studies. Initial tests of the MRI-detectable gadolinium(III) texaphyrin complexes 1 and 2 (Gd-tex^{2+}) as a radiation sensitizer utilized pulse radiolysis (29, 30). Short bursts of ionizing radiation (100-ns duration at 4 MeV) were delivered into aqueous solutions of these complexes and the subsequent reactions monitored by transient absorption spectroscopy. The conditions were chosen so as to favor a reducing environment. The initial texaphyrin solutions (aqueous, pH 7, 1×10^{-4} M) were saturated with nitrogen after the addition of 2-propanol (0.1 M).^{††} Under these conditions, hydroxyl radicals formed in the primary radiolysis event rapidly abstract the tertiary hydrogen atom from 2-propanol, forming highly reducing ketyl radicals (Eq. 1).



Both this ketyl radical and the hydrated electrons (also present in the medium) reduce the Gd-tex^{2+} complexes 1 and 2 via one-electron processes (Eqs. 2 and 3):

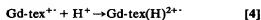


It was further shown that superoxide ions reduced Gd-tex^{2+} .



^{††}In our discussion, we treat the gadolinium(III) texaphyrin complexes 1 and 2 as monomers since, although these species are aggregated at higher concentrations (≥ 0.2 and ≥ 0.1 mM in the case of compounds 1 and 2, respectively), we have not found experimental evidence to suggest that adjacent molecules affect the radiation chemistry to any significant extent. Adding mannitol (5% by weight) serves to reduce the degree of aggregation; under these conditions, critical aggregation concentrations of 2.6 and 1.0 mM are recorded for compounds 1 and 2, respectively.

Thus, all of the reducing equivalents can be utilized to reduce Gd-tex^{2+} to $\text{Gd-tex}^{+ \cdot}$, regardless of the reaction conditions.^{§§} The resultant π -radical cation of $\text{Gd-tex}^{+ \cdot}$ ($\text{Gd-tex}^{+ \cdot}$), which is readily detected by monitoring the appropriate absorption spectral changes (Fig. 1), was found to decay over several hundred microseconds. This decay process, studied most closely in the case of complex 2, does not result in restoration of Gd-tex^{2+} . However, the rate increases with decreasing pH and is thus attributed to protonation of the initially formed π -radical cation (Eq. 4):



The resulting protonated radical ($\text{Gd-tex}(\text{H})^{2+ \cdot}$) decays very slowly by complex reactions that do not restore the original Gd-tex^{2+} complex (the life time is on the order of 30 s and is unaffected by the presence of oxygen).

In view of the high intrinsic stability of the Gd(III) oxidation state, Gd-tex^{2+} and $\text{Gd-tex}(\text{H})^{2+ \cdot}$ are presumed to be π -radical cations that have the reducing equivalent stored on the macrocyclic ring and not on the metal center. While it is clear that other factors, such as reduction of glutathione levels or inhibition of DNA repair processes might be serving to potentiate a putative sensitization effect *in vitro* or *in vivo*, the promise inherent in this seemingly unique mechanism of action prompted us to test Gd-tex^{2+} under more clinically relevant conditions. Summaries of these studies follow.

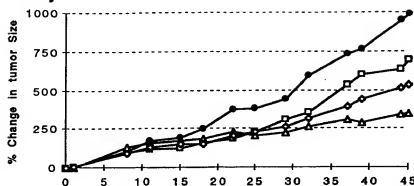
Radiation Sensitization of Cancer Cells *In Vitro*. Both compounds 1 and 2 were tested for their *in vitro* radiation sensitizing ability. These studies indicated that texaphyrins (compounds 1 and 2) are effective radiosensitizers for L1210 cells under aerobic conditions. In fact, for both complexes 1 and 2, the amount of cell killing [$(\text{L1210} + 2 \text{ Gy})/(\text{L1210} + 2 \text{ Gy} + \text{Gd-tex}^{2+})$] was found to increase progressively with increasing concentration of drug beginning at 10^{-5} M and reaching a maximum value of 2.2 ± 0.03 at 10^{-3} M and above. Of course intracellular concentration of Gd-tex^{2+} may be and probably is different than the extracellular concentration. Gd-tex^{2+} (complex 1) was also found to be an effective radiation sensitizer for HT29, a human colon cancer cell line (Fig. 2). Each data point is the mean of three separate runs (SD less than $\pm 10\%$). The sensitization enhancement ratio for this experiment is 1.92 and is derived by comparing the radiation dose needed to kill 95% of the exposed cells in the absence and presence of sensitizer. These studies provided an indication that systems such as compounds 1 and 2 could function as effective *in vivo* radiosensitizers. The results of these studies were found to be independent of the specific complex employed (i.e., compounds 1 or 2), suggesting that the sensitizing effect of Gd-tex^{2+} derives from the basic macrocyclic structure and its properties (e.g., ease of reduction) rather than a judicious choice of exocyclic substituents.

MRI and Radiation Sensitization in Animals. Based on the positive results obtained in cell culture, MRI and radiation sensitization studies were performed in DBA/2N mice with SMT-F tumors or EMT6 tumors in BALB/c mice (as noted both are transplantable mouse mammary carcinomas).

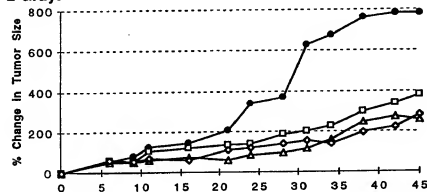
MRI scans after i.v. administration of Gd-tex^{2+} (2 $\mu\text{M}/\text{ml}$ in sterile 5% aqueous mannitol) revealed contrast enhancement of the SMT-F neoplasms. Maximal contrast enhancement was noted immediately after injection but at least 30% enhancement of the tumor (as opposed to surrounding tissue) was observed up to 5 h (Fig. 3) after injection. The observed

^{§§}Additional pulse radiolysis experiments showed that the $\text{Gd-tex}^{+ \cdot}$ radical can also be formed by reduction of Gd-tex^{2+} with carbon dioxide π -radical anion ($\text{CO}_2^{\cdot -}$), and the carbon-centered radicals formed by hydrogen abstraction from ethanol and methanol; protonation in accord with Eq. 4 yields the $\text{Gd-tex}(\text{H})^{2+ \cdot}$ species. This protonated radical is also obtained directly via the reaction of hydrogen atoms and Gd-tex^{2+} .

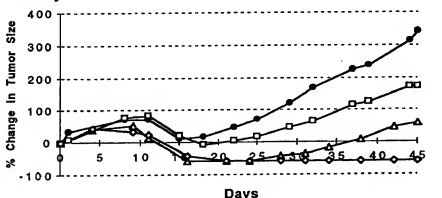
1 Gray



2 Gray:



4 Gray:



—●— Control —□— 5μmol/kg —△— 20μmol/kg —◇— 40μmol/kg

FIG. 5. Percent change in tumor size after i.v. injection of Gd-tex²⁺ at 5, 20, or 40 μmol/kg into BALB/c mice with EMT6 neoplasms irradiated for five consecutive days with either 1, 2, or 4 Gy per fraction.

augmentations in tumor signal intensity (after 40 μmol/kg) were as follows: 94%, 10 min; 79%, 1 h; 55%, 2 h; 44%, 3 h; 39%, 4 h; 32%, 5 h; 9%, 12 h; 7%, 24 h.

Administration of Gd-tex²⁺ (40 μmol/kg i.v.) prior to a single fraction of radiation provided a significant improvement in survival in SMT-F-bearing DBA/2N mice compared with animals receiving 30-Gy radiation alone ($P = 0.0034$) (Fig. 4). For animals receiving irradiation at both 2 h ($n = 32$) and 5 h ($n = 34$) after administration of gadolinium texaphyrin, significant therapeutic effects on tumor size were observed ($P = 0.0439$ and 0.0317 , respectively). There were no significant differences in survival between the groups receiving Gd-tex²⁺ at 2 h versus 5 h prior to 30 Gy of irradiation ($P > 0.3495$, unpaired t test).

A significant radiation sensitization effect was shown in the five consecutive day multifraction studies with BALB/C mice bearing EMT6 neoplasms in the right leg that were injected with compound 1 (5, 20, or 40 μmol/kg) or control solutions

of 5% aqueous mannitol 2 h prior to 1, 2, or 4 Gy of radiation therapy (Fig. 5). Even after 1 Gy of radiation for 5 days, there was a significant difference between the groups receiving 20 and 40 μmol/kg and controls ($P = 0.003$ and $P = 0.005$, respectively), although the group receiving 5 μmol/kg was not significantly different than controls ($P = 0.105$). Similarly, for all test groups in the 2- and 4-Gy study, EMT6 tumors were at least 50% smaller than control tumors at 45 days, and in the 4-Gy studies, there was a clear drug dose-response relationship for tumor size change (Fig. 5). By using a modification of methods to evaluate radiation induced toxicity to normal tissues, we evaluated short-term skin erythema (34) and long-term leg contracture (35) after treatment with the gadolinium complex 1 in conjunction with radiation. These results indicated that there was no enhanced radiosensitization of normal tissues when Gd-tex²⁺ was present.

Consistent with chemical findings from pulse radiolysis and cyclic voltammetry, the gadolinium(III) texaphyrin complex 1

was found to be a very efficient radiation sensitizer, as judged from experiments involving tumor cells *in vitro* and SMT-F and EMT6 neoplasms in mice. Selective localization of Gd- tex^{2+} in tumors was confirmed through the MRI contrast enhancement afforded by the paramagnetic nature of the agent. The imaging studies serve to highlight the possibility of using the MRI contrast enhancement properties of this particular texaphyrin complex to facilitate treatment planning and response monitoring in the context of x-ray therapy of cancer.

We greatly appreciate the assistance of Denise Hakala in manuscript preparation. We thank Drs. Kathryn Woodburn, Richard Zare, Charles Tancian, Raymond Ziessel, and Dominique Matt for review of the manuscript. We thank Dr. Donald O'Connor and Billy Naumann of Center for Fast Kinetics Research for their assistance in carrying out the pulse radiolytic studies. We thank Julie Engel and Lynn Parker for protocol assistance. Partial support for this work was provided by National Institutes of Health Grants A128845 and CA68652 (to J.L.S.). The Center for Fast Kinetics Research was supported in part by the University of Texas at Austin.

- Weiss, G. R. (1993) in *Clinical Oncology*, ed. Weiss, G. R. (Appleton & Lange, Norwalk, CT), pp. 74-88.
- Hendrickson, F. R. & Withers, H. R. (1991) in *American Cancer Society Textbook of Clinical Oncology*, eds. Holleb, A. I., Fink, D. J. & Murphy, G. P. (American Cancer Society, Washington, DC), pp. 35-37.
- Kirchgessner, C. U., Patil, C. K., Evans, J. W., Cuomo, C. A., Fried, L. M., Carter, T., Oettinger, M. A. & Brown, J. M. (1995) *Science* **267**, 1178-1183.
- Lees-Miller, S. P., Godbout, R., Chan, D. W., Weinfeld, M., Day, R. S., III, Barron, G. M. & Allalunis-Turner, J. (1995) *Science* **267**, 1183-1185.
- Tannock, I. F. (1972) *Br. J. Radiol.* **45**, 515-524.
- Watson, E. R., Halnan, K. E., Dische, S., Saunders, M. I., Cade, I. S., McEwan, J. B., Wienik, F., Perrins, D. J. D. & Sutherland, I. (1978) *Br. J. Radiol.* **51**, 879-887.
- Russo, A., Mitchell, J., Kinsella, T., Morstyn, G. & Glatstein, E. (1985) *Semin. Oncol.* **12**, 332-349.
- Brada, M. & Ross, G. (1995) *Curr. Opin. Oncol.* **7**, 214-219.
- Kallman, R. F. (1972) *Radiology* **105**, 135-142.
- Hall, E. J. (1988) *Radiobiology for the Radiologist* (Lippincott, Philadelphia), 3rd Ed.
- Wardman, P. (1982) in *Advanced Topics on Radiosensitizers of Hypoxic Cells*, eds. Breccia, A., Rimondi, C. & Adams, G. E. (Plenum, New York), pp. 49-75.
- Wardman, P. (1987) *Radiat. Phys. Chem.* **30**, 423-432.
- Beard, C. J., Coleman, C. N. & Kinsella, T. J. (1993) in *Cancer: Principles and Practice of Oncology*, eds. DeVita, V. T., Jr., Hellman, S. & Rosenberg, S. A. (Lippincott, Philadelphia), 4th Ed., pp. 2701-2710.
- Dische, S., Saunders, M. I., Bennett, M. H., Chir, B., Dunphy, E. P., Des Rochers, C., Stratford, M. R. L., Minchinton, A. I. & Wardman, P. A. (1986) *Br. J. Radiol.* **59**, 911-917.
- Roberts, J. T., Bleehen, N. M., Workman, P. & Walton, M. I. (1984) *Int. J. Radiat. Oncol. Biol. Phys.* **10**, 1755-1758.
- Saunders, M. I., Anderson, P. J., Bennett, M. H., Dische, S., Minchinton, A., Stratford, M. R. & Tothill, M. (1984) *Int. J. Radiat. Oncol. Biol. Phys.* **10**, 1759-1763.
- Coleman, C. N., Halsey, J., Cox, R. S., Hirst, V. C., Blasahke, T., Howes, A. E., Wasserman, T. H., Urtasun, R. C., Pajak, T., Hancock, S., Phillips, T. L. & Noll, L. (1987) *Cancer Res.* **47**, 319-322.
- Newman, H. F. V., Ward, R., Workman, P. & Bleehen, N. M. (1988) *Int. J. Radiat. Oncol. Biol. Phys.* **15**, 1073-1083.
- Kinsella, T. J., Russo, A., Mitchell, J. B., Rowland, J., Jenkins, J., Schwade, J., Myers, C. E., Collins, J. M., Speyer, J., Kornblith, P., Smith, B., Kufita, C. & Glatstein, E. (1984) *Int. J. Radiat. Oncol. Biol. Phys.* **10**, 69-76.
- O'Connell, M. J., Martenson, J. A., Wieand, H. S., Krook, J. E., MacDonald, J. S., Haller, D. G., Mayer, R. J., Gunderson, L. J. & Rich, T. A. (1994) *N. Engl. J. Med.* **331**, 502-507.
- Kinsella, T. J., Russo, A., Mitchell, J. B., Collins, J. M., Rowland, J., Wright, D. & Glatstein, E. (1985) *Int. J. Radiat. Oncol. Biol. Phys.* **11**, 1941-1946.
- Kinsella, T. J., Dobson, P. P., Mitchell, J. B. & Fornace, A. J. (1987) *Int. J. Radiat. Oncol. Biol. Phys.* **13**, 733-739.
- Iliakis, G., Kurtzman, S., Pantelias, G. & Okayasu, R. (1989) *Radiat. Res.* **119**, 286-304.
- Young, S. W., Sidhu, M. K., Qing, F., Muller, H. H., Neuder, M., Zanassi, G., Mody, T. D., Hemmi, G. W., Dow, W. C., Mutch, J. D., Sessler, J. L. & Miller, R. A. (1994) *Invest. Radiol.* **29**, 330-338.
- Sessler, J. L., Mody, T. D., Hemmi, G. W., Lynch, V., Young, S. W. & Miller, R. A. (1993) *J. Am. Chem. Soc.* **115**, 10368-10369.
- Sessler, J. L., Mody, T. D., Hemmi, G. W. & Lynch, V. (1993) *Inorg. Chem.* **32**, 3175-3187.
- Sessler, J. L., Hemmi, G., Mody, T. D., Mural, T., Burrell, A. & Young, S. W. (1994) *Acc. Chem. Res.* **27**, 43-50.
- Adams, G. E. (1992) *Radiat. Res.* **132**, 129-139.
- Harriman, A., Richoux, M. C. & Neta, P. (1983) *J. Phys. Chem.* **87**, 2629-2636.
- Koch, C. J. & Skov, K. A. (1992) *Radiat. Res.* **132**, 40-49.
- Pavlic, Z. P., Porter, C. W., Allen, C. W. & Mihich, E. (1978) *Cancer Res.* **38**, 1533-1538.
- Rockwell, S. C., Kallman, R. F. & Fajardo, L. F. (1972) *J. Natl. Cancer Inst.* **49**, 735-749.
- Miller, E. M., Fowler, J. F. & Kinsella, T. J. (1992) *Radiat. Res.* **131**, 81-89.
- Brown, J. M. & Lemmon, M. J. (1991) *Int. J. Radiat. Oncol. Biol. Phys.* **20**, 457-461.
- Brown, J. M. & Lemmon, M. J. (1991) *Radiother. Oncol.* **20** (Suppl.), 151-156.

Cell Biology. In the article "ADP-ribosylation factor and phosphatidic acid levels in Golgi membranes during budding of coatamer-coated vesicles" by Mark Starnes, Giampietro Schiavo, Gudrun Stenbeck, Thomas H. Söllner, and James E. Rothman, which appeared in number 23, November 10, 1998, of *Proc. Natl. Acad. Sci. USA* (95, 13676–13680), the authors wish to note the following correction. The label, described correctly in the legend to Fig. 1, incorrectly indicated that coatamer was included in stage 1 of the two-stage reactions. A corrected figure and its legend are shown below.

		One stage			Two stage		
		+	+	+	+	+	+
Stage 1	ARF	+	+	+	+	+	+
	coatamer	+	+	-	-	-	-
	Golgi membranes	+	+	+	+	+	+
	Temperature (°C)	37	37	37	37	37	37
Stage 2	ARF	N/A	-	-	-	-	-
	coatamer	↓	+	-	+	+	+
	Stage 1-incubated membranes		+	+	+	+	+
	Temperature (°C)	↓	37	37	0	37	37
β-COP		[Solid black bar]					
ARF		[Solid black bar]					
		1	2	3	4	5	6

FIG. 1. ARF and coatamer binding in one- and two-stage reactions. The amount of membrane-bound ARF and coatamer (β -COP) determined by Western blot analysis of binding reactions. Lanes 1 and 2 show one-stage reactions in which ARF and coatamer were incubated together. Lanes 3–6 show the results from two-stage reactions in which the membranes were first incubated with ARF but not coatamer, reisolated, and then incubated in a second stage with coatamer but not ARF. As controls, membranes (lane 2) or ARF (lane 3) were excluded from stage 1, or coatamer (lane 4) was excluded from both stages. All incubations were carried out at 37°C except lane 5, which was carried out at 0°C.

Medical Sciences. In the article "Gadolinium(III) texaphyrin: A tumor selective radiation sensitizer that is detectable by MRI" by Stuart W. Young, Fan Qing, Anthony Harriman, Jonathan L. Sessler, William C. Dow, Tarak D. Mody, Gregory W. Hemmi, Yunpeng Hao, and Richard A. Miller, which appeared in number 13, June 25, 1996, of *Proc. Natl. Acad. Sci. USA* (93, 6610–6615), the following correction should be noted. It has come to our attention that the radiation sensitivity of the HT29 control cell line reported in Fig. 2 on page 6611 is inconsistent with that reported in the cited literature (33). Consequently, the *in vitro* HT29 radiation sensitization experiments have been repeated with Gd-tex²⁺ (compound 1). Radiation enhancement comparable to our original findings was observed at doses between 8 and 20 Gy. The results indicate that the Gy scale reported on the x-axis of Fig. 2 is incorrect. We apologize for this error. The conclusions reached in the article remain unchanged.

Medical Sciences. In the article "Production of β -defensins by human airway epithelia" by Pradeep K. Singh, Hong Peng Jia, Kerry Wiles, Jay Hesselberth, Lide Liu, Barbara-Ann D. Conway, Everett P. Greenberg, Erika V. Valore, Michael J. Welsh, Tomas Ganz, Brian F. Tack, and Paul B. McCray, Jr., which appeared in number 25, December 8, 1998, of *Proc. Natl. Acad. Sci. USA* (95, 14961–14966), due to a printer's error, the following change should be noted: the symbol for Brian F. Tack should be f , to indicate that he is affiliated with the Department of Microbiology of the University of Iowa College of Medicine.

Medical Sciences. In the article "A multidrug resistance transporter from human MCF-7 breast cancer cells" by L. Austin Doyle, Weidong Yang, Lynne V. Abruzzo, Tammy Krogmann, Yongming Gao, Arun K. Rishi, and Douglas D. Ross, which appeared in number 26, December 22, 1998, of *Proc. Natl. Acad. Sci. USA* (95, 15665–15670), the following corrections should be noted. In the abstract and text, later analyses reveals that BCRP is a 655 amino acid peptide, not 663 amino acids as stated in the article. The first 8 amino acids displayed in Fig. 2A on page 15667 should be removed, making the initial sequence of the peptide MSSSNVEVFL...

On page 15665 in the data deposition footnote, the GenBank database accession number for BCRP is incorrect. The correct accession number is AF098951.

On page 15670 in the "Note Added in Proof," the accession number for the human EST clone that was homologous to BCRP is incorrect. The correct number is HUEST157481.

Photodynamic Therapy of B16F10 Murine Melanoma with Lutetium Texaphyrin

Kathryn W. Woodburn, Qing Fan, David Kessel,* Yu Luo,* and Stuart W. Young

Pharmacycics, Inc., Sunnyvale, California, U.S.A.; *Department of Pharmacology, Wayne State University School of Medicine, Detroit, Michigan, U.S.A.

Photodynamic therapy (PDT) of pigmented melanoma has generally been unsuccessful because of insufficient light penetration in such tissues. In this study, the responsiveness of the heavily pigmented B16F10 murine melanoma to lutetium texaphyrin (PCI-0123), a water-soluble sensitizer with strong absorbance in the near infrared (700–760 nm), was examined. These studies were carried out in both normal and ApoE deficient C57BL/6 mice. The latter strain exhibits a lipoprotein profile more like humans (low density lipoprotein > high density lipoprotein) than rodents (high density lipoprotein >> low density lipoprotein). Under optimal conditions of drug dose, light dose, and interval between drug administration and irradiation – the median survival time of C57BL/6 tumor bearing mice was approximately doubled (29 d) compared with tumor bearing control animals (13 d). The life-span of the ApoE knockout mice was greater (33 d) than the C57BL/6 animals (23 d) when

irradiation occurred 3 h after administration of a 10 μmol per kg drug dose. The greater efficacy of PDT in the ApoE deficient mice was associated with more rapid clearance of drug from the blood, greater accumulation of sensitizer in tumor tissue, and substantially greater drug binding to the very low density lipoprotein/low density lipoprotein plasma fraction. Confocal laser scanning microscopy showed that the predominant subcellular site of photosensitizer binding was to melanosomes; costaining was performed with Mel-5. Melanosomes are susceptible to oxidative stress. Photo-oxidation, mediated by PCI-0123 PDT, could potentially overload an already highly oxidized stressed state leading to cell death. The good tissue penetration depth achieved by PCI-0123 mediated PDT and the activation of melanosomes makes PDT of pigmented melanoma, for the first time, clinically relevant. **Key words:** cancer/photosensitizer/melanosome. *J Invest Dermatol* 110:746–751, 1998

Photodynamic therapy (PDT) of cancer involves the selective uptake and retention of nontoxic photosensitizers in tumor tissues. Activation of these agents by light at a wavelength corresponding to the drug absorbance band results in the formation of highly cytotoxic products: singlet molecular oxygen and oxygen radicals (Henderson and Dougherty, 1992). PDT has been successfully used for the treatment of cutaneous and subcutaneous tumors (Dougherty, 1981), but pigmented melanomas have been previously unresponsive to PDT with the drug Photofrin because of the poor light penetration of the activating 630 nm light into melanin-rich tissues (Pass, 1993), along with the ability of melanin to markedly reduce singlet oxygen yields (Sealey *et al.*, 1984; Bielek *et al.*, 1986) and scavenge free radical species. Radical scavenging also limits the efficacy of ionizing radiation (Haylett *et al.*, 1995).

The limitations of the porphyrin derived sensitizers with regard to light penetration into tissues (MacRobert *et al.*, 1989) prompted the synthesis of longer wavelength absorbing photosensitizers (Kreimer-Birnbaum, 1989). Among the latter are the texaphyrins, expanded porphyrin compounds that constitute a second generation lineage of photosensitizers. Paramagnetic texaphyrins have exhibited significant

tumor selectivity as detected by magnetic resonance imaging (Sessler *et al.*, 1994; Young *et al.*, 1994, 1996a). PDT treatment with the diamagnetic texaphyrin, lutetium texaphyrin (PCI-0123), has been effective in murine mammary carcinoma models (Young *et al.*, 1996b; Woodburn *et al.*, 1996, 1997). PCI-0123 is a water soluble agent with strong absorbance in the near infrared. A molar extinction coefficient of $42,000 \text{ M}^{-1} \text{ cm}^{-1}$ (MeOH) was obtained at 732 nm, the wavelength used for laser irradiation in this study (Young *et al.*, 1996b). We report here the pharmacokinetics, subcellular localization site, and PDT efficacy of PCI-0123 against the heavily pigmented and metastatic B16F10 murine melanoma subcutaneously implanted in both C57BL/6 and ApoE deficient mice.

MATERIALS AND METHODS

PCI-0123 The synthesis and chemical analysis of PCI-0123 has previously been described (Young *et al.*, 1996b). The drug was dissolved in 5% aqueous mannitol at a 2 mM concentration.

Cells B16F10 melanotic melanoma cells were obtained from the University of California, San Francisco Cell Culture Facility. Cells were grown in Waymouth's Medium (MB752/1, Gibco BRL, Grand Island, NY) supplemented with 14% fetal bovine serum (JRH Biosciences, Woodland, CA) and penicillin/streptomycin (Sigma, St. Louis, MO).

Animals and tumor model Inbred C57BL/6 female mice, aged 7–8 wk, were obtained from Simonsen Laboratories (Gilroy, CA). ApoE knockout mice, C57BL/6-*ApoE*^{0/0}, were obtained from the Jackson Laboratory (Bar Harbor, ME). Female mice from the N10 colony were used. The right flanks of the mice were shaved and depilated the day prior to tumor inoculation. B16F10 cells [5×10^5 cells in 50 μl Dulbecco's phosphate buffered saline (PBS), without

Manuscript received August 29, 1997; revised December 21, 1997; accepted for publication January 20, 1998.

Reprint requests to: Dr. Kathryn Woodburn, Pharmacycics, Inc., 995 E. Arques Avenue, Sunnyvale, CA 94086.

Abbreviations: HDL, high density lipoprotein; LDL, low density lipoprotein; MST, median survival time; PCI-0123, lutetium texaphyrin, PDT, photodynamic therapy; VLDL, very low density lipoprotein.

calcium or magnesium; Gibco BRL) were injected subcutaneously into the right hind flanks. Tumor volume V was measured three times a week with a vernier caliper. The length, width w , and height h were measured. Tumor volumes were calculated using the formula for a hemiellipsoid (Rockwell and Kallman, 1972):

$$V = \pi/6 \times L \times w \times h$$

Animals were used for PDT experiments when the tumors reached surface diameters of between 4 and 6 mm and a depth of 2.5–3 mm. Animals were sacrificed by cervical dislocation when they appeared moribund, and necropsies were performed. Biodistribution studies were performed on slightly larger tumors, i.e., with surface diameters between 5 and 7 mm and a depth of 3–4 mm.

PDT protocol PCI-0123 (10 or 20 μ mol per kg) was administered to mice by tail-vein injection, and the tumor loci were then irradiated 3, 5, or 24 h later by localized laser irradiation at 732 nm using a Lambda Plus argon pumped dye laser (Coherent, Palo Alto, CA). A 400 μ m diameter fiberoptic cable coupled the laser to a microprobe that produced uniform light intensity in the treatment field. Light fluences ranged between 150 and 600 J cm^{-2} , and the power density was set at 150 mW cm^{-2} as measured with a power meter (Scientech, Boulder, CO). The mice were restrained with laboratory tape during irradiation.

Tumor temperature measurements Tumor temperature measurements were performed on a subpopulation of animals, which were not included in the final efficacy analysis. The tumor temperature before, during, and 5 min after laser irradiation was monitored, every minute, with a 33 gauge hypodermic thermocouple probe (Omega Engineering, Stamford, CT). The probe was placed percutaneously at the base of the tumor. Groups of tumor-bearing animals were injected with 10 μ mol ($n = 6$) and 20 μ mol ($n = 4$) PCI-0123 per kg and irradiated with 150 J cm^{-2} at 150 mW cm^{-2} 3 h post-sensitizer administration. Control animals received light alone ($n = 4$).

DNA fragmentation and histologic analysis B16F10 bearing mice were injected with drug (10 μ mol per kg) and irradiated 3 h later using a 150 J cm^{-2} light dose (150 mW cm^{-2}). Animals were sacrificed by cervical dislocation 4, 8, 12, 24, and 48 h after irradiation, and the tumors excised. Controls included mice treated with light alone or drug alone (tumors excised at 24 h) and untreated tumor-bearing animals. Four mice were included in each group with two of the tumors being used in the DNA fragmentation study, whereas the remaining two were fixed in 10% buffered formalin for histologic analysis. For histopathologic evaluation, the tumors were sectioned perpendicular to the skin surface, embedded in paraffin and stained with hematoxylin and eosin, and viewed via light microscopy. DNA fragmentation was measured by static gel electrophoresis (Zaidi *et al.*, 1993). Briefly, the tumors were minced and incubated for 12 h at 50°C with proteinase K (0.5 mg/ml in buffer (0.5 M) containing 150 mM NaCl, 15 mM sodium citrate, 10 mM ethylenediamine tetraacetic acid (EDTA), and 25 mg of N-laurylsarcosine sodium salt). The mixtures were cooled to 0°C, the DNA was precipitated with cold ethanol, centrifuged, air dried, and then resuspended in 50 μ l of 10 mM Tris HCl, 1 mM EDTA at pH 8.0. The DNA mixtures were treated with 1 ml RNase (10 mg per ml) for 30 min at 37°C, loaded onto 1.5% agarose gels, and electrophoresed for 3.5 h (2 V per cm gradient). The Boehringer Mannheim (Indianapolis, IN) molecular weight marker kit VI was used to estimate the size of the DNA fragments. The gels were stained with ethidium bromide and the DNA bands were viewed under 312 nm light.

Tissue extraction procedure The sensitizer was administered via tail-vein injection at either 10 or 20 μ mol per kg. Tissues and plasma were analyzed 3, 5, or 24 h later and were also collected from tumor-bearing animals that were not injected with PCI-0123. Blood was collected in tubes containing 5 mg of solid EDTA and erythrocytes were removed by centrifugation. Plasma samples (125 μ l) were mixed with 10 mM Tris X-100 and analyzed for tetraphyrin content by fluorescence (see below). Weighed tissue samples were frozen in liquid nitrogen, then pulverized using a stainless steel pulverizer chilled to -40°C. The powdered material was homogenized (Polytron[®], Brinkman) in 1.6 M phosphate buffer (50 mM, pH 8.0). These homogenates were then mixed thoroughly with 3.0 ml methanol, and chloroform (3.0 ml) was added. After vigorous shaking on a Thomas Shaking Apparatus (Arthur H. Thomas, Philadelphia, PA), the phases were separated by centrifugation (10,000 \times g, 10 min, room temperature). The chloroform-rich bottom phase was carefully removed and brought to a volume of 3 ml with methanol. Samples were then analyzed for PCI-0123 content by fluorescence (excitation = 450 nm, emission = 700–800 nm). Recovery of sensitizer was >90%. Sensitizer concentration is expressed as micrograms of drug tissue per gram (wet weight) or per milliliter of plasma. The minimal level of detection is 0.05 μ g PCI-0123 per g.

Plasma cholesterol analysis Mice ($n = 6$) from each strain were fasted overnight and blood (300 μ l) drawn retro-orbitally. Blood was anti-coagulated

with EDTA, erythrocytes removed by centrifugation, and the resulting plasma sent to CVD (West Sacramento, CA) for cholesterol analysis by an enzymatic method involving cholesterol oxidase (EM Science, Gibbstown, NJ).

Density-gradient ultracentrifugation The distribution of drug to murine plasma lipoproteins and proteins was assessed as previously described (Woodburn and Kessel, 1995). A potassium bromide solution (750 μ l, 1.27 g per ml) was placed in the bottom of 13 \times 38 mm polyallomer tubes. This was gently overlaid with 750 μ l of a solution containing 100 μ l of murine plasma and isotonic sodium chloride, and the density was adjusted to 1.21 g per ml by the addition of solid potassium bromide. The tubes were then filled with isotonic saline, capped, and centrifuged in a TLN rotor for 60 min at 254,000 \times g in a Beckman (Fullerton, CA) TL-100 ultracentrifuge. The tubes were then fractionated from the top, using a Harvard syringe pump (Harvard Apparatus, South Natick, MA) that injected Fluorinert FC-40 (0.5 μ l per min) into the bottom of the tubes; 25 equal fractions were obtained. Triton X-100 (3 ml, 10 mM) was added to each fraction and the fluorescence measured between 700 and 800 nm (excitation was at 450 nm).

Confocal fluorescence microscopy and immunostaining B16F10 cells (2×10^5) were cultured in Flakette Chamber Slide culture chambers (Nunc, Naperville, IL) containing 4 ml Waymouth's MB/L medium (Gibco BRL) supplemented with 14% fetal bovine serum (Irvine Scientific, Santa Ana, CA). The cells were allowed to incubate for 18 h to enable adherence. PCI-0123 (20 μ g medium per ml) was added to the flasks and incubated for 1–24 h. The adherent cells were rinsed thoroughly with PBS (four times) before being examined with confocal laser scanning microscopy.

Melanomas were detected with Mel-5 (Signet Laboratories, Dedham, MA), a murine monoclonal antibody that specifically targets a 75 kDa glycoprotein, tyrosinase related protein-1, within melanosomes (Hsu *et al.*, 1996). Monoclonals containing PCI-0123, 20 μ g medium per ml and incubated for 4 h, and no sensitizer were washed with PBS (four times) and fixed in methanol for 15 min at -20°C. The cells were then blocked with 5% normal goat serum (Gibco BRL) and 5% nonfat dry milk in PBS at room temperature for 30 min. Mel-5 (10 μ g per ml) was added to the chambers and incubated for 1 h at 37°C. The flasks were washed again with PBS (six times) and then blocked for another 30 min. Fluorescein isothiocyanate conjugated anti-mouse IgG (Boehringer Mannheim) was used as the secondary antibody, 1 μ g per ml in 4 ml blocking solution was added to the cells and incubated for 1 h at 37°C. A subgroup of flasks were treated with the secondary antibody alone. All cells were washed thoroughly with PBS (six times) rinsed with water and mounted in Vectashield[®] mounting medium (Vector Laboratories, Burlingame, CA). A coverslip was placed over the cells and the perimeter sealed with clear nail polish.

The specimens were examined either with a Saratog 2000 Upright (Molecular Dynamics, Sunnyvale, CA) or an Insight Point laser scanning confocal microscope (Meridian Instruments, Okemos, MI). The samples were excited with 488 nm light from an argon ion laser and various filters were employed in the collection of the fluorescence emission signal (FITC band pass, 625 and 660 nm long pass filters).

Statistical analysis Values are expressed as mean \pm SD. Values were compared using the unpaired Student's t test. In the longevity analysis, Kaplan-Meier survival curves and log rank analysis for statistical significance were used. Statistical significance was assumed if $p < 0.05$.

RESULTS

Select accumulation in melanoma The synthesis of PCI-0123 (Fig 1) has been previously described (Young *et al.*, 1996b). The distribution of PCI-0123 in tissues and plasma of tumor-bearing mice after administration of 10 or 20 μ mol sensitizer per kg is shown in Table I. The tetraphyrin exhibited good melanoma localizing capacity. Although there was substantial drug accumulation by liver and kidney, the tumor:muscle ratios were generally high. The tumor to muscle ratios, for the 10 μ mol per kg dose, were 8.6, 15, and 10.1 for 3, 5, and 24 h post-injection times. Use of the 20 μ mol per kg dose generally afforded higher tissue concentrations, with the exception of the 24 h time point. The 20 μ mol per kg dose yielded ratios of 15.3 and 2.8 at 5 and 24 h, respectively. Some sensitizer was present in the skin; melanoma to normal skin ratios were between 0.7–3 to 1.

PCI-0123 mediated phototherapy enhances tumor retardation Results of PDT with PCI-0123 in B16F10 melanotic neoplasms are shown in Tables II and III. The light irradiation conditions utilized (150 mW cm^{-2}) did not induce hyperthermia as the steady state maximal increases for the 20 and 10 μ mol PCI-0123

per kg groups and those animals not injected with sensitizer were 4.0 ± 0.4 , 2.8 ± 0.5 , and $3.0 \pm 0.5^\circ\text{C}$, respectively. With all studied light fluences, steady state was obtained within the first 7 min of irradiation. Table II summarizes melanoma regrowth using a sensitizer dose of 20 μmol per kg and light doses of 150 or 300 J per cm^2 , 5 or 24 h, respectively, after drug administration.

There was no significant difference in melanoma regrowth between untreated animals *versus* controls either irradiated with 400 J per cm^2 alone or treated with sensitizer alone. A significant response was seen when tumors were irradiated 5 h after sensitizer administration ($p < 0.001$ *versus* untreated control animals). The time for the tumors to grow (to 10 times their original volume) was increased to 15.3 d with PCI-0123 and a light fluence of 300 J per cm^2 compared with 5.9 d for the control group. Irradiation 24 h after sensitizer injection with a light fluence of 150 J per cm^2 did not yield any significant change in tumor regrowth when compared with controls; however, an increase in light fluence to 300 J per cm^2 significantly prolonged the regrowth interval to 9.6 d ($p = 0.002$).

Table III summarizes PDT responses using a 10 μmol per kg drug dose. The effect of varying the light dose 5 h after drug administration (10 μmol per kg) is also shown. Following an intravenous injection of 10 μmol per kg and a light fluence of 300 J per cm^2 , there was no significant inhibition of tumor regrowth. But light doses of 400, 500, and 600 J per cm^2 significantly increased the PDT effect of PCI-0123. Using a 600 J per cm^2 light dose, the time required for a tumor to grow to 10 times the initial volume was 15.6 d, compared with 5.9 d for untreated tumor bearing animals (Fig 2, $p < 0.0084$). A 150 J per cm^2 light dose 3 h after drug administration yielded a response very similar to a result obtained with a 600 J per cm^2 light dose 5 h after drug administration ($p = 0.9021$).

PCI-0123 phototherapy increases longevity The B16F10 melanoma line characteristically metastasizes. Tables II and III show the median survival times in the 20 and 10 μmol per kg groups, respectively, after PDT. With regard to both drug doses, there was no apparent difference in survival between matched sets of neoplasms with intravenous drug or light alone and untreated animals. Groups receiving

both drug and light, however, did show increased survival. A significant increase in survival time was observed when irradiation was performed 5 h after intravenous injection of 20 μmol PCI-0123 per kg at both 150 and 300 J per cm^2 : to 26 d ($p = 0.011$) and 27 d ($p = 0.0002$), respectively. The median survival time (MST) for untreated B16F10 neoplasms was 13 d.

PDT 5 h after administration of a 10 μmol per kg drug dose significantly increased the survival time of animals receiving light fluences of 500 and 600 J per cm^2 . The MST of the group treated with 10 μmol sensitizer per kg alone was 17.5 d, compared with 23 d for 500 J per cm^2 and 29 d for 600 J per cm^2 . The MST was increased in the animals treated with 150 J per cm^2 3 h post-injection. The survival analysis using a 10 μmol per kg drug dose and a 150 J per cm^2 light fluence 3 h later (MST = 23 d) is compared (Fig 3) with a light dose of 600 J per cm^2 5 h later (MST = 29 d). Unlike the regrowth analysis, the MST for these latter PDT protocols were statistically different ($p = 0.0278$).

Phototherapy induces apoptosis B16F10 neoplasms were treated with PCI-0123 *in vivo* and then evaluated for apoptosis as assessed by gel electrophoresis. Controls (matched sets of B16F10 and sensitizer, B16F10 and light, and B16F10 alone animals) showed no evidence of DNA degradation. Distinct DNA ladder fragmentation patterns were

Table II. PDT response to 20 μmol PCI-0123 per kg in B16F10 melanoma bearing mice

PCI-0123 (μmol per kg)	Fluence (J per cm^2)	Interval* (h)	Animals	Regrowth* (d)	MST* (d)
—	—	—	16	5.9 ± 1.8	13
—	400	—	5	6.2 ± 1.6	16
20	—	—	5	8.2 ± 2.3	15
20	150	5	8	10.6 ± 2.9	26
20	300	5	13	15.3 ± 2.6	27
20	150	24	7	6.7 ± 0.8	19
20	300	24	7	9.6 ± 2.1	20

*Time between sensitizer administration and irradiation. Power density was 150 mW per cm^2 .

*Time to reach 10 times the original tumor volume (mean \pm SD).

*Median survival time following PDT.

Table III. PDT response to 10 μmol PCI-0123 per kg in B16F10 melanoma bearing mice

PCI-0123 (μmol per kg)	Fluence (J per cm^2)	Interval* (h)	Animals	Regrowth* (d)	MST* (d)
—	—	—	16	5.9 ± 1.8	13
—	400	—	5	6.2 ± 1.6	16
10	—	—	5	7.8 ± 0.8	17.5
10	150	3	12	15.0 ± 3.4	23
10	300	5	6	8.5 ± 3.0	17
10	400	5	7	11.6 ± 2.1	18.5
10	500	5	11	13.2 ± 3.5	23
10	600	5	5	15.6 ± 3.6	29

*Time between sensitizer administration and irradiation. Power density was 150 mW per cm^2 .

*Time to reach 10 times the original tumor volume (mean \pm SD).

*Median survival time following PDT.

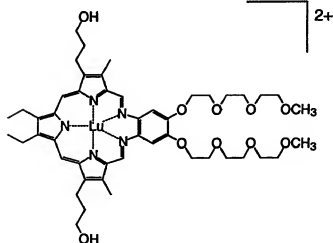


Figure 1. Structure of PCI-0123.

Table I. Biodistribution of PCI-0123 in B16F10 melanoma bearing mice*

PCI-0123 (μmol per kg)	Time (h)	Plasma	Melanoma	Muscle	Liver	Kidney	Skin
10	3	8.9 ± 1.0	11.3 ± 3.7	1.3 ± 0.4	94.5 ± 11.6	63.8 ± 19.0	5.9 ± 1.3
10	5	1.2 ± 0.2	11.4 ± 1.1	0.8 ± 0.2	61.9 ± 8.3	68.8 ± 10.0	3.8 ± 1.1
10	24	0	6.1 ± 1.8	0.6 ± 0.2	38.7 ± 6.0	42.0 ± 8.9	3.0 ± 0.2
20	5	2.7 ± 0.9	21.4 ± 10.3	1.4 ± 0.5	103.8 ± 13.7	117.7 ± 11.8	7.0 ± 0.7
20	24	0	3.4 ± 1.3	1.2 ± 0.5	65.9 ± 6.4	125.6 ± 7.9	5.2 ± 1.1

*The PCI-0123 distribution is expressed as μg tissue per g (wet weight) or μg per ml for plasma. The values represent the mean \pm SD of five animals.

found in melanoma tissue from animals treated with 10 μmol drug per kg, with a light dose of 150 J per cm^2 given 3 h later. Tissues were analyzed for DNA photodamage 4, 8, 12, 24, and 48 h after irradiation (not shown). The fragmentation appeared at 8 h and was most pronounced at 24 h.

Histologic analysis Histologic analysis (hematoxylin and eosin) was performed on control and PDT treated neoplasms (not shown). Post-treatment sacrifice times were 4, 8, 12, 24, and 48 h. Necrosis was observed in the PDT treated neoplasms. Non-coagulative necrosis (including apoptosis, pyknosis, and karyorrhexis) occurred around foci of coagulative necrosis filled with cells in all stages of degeneration with loss of cytoplasmic and nuclear structure. The necrotic severity of the lesions increased with the time interval between PDT treatment and neoplasm evaluation. Hemorrhage and inflammation were mild and rare.

Photosensitizer biodistribution in ApoE deficient mice The biodistribution of PCI-0123 (10 μmol per kg) was also examined in ApoE deficient mice subcutaneously implanted with B16F10 melanoma

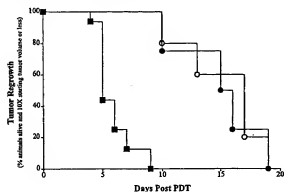


Figure 2. PCI-0123 mediated PDT retards melanoma growth. Kaplan-Meier tumor regrowth curves for B16F10 murine neoplasms in C57BL/6 mice. Photoirradiation was 3 h with 150 J per cm^2 (n = 12, ●) and 5 h with 600 J per cm^2 (n = 5, ○) post-intravenous injection of 10 μmol PCI-0123 per kg. Control animals (n = 16, ■) received no sensitizer and no irradiation.

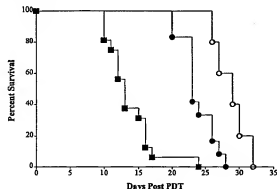


Figure 3. PDT increases MDT. Kaplan-Meier survival curves for B16F10 murine neoplasms in C57BL/6 mice after intravenous injection of 10 μmol PCI-0123 per kg. B16F10 bearing mice (n = 12, ●) were irradiated with 732 nm light 3 h post-injection with 150 J per cm^2 , yielding an MST of 23 d compared with an MST of 29 d for irradiation at 5 h with 600 J per cm^2 (n = 5, ○). Control animals (n = 16, ■), no sensitizer and no irradiation, yielded a MST of 13 d.

(Table IV). The sensitizer was quickly cleared from the plasma; 2.26 μg per ml was found 3 h after injection with none detectable at 24 h. A tumor to muscle ratio of 28.7 was present at 3 h; the ratio fell to 14.6 at 24 h. The kidney PCI-0123 levels were comparable at both 3 and 24 h, and a decrease in liver retention was observed (54.9 μg per ml at 3 h and 39.3 μg per ml at 24 h).

Phototherapy in ApoE deficient mice The MST of ApoE deficient mice bearing B16F10 melanoma treated with 10 μmol PCI-0123 per kg (Table V, Fig 4) and irradiated 3 h post injection was 33 d, compared with 17 d for untreated controls (p = 0.0077) and 17.5 d for animals injected with sensitizer alone (p = 0.0194). No significant difference was observed between the sensitizer alone and untreated groups. Melanoma regrowth was significantly impaired in the PDT treated group (Table V, Fig 5); it required 17 d for the tumor volume to grow to 10 times the preinjection volume, compared with 8.0 d for light alone treated animals (p < 0.0001) and 5.8 d for untreated controls (p < 0.0001).

Plasma protein binding The plasma cholesterol concentration of C57BL/6 mice was 55.2 ± 14.0 mg per dl compared with 730.3 ± 116.0 mg per dl for the ApoE deficient strain. The relative binding of PCI-0123 to both normal and ApoE knockout plasma protein components was assessed using density gradient ultracentrifugation (Fig 6). In the C57BL/6 strain, 4% of the sensitizer was associated with the very low density lipoprotein (VLDL)/low density lipoprotein

Table V. PDT response to 10 μmol PCI-0123 per kg in B16F10 melanoma bearing ApoE knockout mice

PCI-0123 (μmol per kg)	Fluence (J per cm^2)	Interval ^a (h)	Animals	Regrowth ^b (d)	MST ^c (d)
—	—	—	6	5.8 ± 1.2	17
10	—	—	4	8.0 ± 0.82	17.5
10	150	3	13	17.0 ± 3.08	33

^aTime between sensitizer administration and irradiation. Power density was 150 mW per cm^2 .

^bTime to reach 10 times the original tumor volume (mean \pm SD).

^cMedian survival time following PDT.

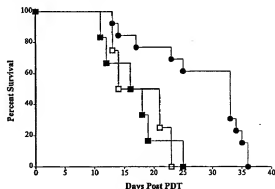


Figure 4. Phototherapy retards tumor growth in ApoE deficient mice. Kaplan-Meier survival curves for B16F10 murine neoplasms in ApoE deficient mice. B16F10 bearing mice (n = 13, ●) were irradiated with 732 nm light 3 h post-injection of 10 μmol PCI-0123 per kg with 150 J per cm^2 and 150 mW per cm^2 , yielding a MST of 33 d. Sensitizer alone control animals (n = 4, □) and no sensitizer and no irradiation control mice (n = 6, ■) yielded respective MST of 17.5 and 17 d.

Table IV. Biodistribution of PCI-0123 in B16F10 melanoma bearing ApoE knockout mice^a

PCI-0123 (μmol per kg)	Time (h)	Plasma	Melanoma	Muscle	Liver	Kidney	Skin
10	3	2.3 ± 0.7	13.8 ± 2.6	0.5 ± 0.1	54.9 ± 3.7	45.1 ± 5.8	2.6 ± 1.3
10	24	0	5.4 ± 0.7	0.4 ± 0.1	39.3 ± 5.4	45.8 ± 5.4	1.1 ± 0.4

^aThe PCI-0123 distribution is expressed as μg tissue per g (wet weight) or μg per ml for plasma. The values represent the mean \pm SD of four animals.

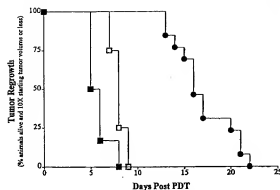


Figure 5. Phototherapy increases longevity in ApoE deficient mice. Kaplan-Meier tumor regrowth curves for B16F10 murine neoplasms in ApoE deficient mice. Irradiation was 3 h post injection of 10 μ mol PCI-0123 per kg with 150 J per cm^2 ($n = 13$, \bullet). The two control groups consisted of sensitizer alone animals ($n = 6$, \blacksquare) and tumor bearing animals that received no sensitizer and no irradiation ($n = 4$, \square).

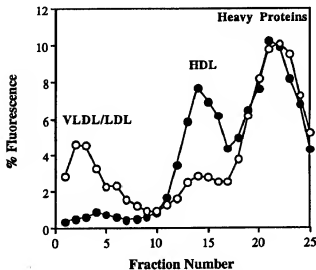


Figure 6. Photosensitizer plasma protein binding. Density gradient ultracentrifugation of C57BL/6 (\bullet) and ApoE deficient (\circ) murine plasma. Plasma was analyzed 1 h after the injection of 10 μ mol PCI-0123 per kg.

(LDL) portion, 35.3% to high density lipoprotein (HDL), and 60.7% to the heavy protein fraction. In contrast, PCI-0123 distribution in the ApoE knockout plasma was 23.4% bound to the VLDL/LDL portion, 15.6% bound to the HDL fraction, and 61% bound to heavy proteins. The data depicted in Fig 6 were obtained from plasma analyzed at 1 h post-intravenous administration of 10 μ mol PCI-0123 per kg; later time points revealed similar relative binding patterns.

Localization in melanosomes The subcellular localization site of PCI-0123 within B16F10 cells was analyzed using confocal laser scanning microscopy. PCI-0123 was found to selectively localize within the melanosome (Fig 7).

DISCUSSION

PDT with PCI-0123 promoted survival of animals bearing the highly pigmented B16F10 melanoma, using both C57BL/6 and ApoE deficient mice. PCI-0123 is a pure, water soluble photosensitizer with strong absorbance in the near infrared, which has previously displayed significant efficacy in treating nonpigmented murine mammary neoplasms (Young *et al*, 1996b; Woodburn *et al*, 1996, 1997). When irradiation occurred 24 h after drug administration, compared with 3 h after drug administration, a higher light dose was required for a statistically significant therapeutic response. A PCI-0123 dose of 20 μ mol per kg proved more efficacious than the 10 μ mol per kg dose when the same irradiation protocols were used. In this case, a

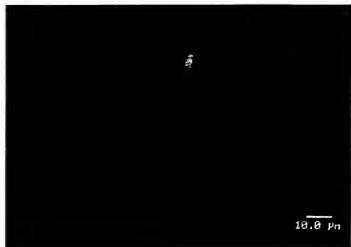


Figure 7. PCI-0123 localization within melanosomes. The confocal scanning micrograph of B16F10 cells after incubation with 20 μ g PCI-0123 per ml for 3 h. Scale bar, 10 μ m.

10 μ mol PCI-0123 per kg drug dose and a 300 J per cm^2 light dose resulted in regrowth to 10 times the original volume in 8.5 d, compared with 15.3 d for the animals that received the 20 μ mol per kg drug dose and 300 J per cm^2 light.

The tissue concentration data 3, 5, and 24 h after drug administration (10 or 20 μ mol per kg) show good selectivity for neoplastic tissue versus adjacent surrounding normal tissue. High melanoma-to-muscle ratios were obtained at all sensitizer doses and study times. High concentrations were found in the organs of excretion (liver and kidney) as expected. Pharmacologic data obtained using radiolabeled [^{14}C]-PCI-0123 in SMT-F bearing mice showed significant but lower tumor-to-muscle ratios (Young *et al*, 1996b). The increased uptake of PCI-0123 in B16F10 melanoma compared with the mammary carcinoma SMT-F (Young *et al*, 1996b) may be related to differences in vascularity or to differences in melanin content of the melanoma. PCI-0123 is cationic, and cationic photosensitizers have been shown to have a strong affinity for the polyanionic melanin (Haylett *et al*, 1995), the photosensitizing properties of PCI-0123:melanin complexes will be addressed in future studies.

Tumor apoptosis, as assessed by gel electrophoresis, was evident in the PDT treated neoplasms 8 h after irradiation. This result was also obtained using the EMT6 murine sarcoma using the same treatment protocol (Woodburn *et al*, 1997). Histologically, the two murine neoplasms responded quite differently to PDT. The B16F10 melanomas contained more pyknosis, whereas the EMT6 sarcomas contained more karyorrhexis. The sarcomas were moderately inflamed and hemorrhagic, whereas inflammation and hemorrhage were rare in the melanomas.

The affinity of photosensitizers for LDL has often been proposed as a mechanism for the preferential uptake of sensitizers by neoplastic tissue (Kessel and Woodburn, 1993). In rodents, HDL is the major lipoprotein and the major cholesterol carrying species, whereas in man, LDL predominates. To assess the likely effects of a high LDL/cholesterol level, as will be pertinent in the clinic, the role of LDL versus HDL levels was investigated using ApoE deficient mice. ApoE is a glycoprotein found in most lipoproteins except LDL, and whose main function is to act as a ligand for the liver receptors that clear chylomicrons and VLDL (Zhang *et al*, 1992). ApoE deficient (knockout) mice, generated by gene targeting, have high plasma cholesterol levels that predispose the mouse to atherosclerosis. PCI-0123 biodistribution analysis within B16F10 bearing ApoE deficient mice, compared with the C57BL/6 strain, showed slightly more tumor uptake with lower sensitizer levels in muscle, kidney, skin, and liver. The latter is not surprising because liver LDL receptors in animals fed a high cholesterol diet are downregulated but the expression of LDL receptors on tumor cells are unaffected (Verluis *et al*, 1996). The sensitizer was cleared more quickly from the plasma in the ApoE deficient mice (10 μ mol per kg dose), and more drug was associated with the VLDL/LDL portion and less with the HDL portion.

No apparent difference in tumor growth and MST was observed between the control groups (normal tumor growth and drug alone controls) for tumor bearing C57BL/6 and ApoE deficient mice. The MST of the ApoE mice that were treated with PCI-0123 and PDT were significantly greater than the normal C57BL/6 strain (33 d compared with 23 d, $p = 0.0077$). The effect of the sensitizer and PDT on tumor metastasis is an important consideration for the clinician. Localized PDT using Photofrin II has been shown not to influence pulmonary metastases of Lewis lung carcinoma (Gomer *et al.*, 1987), but PDT can induce immunosuppression via activation of the complement system (Lim *et al.*, 1985). In this study we have shown that PCI-0123 mediated PDT did increase the MST of the highly metastatic B16F10 melanoma animals (Fidler, 1996).

Confocal laser scanning microscopy revealed that PCI-0123 was concentrated in the melanosome. The melanosome is both an energy absorbing and an energy generating endolysosomal type organelle occupying 40%, by dry weight, of pigmented human melanoma, and it is hoped that it can be utilized to diagnose and treat melanoma (Borovsky, 1993; Orlov, 1995). Methylene blue also has selective affinity for melanosomes and its iodinated radiolabeled counterpart is presently being evaluated in clinical trials (Borovsky, 1993; Link *et al.*, 1996). Melanin is thought to be the skin's photoprotective agent, and it has been proposed that it does this by killing cells that have been exposed to deleterious solar radiation levels (Borovsky, 1993). During melanogenesis, free radical reactions occur that are potentially cytotoxic, but do not kill cells, because they are enclosed within the organelle by the membrane; however, once the cell has been bombarded with too much energy (light), the melanin is overloaded and produces radical species that initiate cell death. PDT is a photo-oxidative process with membranes being a principal target (Henderson and Dougherty, 1992). It is interesting to note that melanoma cells, and melanocytes, are in a continuous state of oxidative stress and are more prone to oxidative damage, i.e., they have lower levels of antioxidant enzymes, than epidermal and dermal cells (Picardo *et al.*, 1995). Therefore it is proposed that melanoma cells cannot cope with oxidative attack as elicited by PCI-0123 PDT. Previous confocal laser scanning microscopy studies with PDT and PCI-0123 on EMT6 sarcoma cells have shown the PDT induced destruction of the lysosomal membrane, eliciting eventual cell death (Woodburn *et al.*, 1997). It is highly likely, based on the present results, that PCI-0123 induced PDT is destroying the melanosomal membrane, leading to a cascade of cytolytic radical reactions.

The B16F10 melanoma model has been used to assess efficacy of several other photosensitizers. Silicon (IV) naphthalocyanine is also a far-red wavelength absorbing photosensitizer with a strong absorption band at 776 nm (Biolo *et al.*, 1994). This naphthalocyanine is highly hydrophobic and requires the use of liposomes for solubilization; however, silicon (IV) naphthalocyanine displayed no tumor selectivity in the B16F10 murine melanoma model, and tumor retardation that was not associated with thermal effects was considered modest (Biolo *et al.*, 1994). In other studies performed with melanoma models, Nelson *et al.* found that human melanotic tumors grown as xenografts were not responsive to PDT with Photofrin II (Nelson *et al.*, 1988), despite containing more sensitizer than amelanotic melanoma.

In summary, PDT of the heavily pigmented and metastatic B16F10 melanoma using the water soluble PCI-0123 resulted in significant tumor growth delay and increased longevity of the treated animals. Animal survival was also increased in ApoE deficient mice. The increased PDT responsiveness of the melanoma was attributed to the high tumor loading achieved by the texaphyrin, in addition to enhanced tissue penetration attained by illumination of the tumor at 732 nm light and selective accumulation within, and activation of, the melanosomes.

the confocal laser scanning microscopes. We also acknowledge Dr. Seth J. Orlov, New York University School of Medicine, for help with the Mel-S staining protocol. Excellent technical assistance was provided by Mr. Jim Hanson and Ms. Veronique Patascil.

REFERENCES

- Bielec J, Pila B, Sarna T, Truscott TG: Photochemical studies of porphyrins-melanin interaction. *J Chem Soc Faraday Trans II* 82:1469-1474, 1986
- Biolo R, Jori G, Soncin M, *et al.*: Photodynamic therapy of B16 pigmented melanoma with liposome-delivered Si (IV)-naphthalocyanine. *Photochem Photobiol* 59:362-365, 1994
- Borovsky J: Properties of melanosomes and their exploitation in the diagnosis and treatment of melanoma. *Melanoma Res* 3:181-186, 1993
- Dougherty TJ: Photodynamic therapy for cutaneous and subcutaneous malignancies. *J Invest Dermatol* 77:122-124, 1981
- Fidler IJ: Critical determinants of melanoma metastasis. *J Invest Derm Symp* 1:203-208, 1996
- Gomer CJ, Ferrario A, Murphree AL: The effect of localized porphyrin photodynamic therapy on the induction of tumor metastasis. *Br J Cancer* 56:27-32, 1987
- Haylet AK, Row S, Truscott TG, Moore JY: Pharmacokinetic and therapeutic outcome in melanoma cells, of the administration of symmetric and asymmetric cationic photosensitizers. *Cancer Lett* 88:191-199, 1995
- Henderson BW, Dougherty TJ: How does photodynamic therapy work? *Photochem Photobiol* 55:145-157, 1992
- Hsu M-Y, Wheelock MJ, Johnson KR, Herlyn M: Shifts in cadherin profiles between human normal melanocytes and melanomas. *J Invest Derm Symp* 1:188-194, 1996
- Kessel D, Woodburn K: Biodistribution of photosensitizing agents. *Int J Biochem* 25:1377-1383, 1993
- Kreimer-Birnbaum M: Modified porphyrins, chlorins, phthalocyanines, and purpurins: Second-generation photosensitizers for photodynamic therapy. *Semin Hematol* 26:157-173, 1989
- Lim HW, Young L, Hagan M, Gigli E: Delayed phase of hematoporphyrin-induced phototoxicity: modulation by complement, leukocytes and antihistamines. *J Invest Derm* 84:114-117, 1985
- Link EM, Carpenter RN, Hansen G: [¹²⁵I]Methylene blue for targeted radiotherapy of human melanoma xenografts: dose fractionation in the treatment of cutaneous tumors. *Eur J Cancer* 32:1240-1247, 1996
- MacRobert AJ, Bown SG, Phillips D: What are the ideal photoprotectors for a sensitizer? In: Lock G, Hansen S (eds): *Photodynamic Therapy: Their Chemistry, Biology and Clinical Use*. Ciba Foundation Symposium 146, Chichester, Wiley, 1989, pp. 4-16
- Nelson JS, McCullough JL, Burns MW: Photodynamic therapy of human malignant melanoma xenografts in athymic nude mice. *J Natl Cancer Inst* 80:56-60, 1988
- Orlov SJ: Melanosomes are specialized members of the lysosomal lineage of organelles. *J Invest Dermatol* 105:3-7, 1995
- Pas H: Photodynamic therapy in oncology: mechanisms and clinical use. *J Natl Cancer Inst* 85:443-456, 1993
- Picardo M, Grammatico P, Rocella F, Rocella M, Grandinetti M, Del Porto G, Passi S: Imbalance in the antioxidant pool in melanoma cells and normal melanocytes from patients with melanoma. *J Invest Dermatol* 107:322-326, 1995
- Rockwell S, Kallman RF: Growth and cell population kinetics of single and multiple RHT sarcomas. *Cell Tissue Res* 5:149-157, 1972
- Sesley RC, Sarna T, Wanner IJ, Reszka K: Photoionization of melanin: an electron spin resonance study of sensitized radical production and oxygen consumption. *Photochem Photobiol* 60:453-459, 1984
- Scudler JL, Hemmi G, Mody TD, Murali T, Burrell A, Young SW: Texaphyrins: Synthesis and applications. *Acc Chem Res* 27:43-50, 1994
- Verschuik AJ, van Geel PJ, Oppelaar H, van Berek TJ, Bijsterveld MK: Receptor-mediated uptake of low-density lipoprotein by B16 melanoma cells *in vivo* and *in vitro*. *Br J Cancer* 74:525-532, 1996
- Woodburn K, Kessel D: Effect of density-gradients on the binding of photosensitizing agents to plasma proteins. *Int J Biochem Cell Biol* 27:499-506, 1995
- Woodburn KW, Fan Q, Kessel D, *et al.*: Phototherapy of cancer and atherosclerotic plaque with texaphyrin. *J Clin Laser Med Surg* 14:343-348, 1996
- Woodburn KW, Fan Q, Miles DR, Kessel D, Luo Y, Young SW: Localization and efficacy analysis of the phototherapeutic lectin texaphyrin (PCI-0123) in the murine EMT6 sarcoma model. *Photochem Photobiol* 65:410-415, 1997
- Young SW, Sidhu MK, Fan Q, *et al.*: Preclinical evaluation of gadolinium (III) complex. A new paramagnetic contrast agent for magnetic resonance imaging. *Invest Rad* 29:330-338, 1994
- Young SW, Fan Q, Hanman A, *et al.*: Gadolinium (III) texaphyrin: A new class of radiation sensitizers which localize in tumors and are detectable by MRI. *Proc Natl Acad Sci* 93:6610-6615, 1996
- Young SW, Woodburn KW, Wright M, *et al.*: Lutetium Texaphyrin (PCI-0123): A near-infrared water-soluble photosensitizer. *Photochem Photobiol* 63:892-897, 1996b
- Zaidi SL, Oleinick NL, Zaim MT, Mukhtar H: Apoptosis during photodynamic therapy-induced ablation of RIF-1 tumor in C3H mice: electron microscopic, histopathologic and biochemical evidence. *Photochem Photobiol* 58:771-776, 1993
- Zhang SH, Reddick RL, Piedrahi JA, Maeda N: Spontaneous hypercholesterolemia and arterial lesions in mice lacking apolipoprotein E. *Am J Pathol* 146:468-471, 1992

We wish to express our sincere thanks to Dr. Margaret Wade of Meridian Instruments and Dr. David K. Hanzel and Mr. Steven Nelson of Molecular Dynamics for use of

Motexafin Gadolinium: A Redox Active Drug That Enhances the Efficacy of Bleomycin and Doxorubicin

Richard A. Miller,¹ Kathryn W. Woodburn, Qing Fan, Intae Lee, Dale Miles, George Duran, Branimir Sikic, and Darren Magda

Pharmacyclics, Inc., Sunnyvale, California 94085 [R. A. M., K. W. W., Q. F., I. L., D. M., D. M.], and Stanford University School of Medicine, Division of Oncology, Stanford, California 94305 [G. D., B. S.]

ABSTRACT

The effect of motexafin gadolinium (MGd), a redox mediator, on tumor response to doxorubicin (Dox) and bleomycin (Bleo) was investigated *in vitro* and *in vivo*. MES-SA human uterine sarcoma cells were studied *in vitro* using a 3-(4,5-dimethylthiazol-2-yl)-2,5-diphenyltetrazolium bromide viability assay. Rif-1, a murine fibrosarcoma cell line, was studied using a clonogenic survival assay. Tumor growth delay assays were performed using the EMT-6 murine mammary sarcoma cell line in BALB/c mice. MGd (25–100 μ M) produced dose-dependent enhancement of Bleo cytotoxicity to MES-SA cells. The IC₅₀ for Bleo was reduced by ~10-fold using 100 μ M MGd. In clonogenic assays using Rif-1 cells, MGd enhanced the activity of Bleo ~1000-fold. This effect was shown to be mediated, in part, by MGd inhibition of potentially lethal damage repair. MGd enhanced the tumor response to bleomycin and Dox *in vivo*. MGd had no significant effect on the systemic exposure to Dox (expressed in terms of the plasma area under the curve, 0–24 h) and did not increase Dox myelosuppression. MGd enhanced the effectiveness of the redox active drugs, Bleo and Dox.

INTRODUCTION

The development of agents that improve or enhance the efficacy of cancer chemotherapy is an important area of research in medical oncology. Some of the approaches have involved the use of drugs that modify the metabolism or inhibit the efflux of cancer drugs from cells. Despite intense efforts in this area, chemosensitization of tumors has met with limited clinical success (1–3).

The tetraphyrins are metal cation-binding macrocycles that bear strong resemblance to naturally occurring porphyrins. For instance, it has now been demonstrated in both animal tumor

models and human clinical trials that tetraphyrins accumulate selectively in cancers, similar to certain porphyrins (4–7). However, tetraphyrins are far easier to reduce (more electron affinity) than typical metalloporphyrins with a half-wave potential of approximately –50 mV (*versus* normal hydrogen electrode; Ref. 8). These properties have led to the consideration that metalloporphyrins might function as radiation-enhancing agents. Animal tumor model studies have demonstrated that the tetraphyrin, MGd,² selectively accumulates in cancers and renders tumors more responsive to ionizing radiation (4, 7, 9). Promising Phase II clinical results also have been reported in patients receiving radiation therapy for brain metastases (6, 10). In human Phase I and II studies, selective tumor localization of MGd has been confirmed using magnetic resonance imaging, which can detect the drug based on its paramagnetic properties (5, 6, 10).

Biological redox reactions are central to metabolism and cellular energy production. Recent studies with MGd have indicated that it catalytically reacts with various intracellular reducing metabolites (antioxidants), such as ascorbate and NADPH, to produce hydrogen peroxide and other reactive oxygen species (11). We hypothesize that the depletion of intracellular reducing metabolites and resulting bioenergetic disruption because of futile redox cycling would lead to increased tumor response to both radiation therapy and chemotherapy. This could explain the results of Bernhard *et al.* (12), who failed to observe radiation enhancement with MGd. In this report, we describe the effects of MGd on tumor response to two chemotherapy drugs, Bleo and Dox. These chemotherapeutic agents were selected because they are redox active and known to generate reactive oxygen species within cells (13, 14).

MATERIALS AND METHODS

Chemicals and Cell Lines. The synthesis and chemical characterization of MGd has been described previously (8). Dox and Bleo were obtained from Sigma Chemical Co. (St. Louis, MO).

The development and characterization of the human cell line, MES-SA, derived from sarcoma elements of a uterine mixed Müllerian tumor, have been described previously (15). Monolayer cultures of MES-SA cells were grown in McCoy's 5A medium supplemented with 10% FCS, 25 mM HEPES (Life Technologies, Inc., Grand Island, NY), 2 mM L-glutamine, and antibiotics (100 units/ml penicillin and 100 μ g/ml streptomycin; Sigma). Murine EMT-6 mammary sarcoma and Rif-1 radiation-induced fibrosarcoma cell lines were maintained through established *in vivo* *in vitro* propagation procedures (16). Rif-1 cells

Received 3/1/01; revised 5/22/01; accepted 6/1/01.

The costs of publication of this article were defrayed in part by the payment of page charges. This article must therefore be hereby marked advertisement in accordance with 18 U.S.C. Section 1734 solely to indicate this fact.

¹To whom requests for reprints should be addressed, at Pharmacyclics, Inc., 995 East Arques Avenue, Sunnyvale, CA 94085. Phone: (408) 774-0330; Fax: (408) 774-0340.

²The abbreviations used are: MGd, motexafin gadolinium; MTT, 3-(4,5-dimethylthiazol-2-yl)-2,5-diphenyltetrazolium bromide; Bleo, bleomycin; Dox, doxorubicin; PLDR, potentially lethal damage repair.

were grown in RPMI 1640 supplemented with 15% FCS and penicillin/streptomycin. EMT-6 cells were grown in Waymouth's medium (MB752/1; Life Technologies, Inc.) supplemented with 15% FCS and penicillin/streptomycin. Cells were maintained at 37°C in a humidified atmosphere containing 5% CO₂.

In Vitro MTT Cytotoxicity Assays. MES-SA cells were allowed to adhere to 96-well microtiter plates (4000 cells/well) overnight in 180 µl of McCoy's 5A medium. A freshly prepared stock solution of Bleo in medium (60 µl) was serially diluted (1:4) down the plate, discarding the final 60 µl. Stock solutions of MGd (1 mM, 750 µM, 500 µM, or 250 µM diluted in medium and 5% mannitol) were added to the plates to give a final volume of 200 µl. Final mannitol concentration was 0.25% in all wells. The plates were incubated at 37°C in a 5% CO₂ in air atmosphere. Medium was exchanged after 24 h, and the plates were incubated an additional 48 h prior to analysis for viability using the tetrazolium dye MTT (17). In brief, a 5-mg/ml solution of dye in PBS (20 µl/well) was added, and after 2 h the medium was removed and replaced with 100 µl of isopropanol to dissolve the formazan crystals formed by the cells. The plate was read at a test wavelength of 570 nm and a reference wavelength of 650 nm on a multiwell spectrophotometer (ThermoMax; Molecular Devices, Sunnyvale, CA). Each concentration of drug was tested in quadruplicate. The percentage of survival was defined as the percentage of the absorbance of the drug-treated cells to that of the control. Data were adjusted to normalize for effect of MGd treatment alone, which produced 15–45% cytotoxicity in the range of MGd concentrations tested. Experiments with Dox were carried out by serial dilution as above, an exchange of medium after 8 h, followed by addition of MGd for 13 h. Medium was exchanged, and cells were incubated for an additional 2 days as above.

In Vitro Clonogenic and PLDR Assays. Rif-1 cells (200 to 10⁵) were plated into 25-cm² plastic tissue culture flasks and allowed to adhere for 24 h. Bleo and MGd were added to final concentrations of 0.88–4.4 and 50 µM, respectively. After a 4- or 24-h drug exposure, the cells were washed twice with Hank's solution, replenished with complete medium, and returned to the incubator for an additional 6–10 days. The colonies were fixed with 10% buffered formalin and stained with crystal violet for counting (plating efficiencies were 43–50%). To evaluate the effects on PLDR, cultures of Rif-1 (4 × 10⁵ cells/flask) were treated with Bleo and MGd for 18 h, washed with fresh medium, and then treated with trypsin either immediately or after incubation in Hank's solution at room temperature for a period of 4 h. Cells were counted and replated, and colonies were determined after further incubation as above (plating efficiencies were 34–46%). To study the effect of drug sequence, Rif-1 cells in medium were exposed under ambient conditions to the following conditions: (a) Bleo for 4 h, rinsed, and then treated with MGd for 4 h; (b) MGd for 4 h, rinsed, and then treated with Bleo for 4 h; (c) both drugs together for 4 h; (d) Bleo alone in medium containing 0.125% mannitol (drug vehicle) for 4 h; (e) Bleo alone for 4 h, rinsed, and then treated with medium containing 0.125% mannitol for 4 h. Colonies were determined after further incubation as above (plating efficiencies were 32–44%). MGd alone had no effect on plating efficiency.

In Vivo Tumor Models. All animals received care in compliance with Guide for the Care and Use of Laboratory Animals (NIH Publication, 1996). Female BALB/c mice, 7–8 weeks of age, were obtained from Simonsen Laboratories (Gilroy, CA). EMT-6 cells (5–7 × 10⁵) were injected s.c. into the right hind flanks. Animals were studied 10–14 days after inoculation with tumor cells when the tumors had reached 5–7 mm diameter and a depth of 2.5–3.5 mm. Tumor volume, measured three times/week using a caliper, was calculated assuming the conformation of a hemiellipsoid (16).

The dose of Dox was selected to produce an ~50% reduction in tumor growth compared with untreated controls. Dox (7.5 mg/kg), Bleo (10 or 20 units/kg), and/or MGd (0.5–40 µmol/kg) were administered i.v. on days 0, 7, and 14. Control animals received either no treatment, Dox, Bleo, or MGd. Kaplan-Meier analyses were performed by scoring events as the time for the tumor to reach four times the pretreatment volume. A log-rank test was used to determine statistical significance.

Pharmacokinetic Measurements. The plasma pharmacokinetics of MGd and Dox was evaluated in 11-week-old male Sprague Dawley rats (Simonsen Laboratories) weighing 295–358 g. Each rat received injections i.v. via the tail vein with either a single administration of 20 µmol/kg MGd, a single administration of 1.3 mg/kg Dox, or an administration of 1.3 mg/kg Dox, followed by an administration of 20 µmol/kg MGd 1 h later. The Dox and MGd infusions were delivered over 30 s and 1 min, respectively. Blood was drawn into EDTA collection tubes by retroorbital bleeding under methoxyflurane anesthesia (Schering-Plough, Kenilworth, NJ). For each drug or drug combination, the combined data from three subgroups of rats (4 rats/subgroup) was used to characterize the 48-h postdosing period.

MGd and Dox concentrations in plasma were measured by high-performance liquid chromatography. MGd was analyzed using a modified technique based on the method of Parise *et al.* (18). Dox was assayed using a modified procedure based on the method of Robert (19), Camaggi *et al.* (20), and Pfeiffer *et al.* (21). Standards for both assays were prepared by adding known amounts of analyte to blank rat plasma. For both MGd and Dox, plasma concentrations at 48 h were below the lower limit of quantitation.

Hematological Toxicity. BALB/c mice receiving Dox (7.5 mg/kg) and MGd (40 µmol/kg) administered on days 0, 7, and 14 were compared with untreated animals and animals receiving Dox alone. There were 8 animals in each group, and complete blood counts were measured on days 14 and 28 by the Cell-dyn system (Abbott Laboratories).

RESULTS

In Vitro Studies with Bleomycin. MES-SA cells were treated *in vitro* with a range of concentrations of Bleo. The cytotoxicity of Bleo to MES-SA cells was enhanced by concomitant treatment with 25–100 µM MGd as shown in Fig. 1 using an MTT assay. The IC₅₀ (50% inhibitory concentration) for Bleo was reduced by ~1 log using 100 µM MGd. These results demonstrate dose-dependent MGd enhancement of the *in*

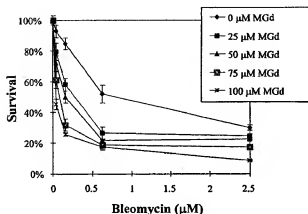


Fig. 1 Bleo cytotoxicity to MES-SA cells measured using an MTT assay. Cells were treated with MGd and Bleo for 24 h before medium exchange and further incubation for 2 days. Bars, SE (n = 4).

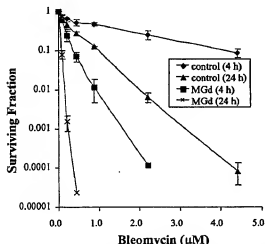


Fig. 2 The effect of Bleo and MGd on the survival of Rif-1 cells measured in a clonogenic assay. Cells were incubated for 4 or 24 h with 50 μ M MGd and the indicated concentration of Bleo. Bars, SE (n = 2).

vitro cytotoxicity of Bleo to MES-SA cells. Similar results were obtained using Rif-1 cells (data not shown).

Enhancement of the cytotoxic activity of Bleo also was studied using the Rif-1 tumor cell line in a clonogenic survival assay (Fig. 2). Plated cells were incubated with MGd for 4 or 24 h with increasing concentrations of Bleo. These data indicated that MGd enhanced the activity of Bleo ~1000-fold in this assay. In another experiment, cultures were incubated with MGd and Bleo and then treated with trypsin and plated, either immediately or after a 4-h "recovery" period. Improved survival was observed in control cultures allowed to recover for 4 h but not in cultures treated with MGd (Fig. 3). This suggests that PLDR was inhibited by MGd. In other experiments, drug treatment sequence was studied by treating Rif-1 cultures with Bleo and MGd for 4 h together or sequentially, after medium exchange (Fig. 4). No change in survival was observed when MGd was added after Bleo treatment. Conversely, the surviving fraction

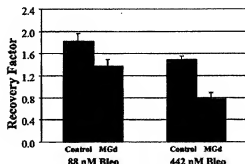


Fig. 3 PLDR inhibition by MGd (50 μ M) in Rif-1 cultures exposed to Bleo. Cultures were detached using trypsin immediately after treatment with Bleo and MGd for 18 h or after a 4-h incubation in Hanks' solution at room temperature. Recovery factors are calculated as the ratio of surviving fractions for control (no MGd) and MGd-treated cultures incubated in Hanks' buffer, divided by the surviving fractions of the corresponding cultures plated immediately after Bleo treatment. MGd treatment led to significant inhibition of PLDR. Bars, SE (n = 4; $P < 0.034$ and 0.001 by two-sided t test for Bleo concentration 88 and 442 μ M, respectively).

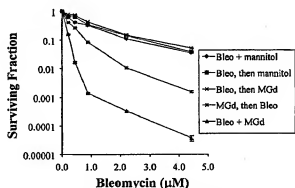


Fig. 4 Effect of order of Bleo and MGd addition on Rif-1 cell survival in a clonogenic assay. Plated cells were incubated with Bleo and mannitol for 4 h; Bleo for 4 h and then mannitol for 4 h; Bleo for 4 h, followed by MGd for 4 h; MGd for 4 h, followed by Bleo for 4 h; or MGd and Bleo for 4 h. Bars, SE (n = 4).

decreased considerably (~2 logs) when MGd was added 4 h before Bleo, although not to as great a degree as when the two drugs were added simultaneously (~3 logs).

Various *in vitro* studies with combinations of Dox and MGd were performed. These studies failed to demonstrate an enhancement of Dox activity. Instead, MGd displayed a dose-dependent cytoprotective effect on MES-SA cells when added before or simultaneously with Dox (Fig. 5). This effect was not seen when MGd was added after Dox. Similar results were found using Rif-1 cells (data not shown). The origins of this *in vitro* antagonism are unknown but could arise from interactions involving Dox and MGd directly or through the intermediacy of reducing metabolites present in the tissue culture medium (thiols, ascorbate, NADPH, and others). An analogous dependence on the scheduling of drug administration was not observed *in vivo* (see below).

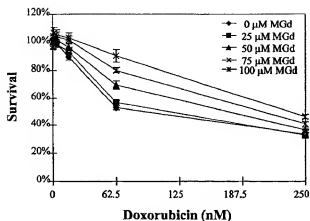


Fig. 5. Dox cytotoxicity to MES-SA cells is inhibited by MGd measured using an MTT assay. Cells were treated with MGd before exchange of medium and addition of Dox. Bars, SD ($n = 4$).

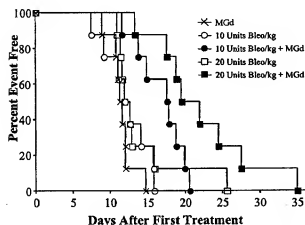


Fig. 6. MGd enhanced the *in vivo* antitumor effect of Bleo on EMT-6. Animals were treated on days 0, 7, and 14 with 10 or 20 units/kg of Bleo and 20 $\mu\text{mol/kg}$ MGd. MGd in combination with either 10 or 20 units/kg of Bleo caused significant tumor growth delay ($P = 0.008$ and $P = 0.015$ for 10 or 20 units/kg of Bleo alone).

MGd Enhances *In Vivo* Tumor Response to Bleo. MGd was found to enhance the effect of Bleo *in vivo* using a tumor growth assay. In these studies, the two drugs were administered within 5 min of each other. As shown in Fig. 6, animals receiving 20 $\mu\text{mol/kg}$ of MGd with each of three weekly doses of Bleo showed significant delay in EMT-6 tumor growth compared with animals receiving Bleo alone. The median time required for tumors to grow to four times their original volume was increased to 17.7 days in animals receiving MGd in combination with a Bleo dose of 10 units/kg compared with 12.3 days for animals receiving Bleo alone ($P = 0.008$). MGd combined with 20 units/kg Bleo delayed tumor growth to 20.8 days ($P = 0.015$, compared with 20 units/kg Bleo alone).

MGd Enhances *In Vivo* Tumor Response to Dox. Animals bearing established EMT-6 tumors were treated with Dox on days 0, 7, and 14. Each Dox injection was followed by

Table 1. Dose-response effect on enhancement of tumor response to Dox by MGd

MGd ^a ($\mu\text{mol/kg}$)	MRT (days) ^b	No. of animals
0	16.8 \pm 1.6	24
0.5	23.5 \pm 9.0 ^c	7
2.5	21.9 \pm 5.7	7
5.0	30.2 \pm 5.4 ^c	19
20	32.2 \pm 7.1 ^c	6
40	33.4 \pm 7.9 ^c	18

^a Animals with established EMT6 tumors were given 7.5 mg/kg Dox and various doses of MGd. Treatment was once a week for 3 weeks. MGd was given 5–10 min after administration of Dox.

^b The mean regrowth time (MRT) is the number of days, \pm SD, for the tumor to reach four times the pretreatment volume.

^c $P < 0.05$ compared with Dox alone.

Table 2. Effect of schedule on enhancement of tumor response to Dox by MGd

Schedule ^a	MRT (days) ^b	No. of animals
Dox + MGd, 10 min	30.2 \pm 5.5 ^c	19
Dox + MGd, 5 h	33.6 \pm 6.9 ^c	6
MGd + Dox, 5 h	27.9 \pm 10.8 ^c	8
MGd alone	9.6 \pm 1.4	8
Dox alone	18.4 \pm 7.9	26
No treatment	10.8 \pm 3.5	6

^a Animals with established EMT6 tumors were given 7.5 mg/kg Dox and/or 5 $\mu\text{mol/kg}$ of MGd. Treatment was given once a week for 3 weeks.

^b The mean regrowth time (MRT) is the number of days, \pm SD, for the tumor to reach four times the pretreatment volume.

^c $P < 0.05$ for the MGd treatment groups plus Dox compared with Dox alone.

administration of MGd within 10 min. At MGd doses of 0.5 and 2.5 $\mu\text{mol/kg}$, some enhancement of tumor response to Dox was seen compared with animals receiving Dox alone. At doses of MGd of 5 $\mu\text{mol/kg}$ or more, considerable enhancement of tumor response to Dox was observed (Table 1). No toxicity was observed with the MGd doses used.

We studied the effect of drug treatment sequence on the enhancement of tumor response to Dox. As shown in Table 2, a dose of 5 $\mu\text{mol/kg}$ of MGd enhanced the tumor response to Dox when given either before or after Dox.

Effect of MGd on the Pharmacokinetics and Hematological Toxicity of Dox. We considered the possibility that enhancement of Dox efficacy could be caused by an alteration of the pharmacokinetics of Dox when given in combination with MGd. As shown in Fig. 7A, a 20- $\mu\text{mol/kg}$ i.v. dose of MGd given 1 h after administration of Dox (1.3 mg/kg i.v.) resulted in a transient increase in the plasma Dox concentration measured ~2 min after MGd administration. At all other time points, Dox concentrations in the Dox plus MGd group were similar to concentrations in the corresponding Dox-alone group. The geometric mean plasma concentration at each time point was used to calculate area under the curve (0–24 h) using linear trapezoidal integration for the Dox-alone and Dox-plus-MGd groups, resulting in values of 204 and 222 ng/h/ml, respectively. Therefore, the transient elevation of Dox concentration seen at 2 min

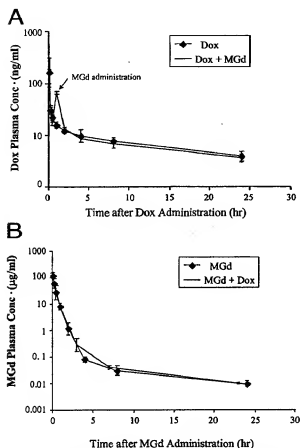


Fig. 7. A, Dox plasma concentration-time profiles for Sprague Dawley rats receiving either a single i.v. administration of 1.3 mg/kg Dox or a single i.v. administration of 1.3 mg/kg Dox, followed 1 h later by a 20- μ mol/kg i.v. dose of MGd. B, MGd plasma concentration-time profiles for Sprague Dawley rats receiving either a single i.v. administration of 20 μ mol/kg MGd or a single i.v. administration of 20 μ mol/kg MGd 1 h after a 1.3-mg/kg i.v. dose of Dox. All values represent the geometric mean for $n = 4$ rats. Bars, 95% confidence intervals back-calculated from the log-transformed data.

resulted in only a 9% increase in systemic Dox exposure when expressed in terms of area under the curve. MGd concentrations at all time points were similar in the Dox-plus-MGd and MGd-alone groups (Fig. 7B), suggesting that a prior administration of Dox did not affect MGd plasma pharmacokinetics under the conditions of this study.

MGd did not increase the hematological toxicity of Dox (data not shown). No effect on WBC or RBC counts, hemoglobin levels, or platelet counts measured both 14 and 28 days after initiation of treatment with Dox and MGd were observed compared with Dox alone.

DISCUSSION

The studies presented here have important implications regarding the mechanism of action of MGd. These findings also suggest potential novel uses for this drug in cancer treatment as an enhancer of chemotherapy or chemosensitizer. MGd has high electron affinity and has been shown to react with various

intracellular reducing metabolites producing reactive oxygen species (11). Hydrogen peroxide and other reactive oxygen species have been shown to enhance radiation response and to be proapoptotic through release of cytochrome *c* from mitochondria (22–26). Cellular reducing metabolites, or antioxidants, such as glutathione, ascorbate, and NADPH protect the cell from the damaging effects of reactive oxygen species (27–29).

MGd enters tumor cells and enhances tumor response to ionizing radiation (4, 7, 9). Ionizing radiation induces the formation of hydroxyl radicals, placing the cells under oxidative stress (30). These radicals damage DNA, which is believed to be the culprit cytotoxic event. The depletion of reducing metabolites and production of reactive oxygen species caused by MGd may render the cells more susceptible to oxidative damage and lower the threshold for apoptosis.

Cytotoxic chemotherapy agents may lead to the generation of reactive oxygen species within cells and cause oxidative stress. Bleo and Dox are two agents known to generate reactive oxygen species (13, 14). Bleo is a glycopeptide that chelates iron inside the cell and binds to DNA. In reactions involving Fe(II) and oxygen, an "activated" Bleo species is formed that damages DNA through free radical intermediates (31). Superoxide and hydrogen peroxide can also react with Fe(II) or Fe(III) bleomycin, respectively, to produce the activated form of the drug. DNA damage from Bleo and ionizing radiation is similar both in induction and repair (32). Dox has several modes of action, including DNA double- and single-strand breakage associated with DNA intercalation and inhibition of topoisomerase II (33). Dox can also form complexes with iron and copper and produce cytotoxic reactive oxygen species (14). In the presence of reducing metabolites, Dox can undergo a one-electron reduction to the semiquinone radical. This radical can rapidly react with oxygen to form superoxide and, in the presence of Fe(II), highly reactive hydroxyl radicals (34). The generation of free radicals is also associated with mitochondrial membrane damage (35).

A dose-response effect was observed for MGd enhancement of tumor responsiveness to Bleo and Dox. The dose-response effect could be readily measured *in vitro* with Bleo (Figs. 1–4) assayed by either MTT viability or clonogenic survival using MES-SA or Rif-1 cells, respectively. The observed enhancement of Bleo activity may partly be attributable to inhibition of PLDR in cells oxidatively stressed by MGd. This assertion is supported by the data presented in Fig. 3, which show that the survival benefit attributable to delayed trypsin treatment was abrogated in MGd-treated cultures. However, the magnitude of the Bleo enhancement suggests that additional mechanisms must be operative that are unique to this agent. One possibility is that reactive oxygen species generated in the presence of MGd contribute to the formation of activated Bleo within cells, either by electron transfer or via the release of Fe(II) ions from intracellular storage sites (31). Another possible mechanism is increased membrane permeabilization by MGd. Electroporation of cells in culture has been reported to enhance Bleo activity by 3 orders of magnitude (36).

Interestingly, activity was enhanced when MGd was added before but not after exposure of cultures to Bleo (Fig. 4). This finding suggests that it may be possible to use the selective

tumor localization of MGd, obtained by its prior administration, to improve the therapeutic index of Bleo. It is important to note that differences in PLDR would not be detected in this experiment, because cells remain in growth phase. Consistent with the above results, administration of MGd and Bleo (MGd within 5 min of Bleo) led to increased tumor responsiveness *in vivo* (Fig. 6).

Dox activity was antagonized when MGd was added to cells before or simultaneously with Dox (Fig. 5). Addition of MGd after Dox had no effect on activity *in vitro* (also observed with Bleo). The source of antagonism is currently unclear. These findings could be explained based on a direct interaction between MGd and Dox or interference with cellular uptake *in vitro*. Alternatively, cells grown in tissue culture may not accurately represent tumor cell concentrations of redox active molecules such as thiols and ascorbate. These differences may mask the effects of redox active drugs such as MGd.

Indeed, as is shown in Table 2, MGd could be given before or after Dox administration *in vivo*. This suggests that the metabolic perturbations induced by MGd do not need to precede the cellular damages caused by Dox. MGd has been found to accumulate in cells and is retained there for long periods of time (6). These findings are consistent with the hypothesis that MGd exerts its effects by depleting intracellular reducing metabolites (11). Xu *et al.* (9) have shown recently, using ^{31}P nuclear magnetic resonance spectroscopy, that MGd treatment leads to a decrease in high-energy phosphates within tumors in mice. This reduction in energy metabolites correlated with increased tumor response to radiation treatment.

Dox is metabolized in the liver. Concomitant use with MGd did not appear to significantly change its plasma pharmacokinetics and did not appear to augment the known myelosuppressive side effects of Dox. Although MGd appeared to cause a transient increase in plasma Dox levels at 2 min, there were no significant effects at other time points or in the area under the curve (Fig. 7A). Future studies must evaluate the potential for enhanced cardiotoxicity with combined use of Dox and MGd.

These findings suggest important potential clinical uses for MGd as a chemotherapy enhancer. MGd selectively accumulates in tumor cells, suggesting the possibility that chemotherapy activity could be enhanced at the tumor but not in normal tissue, thereby increasing the therapeutic margin. Preclinical studies have shown that MGd is excreted primarily by the liver (4). In human clinical trials conducted to date, MGd has shown dose-limiting renal toxicity at 26 $\mu\text{mol/kg}$ in single dose escalation Phase I trial (5). In a Phase Ib/II trial in patients receiving whole brain radiation therapy for brain metastases, dose-limiting hepatotoxicity has been seen at a dose of 8.4 mg/kg given daily for 10 days (6, 10). It is likely that chemotherapy drugs with nonoverlapping toxicities will be best suited for use in combination with MGd.

MGd is a novel redox active drug that may have diverse applications in cancer therapy. It enhances tumor responsiveness to radiation and certain chemotherapy drugs such as Bleo and Dox. Other drugs are currently being tested for use in combination with MGd, and the potential toxicity of combined use will need to be examined for each agent. The studies reported here support redox modulation and inhibition of PLDR as important mechanisms of action for MGd as an enhancer of radi-

ation and chemotherapy. Moreover, these studies and the putative mechanism provide potential new directions for discovering other novel cancer drugs with unique mechanisms of action involving redox reactions in biological systems.

REFERENCES

- Budd, G. T., Bukowski, R. M., Lichtin, A., Bauer, L., Van Kirk, P., and Ganapathi, R. Phase II trial of doxorubicin and trifluoperazine in metastatic breast cancer. *Invest. New Drugs*, 11: 75-79, 1993.
- Miller, T. P., Chase, E. M., Dorr, R., Dalton, W. S., Lam, K. S., and Salmon, S. E. A Phase I/II trial of paclitaxel for non-Hodgkin's lymphoma followed by paclitaxel plus quinine in drug-resistant disease. *Anticancer Drugs*, 9: 135-140, 1998.
- Penmuck, G. D., Dalton, W. S., Roelke, W. R., Appelton, C. P., Mosley, K., Plezia, P., Miller, T. P., and Salmon, S. E. Systemic toxic effects associated with high dose verapamil infusion and chemotherapy administration. *J. Natl. Cancer Inst.*, 83: 105-110, 1991.
- Miller, R. A., Woodburn, K., Fan, Q., Renschler, M. F., Sessler, J. L., and Koutcher, J. A. *In vivo* animal studies with gadolinium(III) texaphyrin as a radiation enhancer. *Int. J. Radiat. Oncol. Biol. Phys.*, 45: 981-989, 1999.
- Rosenthal, D. I., Nurenberg, P., Becerra, C. R., Frenkel, E. P., Carbone, D. P., Lum, B. L., Miller, R., Engel, J., Young, S., Miles, D., and Renschler, M. F. A Phase I single-dose trial of gadolinium texaphyrin (Gd-Tex), a tumor selective sensitizer detectable by magnetic resonance imaging. *Clin. Cancer Res.*, 5: 739-745, 1999.
- Viala, J., Vanel, D., Meignan, P., Larigau, E., Carde, P., and Renschler, M. Phase IB and II multistage trial of gadolinium texaphyrin, a radiation sensitizer detectable at MR imaging: preliminary results in brain metastases. *Radiology*, 212: 755-759, 1999.
- Young, S. W., Qing, F., Harriman, A., Sessler, J. L., Dow, W. C., Mody, T. D., Hemmi, G. W., Hao, Y., and Miller, R. A. Gadolinium(III) texaphyrin: a tumor selective radiation sensitizer that is detectable by MRI. *Proc. Natl. Acad. Sci. USA*, 93: 6610-6615, 1996.
- Sessler, J. L., Tvermoes, N. A., Guidi, D. M., Mody, T. D., and Allen, W. E. One-electron reduction and oxidation studies of the radiation sensitizer gadolinium(III) texaphyrin (PCI-0120) and other water soluble metalotexaphyrins. *J. Phys. Chem.*, 103: 787-794, 1999.
- Xu, S., Zakian, K., Thaler, H., Matei, C., Alfieri, A., Chen, Y., and Koutcher, J. A. Effects of motexafin gadolinium on tumor metabolism and radiation sensitivity. *Int. J. Radiat. Oncol. Biol. Phys.*, 49: 1381-1390, 2001.
- Carde, P., Timmerman, R., Mehta, M. P., Koprowski, C. D., Ford, J., Tishler, R. B., Miles, D., Miller, R. A., and Renschler, M. F. A multicenter Phase Ib/II trial of the radiation enhancer motexafin gadolinium in patients with brain metastases. *J. Clin. Oncol.*, 19: 2074-2083, 2001.
- Magda, D., Lepp, C., Gerasimchuk, N., Lee, I., Sessler, J. L., Lin, A., Biaglow, J. E., and Miller, R. A. Redox cycling by motexafin gadolinium enhances cellular response to ionizing radiation by forming reactive oxygen species. *Int. J. Radiat. Oncol. Biol. Phys.*, in press, 2001.
- Bernhard, E. J., Mitchell, J. B., Deen, D., Cardelli, M., Rosenthal, D. I., and Brown, M. J. Re-evaluating gadolinium(III) texaphyrin as a radiosensitizing agent. *Cancer Res.*, 60: 86-91, 2000.
- Buettner, G. R., and Moseley, P. L. Ascorbate both activates and inactivates bleomycin by free radical generation. *Biochemistry*, 31: 9784-9788, 1992.
- Hassinoff, B. B., and Davey, J. P. Adriamycin and its iron(III) and copper(III) complexes: glutathione-induced dissociation, cytochrome c oxidase inactivation and protection: binding to cardiolipin. *Biochem. Pharmacol.*, 37: 3663-3669, 1988.
- Harker, W. G., MacKintosh, F. R., and Sikic, B. I. Development and characterization of a human sarcoma cell line, MES-SA, sensitive to multiple drugs. *Cancer Res.*, 43: 4943-4950, 1983.
- Rockwell, S. C., Kallman, R. F., and Fajardo, L. F. Characteristics of a serially transplanted mouse mammary tumor and its tissue culture adapted derivative. *J. Natl. Cancer Inst.*, 49: 735-749, 1972.

17. Mosmann, T. Rapid colorimetric assay for cellular growth and survival: application to proliferation and cytotoxicity assays. *Immunological Methods*, 65: 55-63, 1983.
18. Parise, R. A., Miles, D. R., and Egorin, M. J. Sensitive high-performance liquid chromatographic assay for metaxafin gadolinium and metaxafin lutetium in human plasma. *J. Chromatogr. B Biomed. Sci. Appl.*, 749: 145-152, 2000.
19. Robert, J., Extraction of anthracyclines from biological fluids for HPLC evaluation. *J. Liquid Chromatogr.*, 3: 1561-1572, 1980.
20. Comaggi, C. M., Comparsi, R., Stocchi, E., Testoni, F., and Panuti, F. HPLC analysis of doxorubicin, epirubicin, and fluorescent metabolites in biological fluids. *Cancer Chemother. Pharmacol.*, 21: 216-220, 1988.
21. Pfeiffer, T., Krause, U., Thome, U., Skorzek, M., and Scheulen, M. E. Pharmacokinetics of two different delivery regimens of doxorubicin in isolated hyperthermic limb perfusion. *Eur. J. Surg. Oncol.*, 21: 551-554, 1995.
22. Biaglow, J. E., Varnes, M. E., Epp, E. R., Clark, E. P., Tuttle, S. W., and Held, K. D. Role of glutathione in the aerobic radiation response. *Int. J. Radiat. Oncol. Biol. Phys.*, 16: 1311-1314, 1989.
23. Biaglow, J. E., Mitchell, J. B., and Held, K. The importance of peroxide and superoxide in the X-ray response. *Int. J. Radiat. Oncol. Biol. Phys.*, 22: 665-669, 1992.
24. Esposti, M. D., Hatzinisirou, I., McLennan, H., and Ralph, S. Bcl-2 and mitochondrial oxygen radicals. New approaches with reactive oxygen species-sensitive probes. *J. Biol. Chem.*, 274: 29831-29837, 1999.
25. Huang, P., Feng, L., Oldham, E. A., Keating, M. J., and Plunkett, W. Superoxide dismutase as a target for the selective killing of cancer cells. *Nature (Lond.)*, 407: 390-395, 2000.
26. Kuninaka, S., Ichinose, Y., Koja, K., and Toh, Y. Suppression of manganese superoxide dismutase augments sensitivity to radiation, hyperthermia, and doxorubicin in colon cancer cell lines by inducing apoptosis. *Br. J. Cancer*, 83: 928-934, 2000.
27. Deneke, S. M. Thiol-based antioxidants. *Curr. Top. Cell Regul.*, 36: 151-180, 2000.
28. Sastre, J., Pallardo, F. V., Garcia de la Asuncion, J., and Vian, J. Mitochondria, oxidative stress and aging. *Free Radical Res.*, 32: 189-198, 2000.
29. Schulz, J. B., Lindenau, J., Seyfried, J., and Dichgans, J. Glutathione, oxidative stress and neurodegeneration. *Eur. J. Biochem.*, 267: 4904-4911, 2000.
30. Dahm-Daphi, J., Sass, C., and Alberti, W. Comparison of biological effects of DNA damage induced by ionizing radiation and hydrogen peroxide in CHO cells. *Int. J. Radiat. Biol.*, 76: 67-75, 2000.
31. Burger, R. M. Cleavage of nucleic acids by bleomycin. *Chem. Rev.*, 98: 1153-1169, 1998.
32. Byfield, J. E., Lee, Y. C., Tu, L., and Kullhanian, F. Molecular interactions of the combined effects of bleomycin and X-rays on mammalian cell survival. *Cancer Res.*, 36: 1138-1143, 1976.
33. Driscoll, J. S., Hazard, G. F., and Wood, H. B. Structure-activity relationships among quinone derivatives. *Cancer Chemother. Rep. Part 2*, 4: 1-362, 1974.
34. Goodman, J., and Hochstein, P. Generation of free radicals and lipid peroxidation by redox cycling of Adriamycin and daunomycin. *Biochem. Biophys. Res. Commun.*, 77: 797-803, 1977.
35. Dorr, R. T., and Von Hoff, D. D. Doxorubicin. In: *Cancer Chemotherapy Handbook*, Ed. 2, pp. 395-416. Norwalk, CT: Appleton & Lange, 1991.
36. Poddevin, B., Orlowski, S., Belehradec, J. Jr., and Mir, L. M. Very high cytotoxicity of bleomycin introduced into the cytosol of cells in culture. *Biochem. Pharmacol.*, 42: S67-S75, 1991.


A service of the National Library of Medicine
and the National Institutes of Health

My NCBI
[Sign In] [Register]
Entrez 2.0

All Databases	PubMed	Nucleotide	Protein	Genome	Structure	OMIM	PMC	Journals	Book
Search PubMed		for							
				Go Clear					
Limits	Preview/Index	History	Clipboard	Details					
Display AbstractPlus		Show 20		Sort by		Send to			
All: 1		Review: 1							

☐ 1: Curr Treat Options Oncol. 2005 Jul;6(4):289-96.

Links

Motexafin gadolinium induces oxidative stress and apoptosis in hematologic malignancies.

Evens AM, Balasubramanian L, Gordon LT.

Division of Hematology/Oncology, Northwestern University Feinberg School of Medicine and the Robert H. Lurie Comprehensive Cancer Center of Northwestern University, 676 N. St. Clair, Suite 850, Chicago, IL 60611, USA. a-evens@northwestern.edu

Redox mechanisms have been shown to be important in malignant cell survival and are a system that may be modified for the treatment of hematologic malignancies. Motexafin gadolinium (MGd) is a synthetic expanded porphyrin that selectively accumulates in tumor cells and oxidizes various intracellular metabolites, including ascorbate, nicotinamide adenine dinucleotide phosphate, glutathione, and protein thiols, to generate reactive oxygen species in a process known as futile redox cycling. The rationale for its use in hematologic malignancies is that, like naturally occurring porphyrins, it tends to concentrate selectively in cancer cells, and it has a novel mechanism of action of inducing redox stress and triggering apoptosis in a broad range of malignancies. MGd induces apoptosis in B-cell non-Hodgkin's lymphoma, chronic lymphocytic leukemia, and highly resistant myeloma cell lines. Furthermore, MGd is additive or synergistic with ionizing radiation, several chemotherapy agents, and rituximab in vitro and in vivo tumor models. Through gene expression profiling, various stress-related genes are upregulated in response to MGd, including genes encoding metallothioneins, heat shock proteins, and heme oxygenase. Preliminary results from clinical trials with MGd in hematopoietic malignancies have shown that it is well tolerated, with minimal hematologic side effects in both; it has single agent activity in very heavily pretreated chronic lymphocytic leukemia /small lymphocytic lymphoma patients, and it has induced prompt complete remissions in combination with 90Yttrium-ibritumomab (Y-90 Zevalin; Biogen Idec Inc., Cambridge, MA) for relapsed non-Hodgkin's lymphoma in the first two cohorts of patients enrolled. Various clinical trials studying MGd as a single agent and in combination with radiation and/or chemotherapy for the treatment of hematologic malignancies are ongoing.

Related Links

- ▶ Motexafin gadolinium: a redox-active tumor selective agent for the treatment of cancer [Curr Opin Oncol. 2004]
- ▶ Motexafin gadolinium generates reactive oxygen species and induces apoptosis in sensitive and highly resistant multiple myeloma [Blood. 2005]
- ▶ Motexafin gadolinium and zinc induce oxidative stress responses and apoptosis in B-cell lymphoma [Blood. 2005]
- ▶ Motexafin gadolinium-induced cell death correlates with heme oxygenase-1 expression and inhibition of P450 reductase-dependent activities. [Mol Pharmacol. 2007]
- ▶ Motexafin gadolinium: a novel redox active drug for cancer therapy [Cancer Res. 2006]

See all Related Articles...

Motexafin gadolinium modulates levels of phosphorylated Akt and synergizes with inhibitors of Akt phosphorylation

Jason Ramos, Mint Sirisawad, Richard Miller, and Louie Naumovski

Pharmacyclics, Inc., Sunnyvale, California

Abstract

Motexafin gadolinium (MGd, Xcytrin) is a tumor-selective expanded porphyrin that targets oxidative stress-related proteins. MGd treatment of the follicular lymphoma-derived cell line HF-1 resulted in growth suppression and apoptosis whereas MGd treatment of the Burkitt's lymphoma-derived cell line Ramos resulted in growth suppression but not apoptosis. Because phosphorylation status of Akt/protein kinase B is regulated by oxidative stress, we monitored total and phosphorylated Akt (pAkt) in MGd-treated HF-1 and Ramos cells. Levels of pAkt increased within 30 minutes after MGd treatment of HF-1 but after 4 hours began to show a progressive decline to below baseline levels before cells underwent apoptosis. In MGd-treated Ramos cells, pAkt increased ~2-fold within 4 hours and remained persistently elevated. Because pAkt activates survival pathways, we determined if MGd-induced cell death could be enhanced by inhibiting phosphorylation of Akt. The addition of specific inhibitors of Akt phosphorylation (Akt inhibitor 1 or SH-5) reduced pAkt levels in MGd-treated HF-1 and Ramos cells and synergistically enhanced MGd-induced cell death. MGd was also evaluated in combination with celecoxib, an inhibitor of Akt phosphorylation, or docetaxel, a microtubule inhibitor that can decrease Akt phosphorylation. The combination of MGd/celecoxib or MGd/docetaxel resulted in decreased Akt phosphorylation and in synergistic cytotoxicity compared with either agent alone. These data point to a potential protective role for pAkt in MGd-induced apoptosis and suggest that MGd activity may be enhanced by combining it with agents that inhibit Akt phosphorylation. [Mol Cancer Ther 2006;5(5):1176-82]

Introduction

Motexafin gadolinium (MGd) is an expanded porphyrin molecule that disrupts redox-dependent pathways by

targeting oxidative stress-related proteins (1). MGd treatment of A549 lung cancer and Ramos lymphoma cells has been found to induce up-regulation of metallothionein and zinc transporter genes, which leads to disruption of zinc ion homeostasis and redox stress (1, 2). MGd contains the paramagnetic Gd^{3+} ion in its central cavity and is detectable by magnetic resonance imaging (3, 4). Preclinical studies have shown that MGd localizes to tumor cells and enhances the efficacy of radiation and chemotherapy in tissue culture and in animal tumor models (4-7). Tumor-selective localization has also been confirmed in both animal models and human clinical trials using magnetic resonance imaging (4, 8-11). MGd is now in several clinical trials for the evaluation of its efficacy as a single agent and in combination with chemotherapy or radiation therapy for cancer treatment (12, 13).

Akt/protein kinase B is a serine/threonine kinase that acts in cell survival pathways to suppress apoptosis (14). After growth factor or stress signaling including oxidative stress, Akt is recruited to the plasma membrane and activated by phosphorylation (14, 15). Akt functions as an antiapoptotic factor through numerous mechanisms, including phosphorylation and inactivation of several proapoptotic factors such as Bad and caspase-9 (14). Akt also acts in survival pathways by promoting glycolysis and maintaining a physiologic mitochondrial membrane potential (16). Consistent with studies in tissue culture cells using overexpression and dominant-negative models, thymocytes and mouse embryonic fibroblasts derived from mice carrying a homozygous disruption of the *akt1* gene are more susceptible to apoptosis induced by a wide variety of agents (17). Akt is initially phosphorylated and activated in response to proapoptotic agents such as cisplatin, vincristine, and etoposide but levels of phosphorylated Akt (pAkt) and Akt decrease as cells begin to die (18, 19). The decrease may be due to a combination of cleavage of Akt by caspases, ubiquitination and degradation by the proteasome, and/or down-regulation of mRNA levels (20-22).

Because MGd can target redox pathways and Akt is redox regulated, we examined the effects of MGd on total Akt and pAkt in two lymphoma-derived cell lines. Levels of pAkt increased after MGd treatment in both lines, but only in the cell line in which MGd induced apoptosis did levels of total and pAkt drop before cell death. Treatment of both cell lines with inhibitors of Akt phosphorylation in combination with MGd resulted in synergistic cytotoxicity, suggesting that the increase in pAkt after treatment with MGd plays a protective role. Cotreatment of cells with MGd and celecoxib or docetaxel, drugs which inhibit Akt phosphorylation, resulted in synergistic cytotoxicity. Our data show that MGd results in increased phosphorylation of Akt and that MGd can be used in conjunction with Akt kinase inhibitors to achieve synergistic cytotoxicity.

Received 7/25/05; revised 2/1/06; accepted 3/6/06.

The costs of publication of this article were defrayed in part by the payment of page charges. This article must therefore be hereby marked advertisement in accordance with 18 U.S.C. Section 1734 solely to indicate this fact.

Requests for reprints: Louie Naumovski, Pharmacyclics, Inc., 995 Argus Avenue, Sunnyvale, CA 94085. Phone: 408-215-3450; Fax: 408-328-3689. E-mail: lnaumovski@pcyc.com

Copyright © 2006 American Association for Cancer Research. doi:10.1158/1535-7163.MCT-05-0280

Materials and Methods

Reagents

MGd (as a stock solution of 2 mmol/L in aqueous 5% mannitol) was directly added to cultures to the concentrations specified in the text and figure legends. The inhibitors of Akt phosphorylation, SH-5 and Akt inhibitor 1, were from Calbiochem (San Diego, CA). Caspase inhibitor Quinoline-Valine-Aspartic-CH₂-O-Phenyl (Q-VD-OPH) was from Enzyme System Products (Aurora, OH).

Cell Lines and Growth Conditions

The HF-1 cell line was obtained from Ronald Levy, M.D. (Stanford University, Stanford, CA). The HF-1 cell line was derived from a patient with follicular lymphoma (23). The Ramos cell line was derived from a patient with Burkitt's lymphoma. Cells were grown in RPMI 1640 with 10% fetal bovine serum in a 5% CO₂/air incubator at 37°C. For assays determining growth inhibition or apoptosis, cells were plated and treated with various concentrations of MGd, as specified in the text and figure legends, before analysis. The concentrations of MGd used in this study have been achieved in clinical trials (8, 10).

Analysis of MGd-Treated Cells

Cell numbers were determined using a Model Z2 counter (Beckman-Coulter, Miami, FL). Annexin V binding and propidium iodide exclusion were assayed with a FACSCalibur instrument (Becton Dickinson, San Jose, CA) using reagents from BioVision (Mountain View, CA) per protocol of the manufacturer.

For drug combination studies, cytotoxicity was evaluated after 2 days of treatment with MGd and various drug combinations (as described in the figure legends) using Annexin V staining. The data were then analyzed using the CalcuSyn program (Biosoft, Ferguson, MO) to determine the combination index (CI). CI > 1 indicates antagonism, CI = 1 additivity, and CI < 1 synergy.

Caspase-3 activity was assayed using the EnzChek Caspase-3 Assay Kit #2, which monitors the cleavage of a DEVD substrate (Molecular Probes, Eugene, OR). This activity assay also detects activated caspase-6, caspase-7, caspase-8, and caspase-10. Cell lysates were analyzed according to the protocol of the manufacturer except that catalase was added at 10 units/mL in the lysis buffer to degrade hydrogen peroxide that might potentially be produced by MGd *in vitro* because hydrogen peroxide can inactivate caspase-3 (24). For each cell line, measured fluorescence levels were normalized to fluorescence levels of nontreated cell lysates.

Cellular uptake of MGd was measured by flow cytometry using a 650-nm long pass filter to detect MGd fluorescence emission (peak at 760 nm) after excitation at 488 nm (25). Cells were washed once in Hanks solution and a "live-cell" gate was drawn based on forward/side scatter properties to determine MGd uptake in viable cells.

Western Blotting for Caspase Activation and Substrate Cleavage

Cells were lysed in triple-detergent lysis buffer [50 mmol/L Tris-Cl (pH 8.0), 150 mmol/L NaCl, 0.1% SDS,

0.5% deoxycholic acid, 1.0% NP40, supplemented with 1 mmol/L EDTA, 1 mmol/L phenylmethylsulfonyl fluoride, 1 mmol/L Na₃VO₄, 2 mmol/L β -glycerophosphate, and the COMPLETE protease inhibitor cocktail (Roche Molecular Biochemicals, Indianapolis, IN)] on ice for 10 minutes. After centrifugation at 10,000 \times g for 10 minutes, protein concentration was quantitated in the supernatant and equal quantities of protein were resolved on the appropriate percentage SDS-polyacrylamide gels (Bio-Rad, Hercules, CA). Gels were transferred to polyvinylidene difluoride membrane using a Semi-Dry Transfer Cell (Bio-Rad) and Western blotting was done using primary and antimouse and antirabbit secondary antibodies conjugated to Alexa Fluor 680 (Molecular Probes) and IRdye800 (Rockland Immunochemicals, Gilbertsville, PA), respectively. Antibodies to caspases and poly(ADP-ribose) polymerase (Cell Signaling Technologies, Beverly, MA) recognized the full-length and cleaved forms of their respective antigens. Antibodies against the Akt proteins recognized either the phosphorylated serine-473 (pAkt) or total fraction (Akt) of the protein, respectively (Santa Cruz Biotechnology, Inc., Santa Cruz, CA). All membranes were blotted with an anti-Hsc70 (Santa Cruz Biotechnology) antibody to control for loading and transfer. Bands were imaged and quantified in the linear range and normalized to Hsc70 using the Odyssey Infrared Imaging System (LICOR, Lincoln, NE).

Statistical Analysis

Data in figures are from representative experiments done in triplicate. Data are presented as mean \pm SD. Asterisks are used to represent values that are statistically significantly different than the corresponding controls at $P < 0.05$.

Results

Inhibition of Growth and Induction of Apoptosis by MGd in Lymphoma Cell Line HF-1

HF-1 and Ramos cells were treated *in vitro* with 50 μ mol/L MGd for 5 days and cell numbers, Annexin V-positive cells, caspase-3 activity, and MGd uptake were measured. Both cell lines showed a delay in cell growth (Fig. 1A) but only HF-1 cells underwent apoptosis as shown by an increase in Annexin V-positive cells and caspase activity (Fig. 1B and C). Drug uptake (as measured by FL3 channel fluorescence) was similar in both lines (Fig. 1D).

Western blotting of cells treated with MGd for 0 to 5 days revealed progressive cleavage of caspase-9 and caspase-3 and the caspase substrate poly(ADP-ribose) polymerase in HF-1 cells but not in Ramos cells (Fig. 1E and F).

Treatment with MGd Results in Increased Levels of pAkt

Treatment of FL5.12, a non-transformed growth factor-dependent murine hematopoietic cell line, with chemotherapy drug etoposide, cisplatin, or vincristine results in an initial increase in pAkt levels followed by a decrease as cells die (19). To determine if MGd resulted in a similar pattern of Akt phosphorylation in HF-1 cells, we evaluated MGd (50 μ mol/L) modulation of Akt phosphorylation from

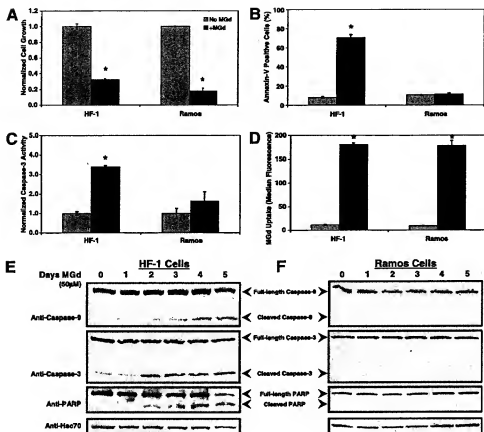


Figure 1. MGD inhibits growth in HF-1 and Ramos cells but only induces apoptosis in HF-1. Cell lines were treated at 25,000 cells/mL with 50 μ M MGD or mannitol control for 5 d before analysis. **A**, normalized growth; **B**, Annexin V-positive cells; **C**, normalized caspase-3 activity; **D**, MGD uptake as assessed by FL3 fluorescence. **E** and **F**, Western blot analysis showing cleavage of caspase-9 and caspase-3 and cleavage of poly(ADP-ribose) polymerase (PARP) during a 5-d time course in HF-1 (**E**) but not in Ramos (**F**). Hsc70 served as a loading control.

30 minutes to 48 hours. MGD initially induced an increase in pAkt, followed by a decrease to below baseline levels before cell death (Fig. 2A). Levels of total Akt increased as levels of pAkt decreased (Fig. 2A).

Decreased levels of Akt have been attributed to caspase cleavage in apoptotic cells although distinct fragments are not detected by Western blotting because the decrease in Akt can be blocked by caspase inhibitors and Akt can be cleaved by caspases *in vitro* (20–22). We determined if apoptosis was responsible for the decrease in pAkt observed in MGD-treated HF-1. Q-VD-OPH, an irreversible caspase inhibitor that is less toxic and more potent than other caspase inhibitors, inhibits MGD-induced apoptosis in HF-1 (26, 27). HF-1 cells were either untreated or treated with MGD, Q-VD-OPH, or MGD, along with Q-VD-OPH, for 48 hours. Western blotting revealed that pAkt decreased in MGD-treated cells but not in MGD/Q-VD-OPH treated cells (Fig. 2B). Total Akt was also elevated in Q-VD-OPH-treated cells compared with control cells possibly because Q-VD-OPH blocks spontaneous apoptosis in HF-1 (27). These data suggest that caspases activated during apoptosis may be responsible, at least in part, for the decrease in pAkt levels in MGD-treated HF-1.

Ramos cells, which do not undergo MGD-induced apoptosis, were treated with 50 μ M MGD and examined from 30 minutes to 48 hours to determine if MGD modulated Akt phosphorylation in these cells. Levels

of pAkt were elevated up to 2-fold by 4 hours and did not return to baseline within 48 hours (Fig. 2C). Levels of total Akt, although somewhat variable, remained close to baseline (Fig. 2C).

MGd and Inhibitors of Akt Kinase Phosphorylation Display Synergistic Cytotoxicity

The increase seen in pAkt in HF-1 and Ramos cells detected early after MGD treatment might have a cytoprotective role and decrease the cytotoxic effects of MGD. To determine if the increase in pAkt has a protective role, we used two different inhibitors of Akt phosphorylation in combination with MGD. Akt inhibitor 1 binds to the pleckstrin homology domain of Akt, disrupting the translocation of Akt to plasma membrane and its ability to be phosphorylated and activated by membrane-bound phosphatidylinositol-dependent kinases (28). SH-5 inhibits the phosphorylation of Akt by inhibiting the upstream kinase phosphatidylinositol-3 kinase (29). HF-1 cells were treated with various doses of MGD or Akt inhibitor 1 or combinations of the two. Although MGD treatment resulted in an increase in pAkt levels and Akt inhibitor 1 resulted in a small decrease in pAkt levels, the combination resulted in a significant drop in pAkt levels after 2 hours of treatment (Fig. 3A). To determine if the combination of MGD and Akt inhibitor 1 had synergistic cytotoxicity, HF-1 cells were treated with MGD, Akt inhibitor 1, and combinations of the drugs for 48 hours and Annexin V-positive cells were

enumerated (Fig. 3B). A CI < 1 was observed, indicating that the drug combinations resulted in synergistic cytotoxicity (Fig. 3C). HF-1 cells were also treated with MGd, SH-5, and combinations of the two and analyzed by Western blotting for pAkt and apoptosis. The combination of MGd and SH-5 resulted in suppression of pAkt levels greater than either drug alone and enhanced cytotoxicity (data not shown). Calculation of the CI based on the Annexin data using the Calcsyn program revealed a CI < 1, consistent with synergy cytotoxicity (Fig. 3D).

To determine if inhibition of Akt phosphorylation was also synergistic with MGd in Ramos cells, we treated Ramos cells with various concentrations of MGd and Akt inhibitor 1, individually and in various combinations. After 2 hours of drug exposure, Western blotting showed that MGd alone resulted in slightly increased pAkt levels whereas Akt inhibitor 1 showed a dose-dependent decrease in pAkt levels (Fig. 4A). Combined treatment with MGd and Akt inhibitor 1 resulted in even further suppression of pAkt levels (Fig. 4A). To determine if the combination of MGd and Akt inhibitor 1 had synergistic cytotoxicity, Ramos cells were treated with MGd, Akt inhibitor 1, and various combinations of the drugs for 48 hours and

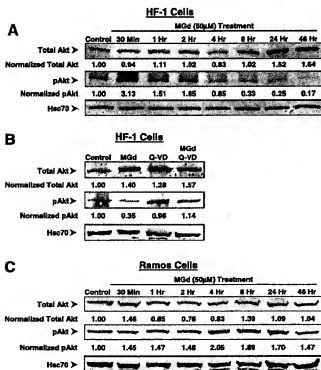


Figure 2. Phosphorylation status of Akt in MGd-treated cells. **A**, total and pAkt in MGd-treated HF-1; **B**, caspase inhibitor Q-VD-OPh blocks decrease in pAkt after MGd treatment of HF-1 for 48 h; **C**, total and pAkt in MGd-treated Ramos. Cells were treated with 50 μmol/L MGd and samples were taken at the indicated time points between 30 min and 48 h. Western blots were probed with antibody to total Akt, pAkt, and Hsc70 as a loading control. Total Akt and pAkt levels were normalized to Hsc70.

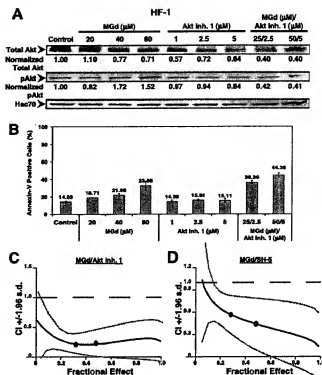


Figure 3. MGd synergizes with Akt inhibitor 1, an inhibitor of Akt phosphorylation, to kill HF-1 cells. **A**, Western blot of Akt, pAkt, and Hsc70 in MGd, Akt inhibitor 1, or combination drug-treated HF-1 cells. Cells were treated with control, MGd, Akt inhibitor 1, or combination of the drugs at concentrations shown in the figure and then analyzed by Western blotting after 2 h. **B**, Annexin V-positive cells 48 h after treatment of HF-1 with MGd, Akt inhibitor 1, or combinations. **C**, combination index plot showing a CI < 1, indicating synergy for the MGd/Akt inhibitor 1 combinations. **D**, combination index plot showing a CI < 1, indicating synergy for Annexin V values from MGd/SH-5 combinations. The following concentrations were used for the MGd/SH-5 combination: 25 μmol/L/2.5 μmol/L and 50 μmol/L/5 μmol/L.

Annexin V-positive cells were enumerated (Fig. 4B). A CI < 1 was observed, indicating that the drug combinations resulted in synergistic cytotoxicity (Fig. 4C). Ramos cells were also treated with MGd, SH-5, and combinations of the two and analyzed by Western blotting for pAkt and apoptosis. The combination of MGd and SH-5 resulted in suppression of pAkt levels greater than either drug alone and enhanced cytotoxicity (data not shown). Calculation of the CI based on the Annexin data using the Calcsyn program revealed a CI < 1, consistent with synergy cytotoxicity (Fig. 4D). These studies show cytotoxic synergy between MGd and inhibition of Akt phosphorylation in both HF-1 and Ramos cells.

Synergistic Activity of MGd with Celecoxib or Docetaxel Correlates with Inhibition of Akt Phosphorylation

We hypothesized that MGd might synergize with other drugs that modulate pAkt. Celecoxib, a specific cyclooxygenase-2 inhibitor, has also been reported to inhibit the phosphorylation of Akt kinase (30–33). To determine if MGd or celecoxib perturbed pAkt levels, we treated Ramos

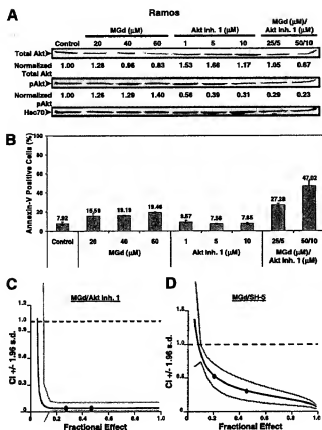


Figure 4. MGD synergizes with Akt inhibitor 1, an inhibitor of Akt phosphorylation, to kill Ramos cells. **A**, Western blot of Akt, pAkt, and Hsc70 in MGD, Akt inhibitor 1, or combination drug-treated Ramos cells. Cells were treated with control, MGD, Akt inhibitor 1, or combinations of the drugs for 2 h and then analyzed by Western blotting. **B**, Annexin V-positive cells after treatment of Ramos cells with MGD, Akt inhibitor 1, or combinations for 48 h. **C**, combination index plot showing a CI < 1, indicating synergy for the MGD/Akt inhibitor 1 combinations in Ramos cells. **D**, combination index plot showing a CI < 1, indicating synergy for Annexin V values from MGD/SH-5 combinations in Ramos cells. The following concentrations were used for the MGD/SH-5 combination: 25 μ mol/L/10 μ mol/L and 50 μ mol/L/20 μ mol/L.

cells with each drug or the combination for 2, 24, and 48 hours and probed for total Akt and pAkt. We noted a time-dependent decrease in the levels of pAkt in the combination treated cells (Fig. 5A-C). With the combination of MGD and celecoxib, a small but reproducible difference was seen in levels of pAkt even at 2 hours, suggesting that this is an early event (Fig. 5A). The decrease in pAkt levels was associated with synergistic increases in cell death as shown by enhanced caspase-3 activity and Annexin V-positive cells in the MGD plus celecoxib-treated cells at 72 hours (Fig. 5D and E).

It is known that Akt mediates resistance to antimicrotubule agents and inhibition of Akt signaling results in sensitization to antimicrotubule agents (19, 34–36). We treated Ramos cells with various concentrations of MGD or the antimicrotubule agent docetaxel, separately and in

combination, and assayed for total Akt and pAkt after 2 hours. Neither MGD nor docetaxel influenced levels of total Akt, but MGD resulted in a 25% to 50% increase in pAkt whereas docetaxel (50 and 75 nmol/L) resulted in decreased pAkt levels to ~50% of normal (Fig. 6A). The combination of the two drugs (MGD 50 μ mol/L and docetaxel 50 nmol/L) resulted in a dramatic decrease in pAkt levels to ~20% of normal (Fig. 6A). Cell death, determined by measuring Annexin V-positive cells at 48 hours, showed that the combination therapy killed substantially more cells than either agent alone (Fig. 6B). The combination of MGD and docetaxel was synergistic as indicated by CI < 1 (Fig. 6C).

Discussion

HF-1 and Ramos lymphoma cell lines both respond to MGD treatment with growth inhibition, but additionally, HF-1 cells also undergo apoptosis as shown by increased number of Annexin V-positive cells, caspase-3 activation, cleavage of caspase-9 and caspase-3 and the substrate poly(ADP-ribose) polymerase. Growth suppression in Ramos was not

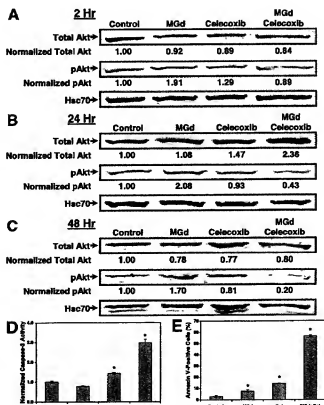


Figure 5. MGD synergizes with celecoxib, a cyclooxygenase-2 inhibitor that also inhibits Akt phosphorylation, to kill Ramos cells. Ramos cells were treated with vehicle or MGD (50 μ mol/L), celecoxib (25 μ mol/L), or MGD/celecoxib for various times. Western blot analysis was with anti-Akt, anti-pAkt, and anti-Hsc70 antibodies at 2 (**A**), 24 (**B**), and 48 (**C**) h. **D**, normalized caspase-3 activity. **E**, Annexin V-positive cells. Total Akt and pAkt levels were normalized to Hsc70.

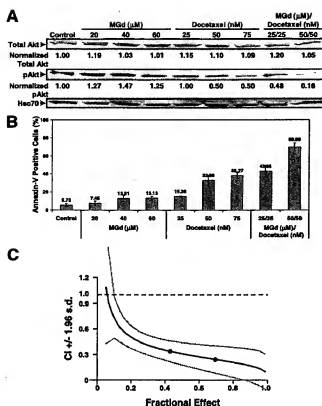


Figure 6. MGd synergizes with docetaxel, an antimicrotubule agent that inhibits Akt phosphorylation, to kill Ramos cells. **A**, Western blot of Akt, pAkt, and Hsc70 in MGd, docetaxel, or combination-treated Ramos. Cells were treated with control, MGd, docetaxel, or combinations of the drugs for 2 h and then analyzed by Western blotting. **B**, Annexin V-positive cells after treatment of Ramos cells with MGd, docetaxel, or combinations for 48 h. **C**, combination index plot from the Annexin V data showing a CI < 1, indicative of synergistic cytotoxicity between MGd and docetaxel.

due to necrosis or a block in any specific phase of the cell cycle.¹ Differences in drug uptake (as measured by FL3 fluorescence) do not explain the cellular responses because uptake was similar in each cell line.

In an effort to better understand the mechanisms that might be involved, we evaluated MGd-treated cells for phosphorylation of Akt, a kinase that is redox regulated and important in metabolism, survival, and apoptosis (14). In the HF-1 cell line in which MGd induces apoptosis and suppresses growth, treatment with MGd (30 minutes–48 hours) resulted in an initial increase in levels of pAkt but after 4 hours resulted in a decrease. The decrease in the levels of pAkt may be related to MGd-induced apoptosis in HF-1 because it could be blocked by caspase inhibition. Because Akt functions in survival pathways, the transient increase in pAkt levels during MGd treatment may represent a cellular adaptive response that could attenuate MGd-induced apoptosis in HF-1.

In the Ramos cell line in which MGd does not induce apoptosis but suppresses growth, MGd treatment resulted in an increase in pAkt levels by 30 minutes, which persistently remained elevated up to 48 hours. These results suggest that the persistent elevation of pAkt may account for the ability of the Ramos cell line to resist the proapoptotic effects of MGd. Therefore, we hypothesized that inhibitors of Akt phosphorylation (Akt inhibitor 1 and SH-5) would sensitize cells to the proapoptotic effects of MGd. For both HF-1 and Ramos cells, specific inhibitors of Akt phosphorylation suppressed the increase in pAkt in MGd-treated cells and synergistically enhanced cell killing by MGd as measured by Annexin V binding. These data suggest that Akt promotes resistance to MGd-induced apoptosis and show that MGd activity is enhanced by inhibition of Akt phosphorylation.

Based on the studies presented here with MGd and Akt inhibitors, we further hypothesized that MGd might also synergize with other drugs that down-regulate pAkt levels such as celecoxib (a cyclooxygenase-2 inhibitor) or docetaxel (an antimicrotubule agent). The ability of celecoxib to induce growth inhibition and apoptosis is most likely an "off-target" effect that may arise, at least in part, through inhibition of Akt phosphorylation via inhibition of 3-phosphoinositide-dependent kinase 1, which seems to be a direct target of celecoxib (30, 32). We found that pAkt levels were decreased in MGd/celecoxib-treated Ramos cells and that this correlated with enhanced cell killing.

The cytotoxic activity of antimicrotubule agents, including docetaxel, is known to be mediated by the Akt pathway (19, 34–36). The combination of MGd with docetaxel resulted in a dramatic decrease in pAkt levels with synergistic cytotoxicity. This result is particularly interesting in view of the recent clinical data from Pandya and Phan (37), which report very promising tumor responses in patients with recurrent non-small-cell lung cancer treated with MGd and docetaxel. These responses were seen even in patients who had failed prior treatment with taxanes (37).

Our results suggest an important role for the Akt pathway in the response of cells to MGd. MGd treatment as a single agent results in an increase in pAkt levels that seem to be protective because MGd-induced cytotoxicity can be enhanced in combination with specific inhibitors of Akt phosphorylation. Additionally, synergistic cytotoxicity of MGd with celecoxib or docetaxel is associated with a decrease in pAkt levels, further highlighting the importance of the Akt pathway in modulating MGd function. Precisely how MGd modulates pAkt levels is currently unclear and under investigation but it may be through induction of oxidative stress, which can enhance the activity of kinases that phosphorylate Akt and attenuate the activity of the Akt phosphatase PTEN (38–42). Similar to what we have shown with MGd, up-regulation of pAkt by other agents that induce redox stress serves a protective role because abrogation of the response with inhibitors of Akt phosphorylation results in enhanced cell death (39, 41, 42). As expected for a protein that functions in a survival pathway, expression of constitutively activated

¹ Unpublished observations.

myristoylated Akt or v-Akt inhibits hydrogen peroxide-induced cell death (42). The results reported here provide valuable insights for maximizing the therapeutic potential of MGD when used in combination with chemotherapy drugs that affect the phosphorylation status of Akt. Clinical trials based on these observations are in progress.

References

- Magda D, Lecane P, Miller RA, et al. Motexafin gadolinium disrupts zinc metabolism in human cancer cell lines. *Cancer Res* 2005;65:3837–45.
- Lecane PS, Karaman MW, Sisrswad M, et al. Motexafin gadolinium and zinc induce oxidative stress responses and apoptosis in B-cell lymphoma lines. *Cancer Res* 2008;68:11676–88.
- Young SW, Sidhu MK, Qing F, et al. Preclinical evaluation of gadolinium (III) texaphyrin complex. A new paramagnetic contrast agent for magnetic resonance imaging. *Invest Radiol* 1994;29:330–8.
- Young SW, Qing F, Harriman A, et al. Gadolinium(III) texaphyrin: a tumor selective radiation sensitizer that is detectable by MRI. *Proc Natl Acad Sci U S A* 1996;93:6610–5.
- Magda D, Lepp C, Gerasimchuk N, et al. Redox cycling by motexafin gadolinium enhances cellular response to ionizing radiation by forming reactive oxygen species. *Int J Radiat Oncol Biol Phys* 2001;51:1025–36.
- Miller RA, Woodburn KW, Fan Q, et al. Motexafin gadolinium: a redox active drug that enhances the efficacy of bleomycin and doxorubicin. *Clin Cancer Res* 2001;7:3215–21.
- Xu S, Zaklen K, Thaler H, et al. Effects of Motexafin gadolinium on tumor metabolism and radiation sensitivity. *Int J Radiat Oncol Biol Phys* 2001;49:1381–90.
- Carde P, Timmerman R, Mehta MP, et al. Multicenter phase I/II trial of the radiation enhancer motexafin gadolinium in patients with brain metastases. *J Clin Oncol* 2001;19:2074–83.
- Mehta MP, Shapiro WR, Glentz MJ, et al. Lead-in phase to randomized trial of motexafin gadolinium and whole-brain radiation for patients with brain metastases: centralized assessment of magnetic resonance imaging, neurocognitive, and neurologic end points. *J Clin Oncol* 2002;20:3445–53.
- Rosenthal DJ, Nurenberg P, Becerra CR, et al. A phase I single-dose trial of gadolinium texaphyrin (Gd-Tex), a tumor selective radiation sensitizer detectable by magnetic resonance imaging. *Clin Cancer Res* 1999;5:739–45.
- Viale J, Vanel D, Melange P, Lertigue E, Carde P, Ranscher M. Phases IB and II multistage trial of gadolinium texaphyrin, a radiation sensitizer detectable by MR imaging: preliminary results in brain metastases. *Radiology* 1999;212:755–9.
- Evans AM. Motexafin gadolinium: a redox-active tumor selective agent for the treatment of cancer. *Curr Opin Oncol* 2004;16:576–80.
- Khuntia D, Mehta M. Motexafin gadolinium: a clinical review of a novel radioenhancer for brain tumors. *Expert Rev Anticancer Ther* 2004;4:981–9.
- Frankie TF, Hornik CP, Segov L, Shostak GA. Supinotin C. PI3K/Akt and apoptosis: size matters. *Oncogene* 2003;22:8953–98.
- Matsuura A, Ichijo H. Stress-responsive protein kinases in redox-regulated apoptosis signaling. *Antioxid Redox Signal* 2005;7:472–81.
- Pla DR, Tadepala S, Edinger AL, Rathmell JC, Thompson CB. Akt and Bcl-XL promote growth factor-independent survival through distinct effects on mitochondrial physiology. *J Biol Chem* 2001;276:12041–8.
- Chen WS, Xu PZ, Gottlieb K, et al. Growth retardation and increased apoptosis in mice with homozygous disruption of the Akt1 gene. *Genes Dev* 2001;15:2203–8.
- Tang D, Okada H, Ruland J, et al. Akt is activated in response to an apoptotic signal. *J Biol Chem* 2001;276:30461–6.
- VanderWeele DJ, Zhou R, Rudin CM. Akt up-regulation increases resistance to microtubule-directed chemotherapeutic agents through mammalian target of rapamycin. *Mol Cancer Ther* 2004;3:1605–13.
- Medina EA, Afari RR, Ravit T, Castillo SS, Erickson KL, Goldkorn T. Tumor necrosis factor- α decreases Akt protein levels in 3T3-L1 adipocytes via the caspase-dependent ubiquitination of Akt. *Endocrinology* 2005;146:2726–35.
- Rokudal S, Fujita N, Hashimoto Y, Tsuruo T. Cleavage and inactivation of antiapoptotic Akt/PKB by caspases during apoptosis. *J Cell Physiol* 2000;182:290–6.
- Widmann C, Gibson S, Johnson GL. Caspase-dependent cleavage of signaling proteins during apoptosis. A turn-off mechanism for anti-apoptotic signals. *J Biol Chem* 1998;273:7141–7.
- Eray M, Tuomikoski T, Wu H, et al. Cross-linking of surface IgG induces apoptosis in a bcl-2 expressing human follicular lymphoma line of mature B cell phenotype. *Int Immunol* 1994;6:1817–27.
- Borutale V, Brown GC. Caspases are reversibly inactivated by hydrogen peroxide. *FEBS Lett* 2001;500:114–8.
- Magda D, Gerasimchuk N, Lecane P, Miller RA, Biaglow JE, Sessler JL. Motexafin gadolinium reacts with ascorbate to produce reactive oxygen species. *Chem Commun (Camb)* 2002;122:2730–1.
- Caserta TM, Smith AN, Gutlice AD, Reedy MA, Brown TL, O-VD-OPH, a broad spectrum caspase inhibitor with potent antiapoptotic properties. *Apoptosis* 2003;8:345–52.
- Chen J, Ramos J, Sisrswad M, Miller RA, Naumovski L. Motexafin gadolinium induces mitochondrially-mediated caspase-dependent apoptosis. *Apoptosis* 2005;10:1131–42.
- Hu Y, Qiao L, Wang S, et al. 3-(Hydroxymethyl)-bearing phosphatidylinositol ether lipid enolates and carbonate surrogates block PI3-K, Akt, and cancer cell growth. *J Med Chem* 2000;43:3045–51.
- Kozikowski AP, Sun H, Brognard J, Dennis PA. Novel PI enolates selectively block activation of the pro-survival serine/threonine kinase Akt. *J Am Chem Soc* 2003;125:1144–5.
- Arico S, Pettinger S, Buvay C, et al. Celecoxib induces apoptosis by inhibiting 3-phosphoinositide-dependent protein kinase-1 activity in the human cell cancer HT-29 cell line. *J Biol Chem* 2002;277:21613–21.
- Hsu AL, Ching TT, Wang DS, Song X, Rengnath VM, Chen CS. The cyclooxygenase-2 inhibitor celecoxib induces apoptosis by blocking Akt activation in human prostate cancer cells independently of Bcl-2. *J Biol Chem* 2000;275:11397–403.
- Kulp SK, Yeng YT, Hung CC, et al. 3-phosphoinositide-dependent protein kinase-1/Akt signaling represents a major cyclooxygenase-2-independent target for celecoxib in prostate cancer cells. *Cancer Res* 2004;64:1444–51.
- Lei GH, Zhang Z, Sirica AE. Celecoxib acts in a cyclooxygenase-2-independent manner and in synergy with emodin to suppress rat cholangiocarcinoma growth in vitro through a mechanism involving enhanced Akt inactivation and increased activation of caspases 9 and 3. *Mol Cancer Ther* 2003;2:265–71.
- Fuino L, Beli P, Wittmann S, et al. Histone deacetylase inhibitor LAQ824 down-regulates Her-2 and sensitizes human breast cancer cells to trastuzumab, taxotere, gemcitabine, and epothilone B. *Mol Cancer Ther* 2003;2:971–84.
- Le XF, Lammayot A, Gold D, et al. Genes affecting the cell cycle, growth, maintenance, and drug sensitivity are preferentially regulated by anti-HER2 antibody through phosphatidylinositol 3-kinase/Akt signaling. *J Biol Chem* 2005;280:2092–104.
- Shingu T, Yamada K, Hara N, et al. Synergistic augmentation of anticarcinogenic agent-induced cytotoxicity by a phosphoinositide 3-kinase inhibitor in human malignant glioma cells. *Cancer Res* 2003;63:4044–7.
- Pandya K, Phan S. Combination motexafin gadolinium (MGd) and docetaxel is active in recurrent lung and other solid tumors: results of a phase I trial. *J Clin Oncol* 2005;23:226–6.
- Ding J, Takeno T, Gao S, et al. Syk is required for the activation of Akt survival pathway in B cells exposed to oxidative stress. *J Biol Chem* 2000;275:30873–7.
- Mone AP, Huang P, Pelicano H, et al. HuD10 induces apoptosis concurrent with activation of the Akt survival pathway in human chronic lymphocytic leukemia cells. *Blood* 2004;103:1846–54.
- Shaw M, Cohen P, Alessi DR. The activation of protein kinase B by H2O2 or heat shock is mediated by phosphoinositide 3-kinase and not by mitogen-activated protein kinase-activated protein kinase-2. *Biochem J* 1998;336:241–6.
- Sonoda Y, Watanabe S, Matsumoto Y, Aizu-Yokote E, Kasahara T. FAK is the upstream signal protein of the phosphatidylinositol 3-kinase/Akt survival pathway in hydrogen peroxide-induced apoptosis of a human glioblastoma cell line. *J Biol Chem* 1999;274:10566–70.
- Wang X, McCullough DL, Franke TF, Holbrook NJ. Epidermal growth factor receptor-dependent Akt activation by oxidative stress enhances cell survival. *J Biol Chem* 2000;275:14624–31.

Intracellular Localization of the Radiation Enhancer Motexafin Gadolinium Using Interferometric Fourier Fluorescence Microscopy

KATHRYN W. WOODBURN

Pharmacycics Inc., Sunnyvale, California

Received October 20, 2000; accepted February 20, 2001

This paper is available online at <http://jpet.aspetjournals.org>

ABSTRACT

Motexafin gadolinium (MGd) is a unique therapeutic agent that localizes in cancer cells and increases tumor response to ionizing radiation and certain chemotherapeutics. The *in vitro* intracellular localization, accumulation, and retention of MGd in murine EMT6 mammary sarcoma and Rif-1 fibrosarcoma cell lines were studied using interferometric Fourier fluorescence microscopy. MGd cellular uptake was semiquantified using its characteristic fluorescence emission band centered at 758 nm. Colocalization studies were performed using mitochondrial, endoplasmic reticulum, Golgi apparatus, nuclear, and lysosomal fluorescent organelle probes, and verified using interferometric Fourier spectroscopy. Cellular uptake was gradual and in-

creased significantly with incubation time. MGd localized primarily within the lysosomes and endoplasmic reticulum, and to a lesser extent within the Golgi apparatus and mitochondria. Mitochondrial staining was increased in media without serum. No nuclear uptake was detected in the Rif-1 cells, but after 48 h nuclear uptake was observed in 15% of EMT6 cells. These results indicated that MGd accumulates within cytoplasmic compartments. The sustained intracellular localization of MGd may, in part, account for its unique radiation and chemotherapy enhancement properties. Interferometric Fourier fluorescence microscopy is a potentially powerful tool in delineating and verifying localization sites of therapeutic agents.

Fluorescence microscopy enables the spatial assignment of fluorophores within cells. The limitations of current fluorescence cellular imaging, which mainly uses filter-based systems, include endogenous autofluorescence, exogenous dye contributions, and spectral overlap between probes and the studied fluorophore. Autofluorescence artifacts occur during biological imaging; these may distort experimental findings. The major endogenous fluorophores responsible for native fluorescence include aromatic amino acids (tryptophan, 340 nm), pyridoxine (390 nm), collagen (390 nm), elastin (410 nm), reduced nicotinamide adenine dinucleotides (470 nm), flavins (550 nm), and porphyrins (630 and 690 nm), all of which may perturb single point or filter detection systems (Richards-Kortum and Sevick-Muraca, 1996). Exogenous fluorophores also may interfere with data interpretation; an example is phenol red, which serves as a pH indicator in some media or fluorescence diagnostics such as organelle probes. Additionally, the cellular microenvironment not only affects fluorescence quantum yields but also the chromophore's emission wavelength maxima and bandwidth. Fluorophores have different photodynamic activities or photobleaching properties that may lead to shifts in emissions signals. There is a need for complete fluorescence spectra

acquisition in cellular environments, which overcomes these limitations.

Fluorescence spectral bioimaging, using Fourier spectroscopy, allows spatial and spectral measurements that enable characterization of the fluorescence emission profile at every acquired pixel. A recent technique, it has been used successfully in fluorescence *in situ* hybridization applications to diagnose genetic defects by fluorescent staining, termed spectral karyotyping, of chromosomes (Schröck et al., 1996). Malik et al. (1996) have used spectral bioimaging microscopically to monitor protoporphyrin IX production after exogenous 5-aminolevulinic acid administration. Subsequent illumination of the cells caused photobleaching and photoproduct formation, with a distinctly different spectral peak appearing in the acquired spectrum.

In this study, a similar system was used to correctly identify the fluorophore motexafin gadolinium (MGd) in intracellular sites after MGd treatment. The biolocalization of MGd was confirmed by co-staining with organelle-specific probes and spectral overlay. MGd is a radiation enhancer that targets tumors and is now in human clinical trials (Rowinsky, 1999). To better understand the biochemical mechanisms that underlie these activities cell culture localization studies

ABBREVIATIONS: MGd, motexafin gadolinium; MTG, MitoTracker Green FM; LTR, LysoTracker red DND-99; C₆-ceramide, BODIPY FL C₆-ceramide; R6, Rhodamine B, hexyl ester, perchlorate; HO342, Hoechst 33342; FBS, fetal bovine serum; CCD, charge-coupled device; FWHM, full-width half-maximum.

were performed. Here, wavelength-dependent microenvironmental changes, photobleaching, and subcellular fluorophore concentrations after MGd treatment were determined in both the murine R1-fibrosarcoma and EMT6 mammary sarcoma cell lines.

Materials and Methods

Chemicals. The synthesis and chemical characterization of MGd (also known as gadolinium texaphyrin, NSC #695238) used in this study has been described previously (Sessler et al., 1999). The compound was formulated in 5% aqueous mannitol, and the pH was adjusted to 5.5 with acetic acid to yield a final MGd concentration of 2.2 mM. Fluorescent probes for staining mitochondria (MitoTracker Green FM; MTG), lysosomes (LysoTracker red DND-99; LTR), Golgi apparatus (BODIPY FL C_2 -ceramide, C_2 -ceramide), endoplasmic reticulum (Rhodamine B, hexyl ester, perchlorate; R6), and the nucleus (Hoechst 33342; HO342) were purchased from Molecular Probes (Eugene, OR).

Cells. Murine EMT6 mammary sarcoma and R1-f radiation-induced fibrosarcoma cell lines were maintained through established *in vivo* vitro propagation procedures (Rockwell et al., 1972; Young et al., 1996). Cells were grown in Waymouth's medium (MB752/1; Life Technologies, Grand Island, NY) supplemented with 14% fetal bovine serum (FBS; JRH Biosciences, Woodland, CA) and penicillin/streptomycin (Sigma, St. Louis, MO).

Colony Survival Assay. EMT6 cells were cultured and harvested into 25-cm² plastic tissue culture flasks at a density of 200 cells/flask. Twenty-four hours was allowed for cell attachment to the flask at 37°C and 5% CO₂. MGd was added to yield a range of final concentrations from 0 to 160 μ M. After 2 or 24 h MGd exposure the cells were washed three times with growth media without serum. The flasks were replenished with serum-supplemented media and returned to the incubator for an additional 6 to 10 days. The colonies were fixed with 10% buffered formalin and stained with crystal violet. Each determination was performed in triplicate and repeated twice for each data point.

Fluorescence Spectral Bioimaging. Female BALB/c mice, 7 to 8 weeks old, were purchased from Simonsen Laboratories, Gilroy, CA. Animals received care in compliance with the Guide for the Care and Use of Laboratory Animals (National Institutes of Health publication, 1996). The right flanks of the mice were shaved and depilated with Nair (Carter-Wallace, Inc., New York, NY) the day prior to tumor inoculation. EMT-6 cells ($5-7 \times 10^5$) were subcutaneously implanted into the right hind flanks of recipient mice. The tumor-bearing animals were studied 7 to 10 days after implantation (tumor size approximately 70 mm³).

EMT6 tumor-bearing mice (four mice per group) were intravenously injected, via the tail vein, with either 40 μ M MGd/kg or control vehicle (5% mannitol in water) and then subject to spectral bioimaging 5 h following administration. Prior to imaging, each mouse was anesthetized with an intraperitoneal injection of xylazine (10 mg/kg; Rompun, Mobay Corporation, Ames, KS) and ketamine (90 mg/kg; Vetalar; Aveco Corporation, Fort Dodge, IA) and placed in the prone position on black cloth. The tumor and surrounding normal skin were illuminated with 470-nm light and the resultant fluorescence captured with the SD200 SpectraCube system (Applied Spectral Imaging, Carlsbad, CA). The spectral bioimaging system incorporates a Sagnac interferometer and a thermoelectrically cooled charge-coupled device (CCD) camera (512EFT; Roper Scientific, Trenton, NJ) that exhibits maximal quantum efficiency in the near-infrared enabling the detection of the unique MGd fluorescence emission band centered at 758 nm. The spectral range used was 400 to 850 nm, the spectral resolution from 400 to 540 nm was 2 nm, whereas from 540 to 850 nm it was typically 3 to 5 nm. The SD200 system is connected, via a C-mount, to a Nikon macro lens enabling the capturing of both black and white fluorescence images. The

excitation light was delivered from a xenon lamp (Cogent Light Technologies, Inc., Santa Clara, CA) via a multimode fiber terminating with a 470-nm interference filter (10-nm bandwidth; Oriol Corporation, Stratford, CT); a 695-nm long-pass filter (Oriol Corporation) was incorporated into the emission path. Each signal was averaged over 5 pixels.

Fluorescence Microscopy. The cells were seeded (4×10^4) into Lab-Tek 10-cm² flaskette glass chamber slides (Nunc, Inc., Naperville, IL) containing 4 ml of media. The cells were allowed to incubate for 24 h to enable attachment to the flask. MGd was added to the media to yield a final concentration of 25 μ M/ml and incubated for predetermined amounts of time. After the incubation, the cells were washed with serum-free media, coverslipped, and sealed with nail polish. The specimens were viewed using a 63 \times oil-immersion objective via a Zeiss AxioPlan-2 microscope. The SD200 SpectraCube system was coupled to the microscope via a C-mount. Both fluorescence and phase contrast micrographs were captured. All cell preparations were performed in triplicate.

Organelle-specific fluorescent probes were used: MTG, used to stain the mitochondria; LTR to stain the lysosomes; R6 to label the endoplasmic reticulum; C_2 -ceramide to stain the Golgi apparatus; and HO342 to stain the nucleus. Filter cubes optimized to match the spectral properties of the dyes and also integrated to match the coincident excitation wavelength of the MGd were chosen. A 360-nm bandpass filter (40 nm FWHM); a 400-nm dichroic filter and 420-nm long-pass filter were used to visualize HO342. A 485-nm bandpass (22-nm FWHM) filter, a 505-nm dichroic filter, and a 530-nm emission bandpass filter (30-nm FWHM) were used to confirm MTG's fluorescence. LTR and R6 both required 535-nm (50-nm FWHM) excitation filters, 565-nm dichroic filters, and 590-nm long-pass emission filters. For visualizing the Golgi apparatus, a 470-nm bandpass filter (40-nm FWHM); a 505-nm dichroic filter, and a 515-nm long-pass filter were used. For MGd detection, the cells were excited using a 470-nm bandpass filter (40-nm FWHM), 505-nm dichroic filter, and either a 515- or a 715-nm long-pass filter.

Caution was used when fluorophores were observed, since some organelle dyes become photosensitizing agents or photobleach (degrade) when subjected to high-intensity illumination, or low intensities for long exposure times (Twentyman et al., 1980; Woodburn et al., 1991). The samples were therefore illuminated with 63 mW/cm² from an HBO/100-W mercury lamp. Neutral red and LysoTracker blue DND-22 were considered candidate lysosomotropic fluorescent probes for this study; however, they proved to be photolabile using the illumination conditions described here. Neutral red is particularly photoreactive; after localization to the lysosomes and following light exposure, the lysosomes ruptured and fluorescence dispersed. LysoTracker blue DND-22 readily photobleached in the presence of MGd, but did not stain well in the absence of serum.

The following dye concentrations and incubation times were used for staining specific organelles: 0.5 μ M of HO342/ml for 10 min; 500 nM R6 for 30 min; 50 nM LTR for 1 h; 0.5 mg/ml BODIPY FL C_2 -ceramide for 10 min; and 250 nM MTG for 30 min. Phase contrast and fluorescence images were stored electronically and color processed using the EasyFISH software (Applied Spectral Imaging).

Results

In Vivo Fluorescence Imaging. The chemical structure, absorption, and fluorescence profile of MGd is shown in Fig. 1. MGd has a large Soret band at 473 nm ($\log \epsilon = 5.06$). Due to its extended porphyrin aromatic conjugation system, the texaphyrin macrocycle has a low-energy band occurring at 740 nm ($\log \epsilon = 4.59$). The signature fluorescence emission band of MGd is centered at 758 nm and was used to monitor real-time MGd biolocalization in EMT6 mammary sarcoma-bearing mice. The animals were intravenously injected with MGd (40 μ M/kg) and then the tumor and surrounding

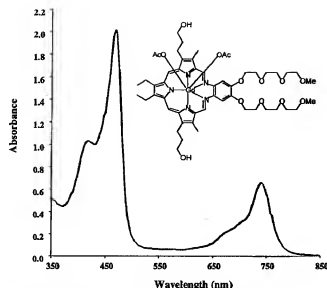


Fig. 1. Chemical structure of MGd and an absorption spectrum of 25 $\mu\text{g/ml}$ MGd in phosphate-buffered saline with 10% FBS.

normal skin were illuminated with 470-nm light, corresponding to the Soret band, 5 h postinjection. The resultant fluorescence emission signals were captured with a CCD camera coupled to an interferometer, and then the signal was Fourier-transformed, allowing spectral identification at each pixel (Fig. 2). Integration of the signal over the emission captured range (720–780 nm), for four animals, and subtraction of the endogenous fluorescence revealed a 6-fold enhancement in the tumor relative to surrounding normal tissue.

MGd Photobleaching. The fluorescence quantum yield of MGd is low. However, it can be used for detection and quantitation due to the large extinction coefficient at the excita-

tion wavelength of 473 nm ($\log \epsilon = 5.06$), a large Stokes shift (758 nm), and a detection system that exhibits optimal quantum efficiencies in the desired wavelengths. Because irreversible destruction or photobleaching of the fluorophore limits the illumination intensity and time of exposure, studies were undertaken to determine the effect of illumination on MGd photobleaching. An illumination intensity of 63 mW/cm² caused no significant photobleaching, whereas using an intensity of 209 mW/cm² did (Fig. 3). Interestingly, repeating an illumination at 63 mW/cm² did not significantly change the fluorescence profile and emission (data not shown).

Uptake Kinetics. The localization of MGd in EMT6 and Rif-1 cells was evaluated for incubation periods up to 72 h in medium supplemented with 14% FBS. No inherent cytotoxicity, measured using a clonogenic assay, was observed using MGd concentrations up to 150 μM in serum supplemented medium (data not shown). Using a 72-h incubation time in serum-free medium the IC₅₀ was 25 μM so for serum-free media experiments incubation periods were confined to 24 h or less.

A time-dependent increase in intracellular MGd fluorescence was seen in both cell lines. Distinct, punctate localization patterns were observed that became more defined with incubation time. A typical fluorescence pattern for EMT6 cells is shown in Fig. 4b that was obtained after incubation of MGd for 4 h. MGd, noted by its characteristic 758-nm profile, was not present in the nuclei. Uptake, based on the use of the previously mentioned organelle probe stains, appeared to occur in the lysosomes, endoplasmic reticulum, and some mitochondria. A large fluorescence signal was detected in the perinuclear region, suggestive of localization of MGd within the Golgi apparatus. Generally, MGd was not present in the nuclei; however, 15% of cells showed nuclear association in the EMT6 cell line after long incubation intervals. In this small subset, as much as 40% of MGd was present within the

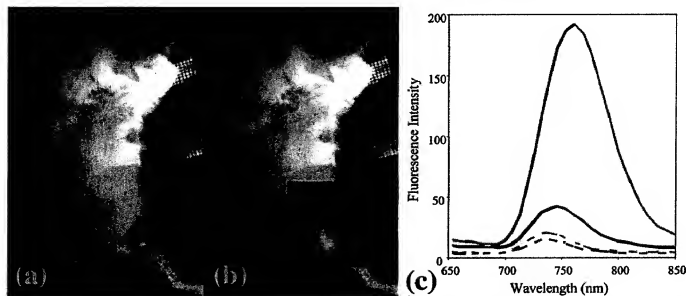


Fig. 2. Fluorescence spectral biocaging of MGd in an EMT-6 mammary sarcoma-bearing mouse. A black-and-white photo illustrating the tumor-bearing mouse in the prone position is shown in a. The mouse received 40 $\mu\text{mol/kg}$ MGd and was spectral-imaged 5 h after intravenous administration. A fluorescence spectral typing map, using a pixel classification of 720 to 780 nm, was obtained and overlaid on the pre-imaged black-and-white photo (b). Two pixel areas, averaged from four animals, showing tumor (orange) and nontumor (green) regions from animals receiving MGd (full lines) and receiving no MGd (dashed lines), were processed to yield fluorescence emission profiles (c). The curves represent average values \pm 20%.

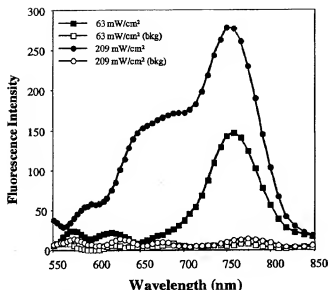


Fig. 3. Fluorescence spectra of MGD-treated Rif-1 cells. Cells were incubated with 25 $\mu\text{g}/\text{ml}$ MGD and then imaged at 24 h with an illumination intensity of 63 mW/cm^2 (■) followed by another acquisition using 209 mW/cm^2 (●). The data reflect fluorescence pixels (3×3) within a punctate fluorescent area compared with background (background, open symbols).

nuclei (Fig. 5, b and c). The nuclear membranes were well defined, and fluorescent areas were seen in a compartmentalized manner throughout the cytoplasm.

The temporal uptake of both cell lines, with and without serum supplementation, is shown in Fig. 6. It is important to note that the obtained spectra were taken from typical punctate localization sites within the cells and, as such, were not reflective of the total cellular content. The fluorescence intensity significantly increased with time; little signal was detected after 2 h, and was sparsely located throughout the cytoplasm. Large signals were clearly defined at the later time points. Omitting serum from the medium increased MGD uptake.

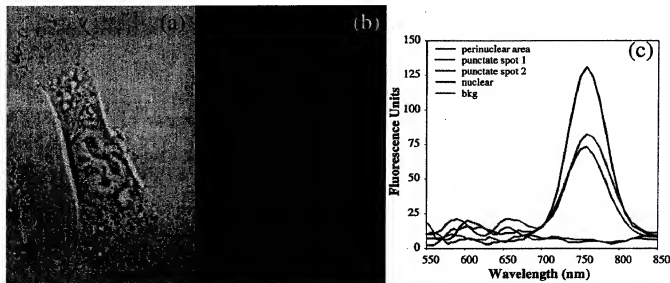


Fig. 4. MGD localization within EMT6 cells. EMT6 cells were treated for 4 h with 25 $\mu\text{g}/\text{ml}$ MGD. The transmission and fluorescence micrographs are illustrated in a and b, respectively. The fluorescence emission spectra, analyzed at various regions, are shown in c.

EXHIBIT 2

PAGE 19

Staining with Organelle Probes. The subcellular localization of each of the studied organelle probes was confirmed based on the unique staining patterns of the Rif-1 and EMT6 murine cell lines. Typical localization patterns for the murine radiation-induced fibrosarcoma cell line (Rif-1) are illustrated in Fig. 7. In Fig. 7b, the cells were sequentially stained with LTR, C5-ceramide, and HO342. The red fluorescent LTR stains the lysosomes, the green C5-ceramide targets the Golgi apparatus, and the blue fluorescent HO342 accumulates in the nuclei. Three exposures, with specific filter cubes matched to each probe, were acquired and then overlaid to yield the depicted image. Figure 7c denotes the distinct green curlicue staining characteristic of the mitochondria, and Fig. 7d shows the red fluorescent R6 accumulating in the endoplasmic reticulum.

The intracellular fluorescence emission profiles of each of the organelle probes was acquired using spectral bioimaging. The normalized fluorescence emission spectra obtained using filter cubes matched to each of the probe's specific spectral properties are shown in Fig. 8. The emission maxima for C5-ceramide, HO342, MTG, R6, and LTR were 522, 527, 533, 599, and 612 nm, respectively. C5-ceramide possesses concentration- and environment-dependent properties. At high concentrations, C5-ceramide forms longer wavelength excimers (excited state dimers) in the Golgi apparatus that result in a wavelength shift from 522 to 637 nm (Fig. 8b). R6 fluorescence can also be observed, but with less fluorescence output, with the MGD/C5-ceramide filter cube, and yields an emission maximum of 584 nm.

Colabeling with Organelle Probes. After exposure of the cells to MGD for varying times, organelle-specific fluorophores were added for colocalization studies. It was necessary to wash the cells with serum-free medium before incubation with the organelle-specific probes, because most probes, and also the MGD, are planar aromatic systems and may interact noncovalently and cause unwanted artifacts that change biolocalization. Dichroic and emission filters were used because, for multispectral labeling, it is ideal that the dye undergoing analysis and the organelle-specific flu-

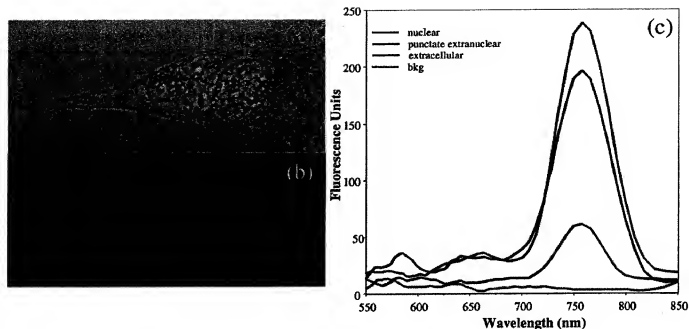


Fig. 5. MGD localization in the nucleus of EMT6 cells after an incubation of 48 h. Transmission and fluorescence micrographs are depicted in a and b, respectively. Emission profiles for the nuclear, extranuclear punctate, cytoplasmic, and extracellular regions are shown in c.

orophore have the same coincident wavelength custom excitation. Special attention was given to the long-pass filters, so the different fluorophores could be simultaneously spectrally resolved at every pixel within the CCD array study area.

Colocalization labeling using the various fluorophores confirmed MGD uptake was within the lysosomes and endoplasmic reticulum, with less partitioning into the mitochondria and Golgi apparatus at early incubation times (<24 h) in both the EMT6 and Rif-1 cell lines. At longer incubation times there was more MGD present within the Golgi appara-

tus. For example, Fig. 9b shows the overlay staining of MGD, HO342, and LTR in Rif-1 cells. The cells were incubated with 25 μ g/ml MGD for 6 h. The overlay involved the three filter cube sets responsible for HO342, LTR, and 715-nm long-pass MGD. The nuclei were distinctly defined by the blue staining of HO342. Both LTR (red) and MGD (yellow) staining were in punctate areas, often overlapping; several areas were distinctly isolated from each other. Spectral analysis for four different extranuclear pixel areas using the 520 nm long-pass filter set, is shown in Fig. 9d. The blue line denotes a distinct yellow pixel area from Fig. 9b, revealing the presence of MGD. The other lines represent colocalization areas of MGD and LTR. It is apparent that MGD was present in nearly all lysosomes, but not all of the MGD was associated with lysosomal uptake.

Longer incubation times (72 h) indicated higher partitioning within the Golgi apparatus (data not shown). Spectral analysis using the 520-nm long-pass filter set, used to capture both the C_2 -ceramide and MGD fluorescence, revealed areas of colocalization of the C_2 -ceramide with MGD. It is interesting to note that not all the Golgi showed MGD association and that which did, did not exhibit excimer formation (data not shown).

Discussion

Motexafin gadolinium, or MGD, is a paramagnetic, aqueous-soluble expanded pentadentate porphyrinoid that is selective for neoplastic cells (Young et al., 1996). MGD alone, using the conditions described here, has no observed therapeutic impact. However, radiation enhancement with MGD in combination with radiation therapy has been seen in single and multifraction studies in experimental tumor models (Miller et al., 1999; Minamikawa et al., 1999). MGD is presently in a phase III clinical trial for patients undergoing whole brain radiation therapy for brain metastases (Rowin-

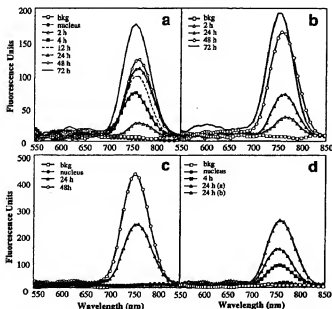


Fig. 6. Time-dependent localization of MGD in punctate regions of EMT6 and Rif-1 cells. Temporal profiles of EMT6 and Rif-1 cells in serum-supplemented medium are shown in a and b, whereas those in medium lacking serum are shown in c and d, respectively. Data were averaged from 10 cells.

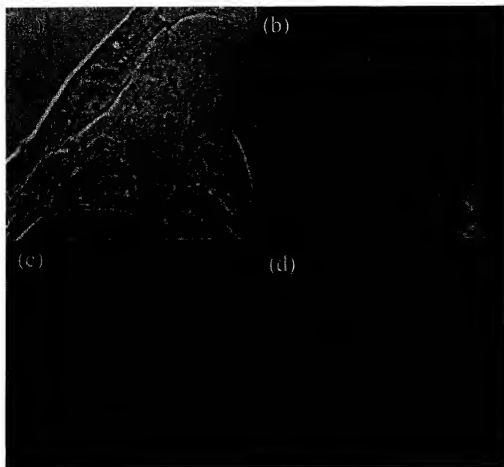


Fig. 7. Representative staining of Rif-1 cells with fluorescent organelle-specific probes. In the transmission micrograph in a, cells were stained with fluorescence probes (b) specific for the nuclei (blue), Golgi apparatus (green), and lysosomes (red). The fluorescence micrograph in c depicts the mitochondria as green and the nuclei as blue. The endoplasmic reticulum is illustrated by the red staining in d, with the nuclei appearing blue.

sky, 1999) and is also being evaluated in nonclinical models as a chemosensitizer with doxorubicin and bleomycin.

Intracellular localization studies may provide mechanistic insights into MGd's mode of action as both a radiation enhancer and a chemosensitizer. Some discordance has been observed when assessing *in vitro* radiation responses as MGd displayed minimal radiation enhancement in *in vitro* clonogenic assays, whereas good tumor responses were recorded in murine models (Miller et al., 1999). It is hoped that interferometric Fourier fluorescence microscopy may aid in defin-

ing the importance of tumor-host interactions versus intracellular interactions.

Noninvasive spectral bioimaging of EMT6 tumor-bearing mice showed enhanced localization of MGd in the sarcoma compared with the surrounding normal tissue, resulting in an enhancement ratio of 6 to 1. The latter fluorescent result was in accord with previous studies using magnetic resonance imaging to detect the paramagnetic gadolinium coordinated into the central core of the macrocycle and ^{14}C -labeled MGd (Miller et al., 1999; Minamikawa et al., 1999). The latter radiolabeled biodistribution study performed in SMT-F mammary tumor-bearing mice yielded a tumor-to-muscle ratio of 8.5 to 1 at 5 h after intravenous administration of 9.9 μmol MGd/kg (Miller et al., 1999). It may also be possible to study the intracellular localization of MGd using subcellular fractionation with radiolabeled MGd. However, cultured cells are difficult to fractionate, they are more problematic than tissues due to differences in cytoskeletal organization, and additionally, with subfractionation it is difficult to cleanly resolve many organelles into distinct fractions (Howell et al., 1989; Pasquali et al., 1999), so alternative more facile approaches to discerning intracellular localization sites of drugs are sought.

The uptake of MGd within EMT6 and Rif-1 cells, assessed using interferometric Fourier fluorescence microscopy was immediate. Retention increased significantly with time and was more pronounced in serum-free media. MGd partitioned within the lysosomes, endoplasmic reticulum, and, to a lesser extent, the Golgi apparatus and mitochondria in serum-sup-

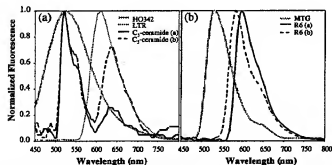


Fig. 8. *In vitro* normalized fluorescence emission spectra of organelle-specific fluorophores. The emission maxima for HO342, C5-ceramide, and LTR are shown in a. C5-ceramide, at high concentrations in the Golgi apparatus, forms longer wavelength excimers that result in a wavelength shift from 522 nm, C5-ceramide (a), to 637 nm, C5-ceramide (b). The normalized fluorescence emission spectra of MTG and R6 are shown in b. R6 fluorescence was observed with two filter cubes, the custom filter cube, R6 (a), and the MGd/C5-ceramide filter cube, R6 (b).

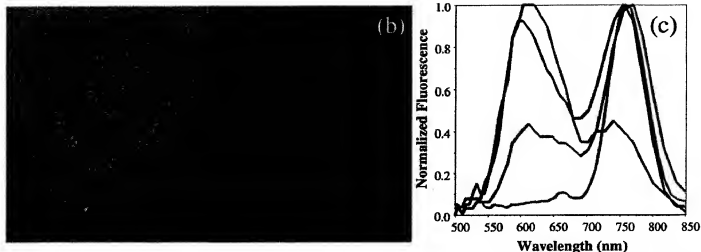


Fig. 9. Colocalization of MGD within lysosomes. Rif-1 cells were incubated with MGD for 6 h in serum-supplemented medium and then incubated with LTR and HO342. A transmission micrograph is shown in a, and a multiple exposure image obtained with filter sets appropriate for HO3423 (blue), LTR (red), and MGD (yellow) is shown in b. Spectral analysis of four extranuclear pixel areas is depicted in c.

plemented medium. Only in 15% of EMT6 cells, at 48 h, was MGD observed in the nucleus. In serum-free medium, more MGD was partitioned within the mitochondria.

Interferometric Fourier fluorescence microscopy is a potentially valuable technique that will resolve subcellular localization of fluorophores using known organelle-specific markers. Fluorescence is often wavelength-dependent, and varies with alterations in kinetic and physiological factors with different cellular compartments. The latter cannot be analyzed from single-point determinations as is obtained using fluorescence filter technology. Monitoring the fluorescence emission range not only aids in subcellular localization studies but is also valuable in assessing cellular changes using different biochemical markers. Experiments of this kind are currently in progress in this laboratory.

References

- Elgohary WG, Sidhu S, Krescoski SO, Petering DH and Byrnes RW (1998) Protection of DNA in HL-60 cells from damage generated by hydroxyl radicals produced by reaction of H_2O_2 with cell iron by zinc-metallothionein. *Chem Biol Interact* 115: 85-107.
- Howell KE, Devaney E and Gruenberg J (1989) Subcellular fractionation of tissue culture cells. *Trends Biol Sci* 14:44-47.
- Malik Z, Dishi M and Garini Y (1996) Fourier transform multipixel spectroscopy and spectral imaging of protoporphyrin in single melanoma cells. *Photochem Photobiol* 63:608-614.
- Minamikawa T, Sriratanana A, Williams DA, Bowser DN, Hill JS and Nagley P (1999)

- Chloromethyl-X-rosamine (MitoTracker Red) photosensitizes mitochondria and induces apoptosis in intact human cells. *J Cell Sci* 112:2419-2430.
- Miller RA, Woodburn K, Fan Q, Renachier MF, Seesler JL and Koutcher JA (1999) In vivo animal studies with gadolinium (III) texaphyrin as a radiation enhancer. *Int J Rad Oncol Biol Phys* 45:981-989.
- Pasquali C, Fialka I and Huber LA (1999) Subcellular fractionation, electromigration analysis and mapping of organelles. *J Chromatogr B* 729:89-102.
- Richards-Kortum R and Sevick-Muraca E (1996) Quantitative optical spectroscopy for tissue diagnosis. *Annu Rev Phys Chem* 47:555-606.
- Rockwell SC, Kallman RF and Fajardo LF (1972) Characterization of a serially transplanted mouse mammary tumor and its tissue culture adapted derivative. *J Natl Cancer Inst* 49:735-745.
- Rowinsky ER (1999) Novel radiation sensitizers targeting tissue hypoxia. *Oncology* 13:61-70.
- Schreck E, du Manoir S, Veldman T, Schoell B, Wienberg J, Ferguson-Smith MA, Ning Y, Ledbetter DH, Bar-Am I, Soenksen D, et al. (1996) Multicolor spectral karyotyping of human chromosomes. *Science (Wash DC)* 273:494-497.
- Seesler JL, Tvermoes NA, Galdi DM, Mody TD and Allen WE (1999) Ona-electron reduction and oxidation studies of the radiation sensitizer gadolinium(III) texaphyrin (PCI-0120) and other water soluble metallotexaphyrins. *J Phys Chem* 103:757-764.
- Twentymann PR, Brown JM, Gray JW, Franko AJ, Scoles MA and Kallman RF (1980) A new mouse tumor model system (Rif-1) for comparison of end-point studies. *J Natl Cancer Inst* 64:585-604.
- Woodburn KW, Vardas NJ, Hill JS, Kaye AH and Phillips DR (1991) Subcellular localization of porphyrins using confocal laser scanning microscopy. *Photochem Photobiol* 54:725-732.
- Young SW, Qing F, Harriman A, Seesler JL, Dow WC, Mody TD, Hemmi GW, Hao Y and Miller RA (1999) Gadolinium(III) texaphyrin: a tumor selective radiation sensitizer that is detectable by MRI. *Proc Natl Acad Sci USA* 93:6610-6615.

Send reprint requests to: Kathryn W. Woodburn, Ph.D., Pharmacycics, 995 East Arques Ave., Sunnyvale, CA 94086. E-mail: KWoodburn@pcyc.com



A service of the National Library of Medicine
and the National Institutes of Health

www.pubmed.gov

My NCBI
[Sign In] [Register]
Entrez 2.0

All Databases PubMed Nucleotide Protein Genome Structure OMIM PMC Journals Book

Search PubMed for

Limits Preview/Index History Clipboard Details

Display AbstractPlus

All: 1 Review: 0

☐ 1: Int J Radiat Oncol Biol Phys. 2001 Apr 1;49(5):1381-90.

ELSEVIER Links
FULL-TEXT ARTICLE

Effects of Motexafin gadolinium on tumor metabolism and radiation sensitivity.

Xu S, Zakian K, Thaler H, Matei C, Alfieri A, Chen Y, Koutcher JA.

Department of Medical Physics, Memorial Sloan Kettering Cancer Center, New York, NY 10021, USA.

PURPOSE: Experiments were undertaken to determine if metabolic changes induced by Motexafin gadolinium (Gd-Tex (+2), XCYTRIN) predict time intervals between drug and radiation wherein there is enhancement of radiation efficacy. **METHODS AND MATERIALS:** We evaluated the effect of Gd-Tex (+2) on tumor metabolism and on tumor growth using a mouse mammary carcinoma model and ^{31}P nuclear magnetic resonance (NMR) experiments. Response to therapy was evaluated based on time for the tumor to regrow to pretreatment size and also tumor doubling time. **RESULTS:** ^{31}P NMR experiments indicated that Gd-Tex (+2) effected tumor energy metabolism during the first 24 hours postadministration. A decrease in phosphocreatine was noted at 2 ($p < 0.04$), 6 ($p < 0.006$), and 24 ($p < 0.001$) hours post Gd-Tex (+2). A decrease in nucleoside triphosphates was noted only at 2 hours ($p < 0.02$), with subsequent recovery at 6 hours. Phosphocreatine in control (saline treated) tumors showed a significant decrease only at 24 hours ($p < 0.01$). Irradiation at 2 and 6 hours post Gd-Tex (+2) induced an enhanced effect compared to radiation alone as measured by analyzing the growth curves, maximum tumor volumes, and the time for the tumors to regrow to their initial volumes. Irradiation at 24 hours post Gd-Tex (+2) induced a modest enhancement in tumor growth delay compared to radiation alone. **DISCUSSION:** NMR spectroscopy may be useful for monitoring tumor metabolism after treatment with Gd-Tex (+2) and administering radiation during the time of maximal efficacy of Gd-Tex (+2).

PMID: 11286846 [PubMed - indexed for MEDLINE]

Related Links

- ▶ In vivo animal studies with gadolinium (III) texaphyrin as a radiation enhancer [Int J Radiat Oncol Biol Phys. 1999]
- ▶ The in vivo effect of bryostatin-1 on paclitaxel-induced tumor growth, mitotic entry, and ~~radiation~~ ^{radiosensitization} [Cancer Res. 2000]
- ▶ Re-evaluating gadolinium(III) texaphyrin as a radiosensitizer [Cancer Res. 2000]
- ▶ Modulation of murine radiation-induced fibrosarcoma-1 tumor metabolism and blood flow in situ via glucose and mannitol administration monitored by ^{31}P and ^2H nuclear magnetic resonance spectroscopy [Cancer Res. 1991]
- ▶ Redox cycling by motexafin gadolinium enhances cellular response to ionizing radiation by forming reactive oxygen species. [Int J Radiat Oncol Biol Phys. 2001]

See all Related Articles...

Display AbstractPlus

EXHIBIT 2
PAGE 23

[Write to the Help Desk](#)



A service of the National Library of Medicine
and the National Institutes of Health

My NCBI
[Sign In] [Register]
Entrez 2.0

All Databases PubMed Nucleotide Protein Genome Structure OMIM PMC Journals Book

Search PubMed for [] Go Clear

Limits Preview/Index History Clipboard Details

Display AbstractPlus Show 20 Sort by Send to

All: 1 Review: 1

1: Expert Opin Pharmacother. 2007 Feb;8(3):351-9.



Links

Motexafin gadolinium in the treatment of brain metastases.

Richards GM, Mehta MP.

University of Wisconsin School of Medicine and Public Health,
Department of Human Oncology, Madison, WI 53792, USA.

Motexafin gadolinium (MGd) is a novel, MRI-detectable, anticancer agent that enhances the cytotoxic potential of radiation therapy through several mechanisms, including depleting intracellular reducing metabolites that are necessary for repairing the oxidative damage induced by irradiation. It has tumor-specific uptake, normal tissue sparing, and tolerable and reversible toxicities in clinical trials. MGd's use in conjunction with whole-brain radiation therapy (WBRT) has demonstrated an improvement in neurocognitive decline, neurologic progression, and quality of life in patients with brain metastases from NSCLC. Its use in conjunction with radiosurgery and whole brain radiation therapy in the setting of brain metastases is currently being studied, as is MGd with radiation and temozolomide in patients with glioblastoma multiforme. MGd is also being actively investigated as a single agent or in combination with chemotherapy or radiation therapy in other tumors, including pediatric brain tumors, NSCLC, lymphoma, renal cell carcinoma, and pancreatic and biliary tumors.

PMID: 17266469 [PubMed - indexed for MEDLINE]

Related Links

- Motexafin gadolinium: a redox-active tumor selective agent for the treatment of cancer (Curr Opin Oncol. 2004)
- Neurocognitive function and progression in patients with brain metastases treated with whole-brain radiation and motexafin gadolinium: results of a randomized trial (J Clin Oncol. 2004)
- Lead-in phase to randomized trial of motexafin gadolinium and whole-brain radiation for patients with brain metastases: centralized assessment of magnetic resonance imaging, neurocognitive, and neurologic endpoints. (J Clin Oncol. 2002)
- Survival and neurologic outcomes in a randomized trial of motexafin gadolinium and whole-brain radiation therapy in brain metastases (J Clin Oncol. 2003)
- Motexafin gadolinium: gadolinium (III) texaphyrin, gadolinium texaphyrin, Gd-Tex. GdT282, PCI 012Q (Drugs R.D. 2004)

See all Related Articles...

Display AbstractPlus Show 20 Sort by Send to

Write to the Help Desk
NCBI | NLM | NIH
Department of Health & Human Services
Privacy Statement | Freedom of Information Act | Disclaimer

EXHIBIT 2
PAGE 24



A service of the National Library of Medicine
and the National Institutes of Health

My NCBI
[Sign In] [Register]
Entrez 2.0

All Databases PubMed Nucleotide Protein Genome Structure OMIM PMC Journals Book

Search PubMed for [Go] [Clear]

Limits Preview/Index History Clipboard Details

Display AbstractPlus Show 20 Sort by Send to

All: 1 Review: 1

1: Expert Opin Investig Drugs, 2003 Jul;12(7):1205-10.



Links

Motexafin gadolinium: a possible new radiosensitiser.

Rodrigus P.

Dr B Verbeeten Institute, PO Box 90120, 5000 LA Tilburg, The Netherlands.

Motexafin gadolinium (MGd, PCI-0120, Xcytrin, a metallotexaphyrin developed by Pharmacyclics, is a redox active drug that selectively targets tumour cells with a potential action as a radiosensitiser. In vitro and in vivo models showed radiation enhancement when radiation followed MGd administration. Phase I and II clinical studies showed that MGd was well-tolerated with a maximum-tolerated dose set at 6.3 mg/kg. Acute side effects of discolouration of the sclera, skin and urine are reversible. The clinical efficacy was determined in an international Phase III trial for brain metastases with a significant difference in time to neurological progression for lung cancer brain metastases in favour of MGd and whole brain radiation versus whole brain radiation only. For the treatment of glioblastoma multiforme, promising results are found in a Phase I trial with a median survival of 17.3 months. Further investigation of the combination of MGd and radiotherapy will be worthwhile.

PMID: 12831354 [PubMed - indexed for MEDLINE]

Related Links

- ▶ Motexafin gadolinium: gadolinium (III) texaphyrin, gadolinium texaphyrin, Gd-Tex, GdT2B2, PCI 0120 [Drugs R.D. 2004]
- ▶ Survival and neurologic outcomes in a randomized trial of motexafin gadolinium and whole-brain radiation therapy in brain metastases [J Clin Oncol. 2003]
- ▶ Motexafin gadolinium: a clinical review of a novel radioenhancer for brain tumors. [Expert Rev Anticancer Ther. 2004]
- ▶ Motexafin gadolinium: a redox-active tumor selective agent for the treatment of cancer [Curr Opin Oncol. 2004]
- ▶ Multicenter phase Ib/II trial of the radiation enhancer motexafin gadolinium in patients with brain metastases. [J Clin Oncol. 2001]

See all Related Articles...

Display AbstractPlus Show 20 Sort by Send to

Write to the Help Desk

NCBI | NLM | NIH

Department of Health & Human Services

[Privacy Statement](#) | [Freedom of Information Act](#) | [Disclaimer](#)

A service of the National Library of Medicine
and the National Institutes of HealthMy NCBI
[Sign In] [Register]
Entrez 2.0

All Databases

PubMed

Nucleotide

Protein

Genome

Structure

OMIM

PMC

Journals

Book

Search PubMed



for

Go

Clear

Limits Preview/Index History Clipboard Details

Display AbstractPlus

Show 20

Sort by

Send to

All: 1 Review: 0

1: Clin Cancer Res. 2006 Jan 1;12(1):206-13.

Final Version FREE Links
Clin Cancer Res**Motexafin-gadolinium taken up in vitro by at least 90% of glioblastoma cell nuclei.****De Stasio G, Rajesh D, Ford JM, Daniels MJ, Erhardt RJ, Frazer BH, Tyliczszak T, Gilles MK, Conhaim RL, Howard SP, Fowler JF, Estève F, Mehta MP.**Department of Physics and Synchrotron Radiation Center, University of Wisconsin-Madison, Stoughton, Wisconsin 53589, USA.
pupa@src.wisc.edu

PURPOSE: We present preclinical data showing the in vitro intranuclear uptake of motexafin gadolinium by glioblastoma multiforme cells, which could serve as a prelude to the future development of radiosensitizing techniques, such as gadolinium synchrotron stereotactic radiotherapy (GdSSR), a new putative treatment for glioblastoma multiforme.

EXPERIMENTAL DESIGN: In this approach, administration of a tumor-seeking Gd-containing compound would be followed by stereotactic external beam radiotherapy with 51-keV photons from a synchrotron source. At least two criteria must be satisfied before this therapy can be established: Gd must accumulate in cancer cells and spare the normal tissue; Gd must be present in almost all the cancer cell nuclei. We address the in vitro intranuclear uptake of motexafin gadolinium in this article. We analyzed the Gd distribution with subcellular resolution in four human glioblastoma cell lines, using three independent methods: two novel synchrotron spectromicroscopic techniques and one confocal microscopy. We present in vitro evidence that the majority of the cell nuclei take up motexafin gadolinium, a drug that is known to selectively reach glioblastoma multiforme.

RESULTS: With all three methods, we found Gd in at least 90% of the cell nuclei. The results are highly reproducible across different cell lines. The present data provide evidence for further studies, with the goal of developing GdSSR, a process that will require further in vivo animal and future clinical studies.

PMID: 16397044 [PubMed - indexed for MEDLINE]

Related Links

- ▶ Motexafin gadolinium: gadolinium (III) texaphyrin, gadolinium texaphyrin, Gd-Tex, GdT282, PCI 012Q [Drugs R.D. 2004]
- ▶ MRI measurement of the uptake and retention of motexafin gadolinium in glioblastoma multiforme and uninvolved normal human brain. [Neurobiol. 2006]
- ▶ Are gadolinium contrast agents suitable for gadolinium neutron capture therapy? [Neurol Res. 2005]
- ▶ Gadolinium in human glioblastoma cells for gadolinium neutron capture therapy. [Cancer Res. 2001]
- ▶ Motexafin gadolinium: a possible new radiosensitizer. [Expert Opin Investig Drugs. 2003]

See all Related Articles...

Display AbstractPlus

Show 20

Sort by

Send to

EXHIBIT 2

PAGE 26

Motexafin Gadolinium Disrupts Zinc Metabolism in Human Cancer Cell Lines

Darren Magda,¹ Philip Lecane,¹ Richard A. Miller,¹ Cheryl Lepp,¹ Dale Miles,¹ Mimi Mesfin,¹ John E. Biaglow,² Vincent V. Ho,³ Danny Chawannakul,³ Shailender Nagpal,³ Mazen W. Karaman,³ and Joseph G. Hacia³

¹Pharmacyclics, Inc., Sunnyvale, California; ²Department of Radiation Oncology, University of Pennsylvania, Philadelphia, Pennsylvania; and ³Institute for Genetic Medicine, University of Southern California, Los Angeles, California

Abstract

To gain a better understanding of the mechanism of action of the metal cation-containing chemotherapeutic drug motexafin gadolinium (MGd), gene expression profiling analyses were conducted on plateau phase human lung cancer (A549) cell cultures treated with MGd. Drug treatment elicited a highly specific response that manifested in elevated levels of metallothionein isoform and zinc transporter 1 (*ZnT1*) transcripts. A549 cultures incubated with MGd in the presence of exogenous zinc acetate displayed synergistic increases in the levels of intracellular free zinc, metallothionein transcripts, inhibition of thioredoxin reductase activity, and cell death. Similar effects were observed in PC3 prostate cancer and Ramos B-cell lymphoma cell lines. Intracellular free zinc levels increased in response to treatment with MGd in the absence of exogenous zinc, indicating that MGd can mobilize bound intracellular zinc. These findings lead us to suggest that an important component of the anticancer activity of MGd is related to its ability to disrupt zinc metabolism and alter cellular availability of zinc. This class of compounds may provide insight into the development of novel cancer drugs targeting control of intracellular free zinc and the roles that zinc and other metal cations play in biochemical pathways relevant to cancer. (Cancer Res 2005; 65(9): 3837-45)

Introduction

The disruption of metal cation homeostasis can play a significant role in the development and progression of cancer (1-5). Intracellular levels of zinc, in particular, are known to regulate biological pathways involved in carcinogenesis (6-10) and in modulating the effectiveness of the immune system (11). For example, intracellular zinc levels can modulate mitogen-activated protein kinase, extracellular signal-regulated kinase, protein kinase C, and nuclear factor- κ B signaling pathways (6-10). Zinc also plays a major role in modulating the effectiveness of the immune system, in part through its effect on the expression of genes associated with the amplification of the Th1 immune response (11). In addition, genes involved in intracellular zinc trafficking (i.e., metallothionein gene family members) are frequently either over- or underexpressed in a variety of tumors (3-5) and may be involved in tumor growth regulation (12).

Interestingly, several classes of chemotherapeutic agents contain metal cations that are essential for their biological activities (13, 14). For example, motexafin gadolinium (MGd, Xcytrin, Fig. 1A), an expanded porphyrin containing the lanthanide cation gadolinium, is currently in clinical trials for the treatment of several forms of cancer (15-23). MGd is an electron-affine compound that mediates electron transfer from a variety of intracellular reducing species, such as ascorbate, NADPH, and thiols, to oxygen to form superoxide and hydrogen peroxide (20-23). Although the relative importance of the impact MGd has on each of these intracellular processes is unknown, it is interesting to note that the most facile redox reaction seems to occur with vicinal thiols, a chemical motif most commonly associated with the binding of zinc (22).

Here, we generated gene expression profiles of plateau phase A549 cell cultures treated with MGd for the purpose of gaining insights into the mechanisms of its biological activity. A remarkably specific cellular response to drug treatment was observed, which resulted in the marked induction of transcript levels of genes that play major roles in controlling free zinc levels. We found that MGd increased intracellular free zinc levels, modulated the cellular toxicity of zinc, and inhibited cellular bioelectronic activity in human cancer cell lines. Based on our findings, we propose a mechanism of MGd activity and suggest that dysregulation of zinc homeostasis represents a potentially important strategy for anticancer therapy.

Materials and Methods

Cells and cell culture reagents. A549 lung cancer, PC3 prostate cancer, and Ramos B-cell lymphoma lines were obtained from the American Type Culture Collection (Manassas, VA). Unless otherwise indicated, all cell culture reagents were purchased from Invitrogen (Carlsbad, CA). Cells were cultured in RPMI 1640 supplemented with 20 mmol/L HEPES, 2 mmol/L L-glutamine, 10% fetal bovine serum (SH30021, Hyclone, Logan, UT) and antibiotics (200 units/mL penicillin and 200 μ g/mL streptomycin). Unless specified otherwise, plateau phase cultures of A549 and PC3 cells were used. The cell density of Ramos cultures was maintained between 0.2×10^6 and 1×10^6 cells/mL. Motexafin gadolinium (MGd) was prepared as a 2 mmol/L (2.3 mg/mL) formulation in 5% aqueous mannitol. Gadolinium acetate, cadmium chloride, and zinc acetate were purchased from Aldrich Chemical (St. Louis, MO) and prepared as 2 mmol/L formulations in 5% aqueous mannitol. The zinc salt of 1-hydroxypyridine-2-thione (Sigma Chemical, St. Louis, MO) was formulated as a 20 mmol/L stock solution in DMSO. Plateau phase cultures were chosen to obviate any effect that drug treatment might have on cell cycle, to reduce experimental variability, and to examine the effect of the drug in a system that might better mimic conditions extant in the tumor microenvironment (24). In other cases, exponential phase cultures were used to assess the effect of treatment on proliferation.

Gene expression profiling. A549 human lung cancer cells (6.5×10^5 cells per T-162 flask in 45 mL complete RPMI 1640) were seeded 10 days

Note: Supplementary data for this article are available at Cancer Research Online (<http://cancerres.aacrjournals.org/>).

Requests for reprints: Joseph G. Hacia, Institute for Genetic Medicine, University of Southern California, 2250 Alcazar Street, IGM 240, Los Angeles, CA 90089. Phone: 323-442-3030; Fax: 323-442-2764; E-mail: hacia@hsc.usc.edu.

©2005 American Association for Cancer Research.

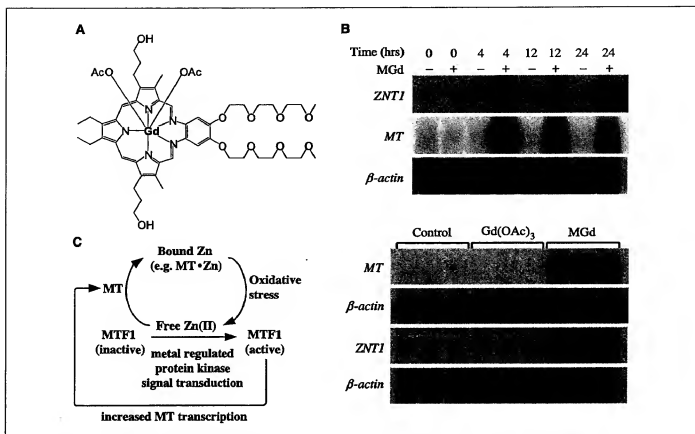


Figure 1. MGD treatment of A549 cultures. **A**, chemical structure of MGD. **B**, MGD up-regulation of RNA expression levels as determined by Northern hybridization in (top) representative microarray samples or (bottom) phase A549 cultures treated for 4 hours with control vehicle (Control), gadolinium acetate [$\text{Gd}(\text{OAc})_3$, 5 $\mu\text{mol/L}$], or MGD (50 $\mu\text{mol/L}$). **C**, schematic diagram of metallothionein (MT) gene regulation in response to oxidative stress.

before treatment of noncycling plateau phase cultures with MGD. At 4, 12, or 24 hours before RNA isolation, MGD (50 $\mu\text{mol/L}$ final concentration) or control (5% mannitol) solution was added to the cultures. Each time course experiment was done in triplicate. After incubation, all cultures were washed once with PBS and total RNA was (25) subjected to analysis on Affymetrix (Santa Clara, CA) U133A microarrays, designed to interrogate the relative abundance of over 15,000 human genes as described (25).

We used Microarray Suite version 5.0 software (Affymetrix) to generate raw gene expression scores and normalized the relative hybridization signal from each experiment as described (25). All gene expression scores were set to a minimum value of 100 to minimize noise associated with less robust measurements of rare transcripts. The permutation-based significance analysis of microarrays (SAM) was used to determine genes differentially expressed in response to MGD treatment compared with the control 5% mannitol-treated cultures (0.125% final) at each time point (26). We report all genes at least 2-fold differentially expressed with a <1% false discovery rate in response to MGD treatment (Table 1). The use of lower fold change cutoffs (down to 1.01-fold) in SAM analysis did not identify any additional differentially expressed genes. All raw fluorescent intensity values from microarray experiments are available in the Supplementary Materials. All cell files are available at http://haciablab.usc.edu/supplement/magda_et_al_2005/.

Northern blot analysis. Plateau phase cultures of A549 cells were prepared as described above, except that T-25 flasks were used and the number of cells initially plated scaled accordingly. Cultures were treated with 50 $\mu\text{mol/L}$ MGD, 5 $\mu\text{mol/L}$ gadolinium acetate or 5% mannitol for 4 hours, whereupon cultures were washed twice with PBS and RNA harvested as above. Alternatively, 7-day plateau phase A549 or PC3 cultures were treated with 50 $\mu\text{mol/L}$ MGD, 50 to 100 $\mu\text{mol/L}$ zinc acetate, 50 $\mu\text{mol/L}$ cadmium chloride, or 5% mannitol for 24 hours (A549) or 4 hours (PC3)

before washing and RNA analysis. Exponential phase Ramos cultures were treated for 6 hours. Northern blots were conducted and analyzed as described (25). Radiolabeled metallothionein probe, designed to bind to a 113-bp region of 3' untranslated region (UTR) sequences from multiple metallothionein gene family members, was generated using 5'-ATGGACCCCACTGCTCCTG-3' (forward) and 5'-GGGCAGCAGGAGCAGCAGCT-3' (reverse) PCR primers and the NEBlot kit (New England Biolabs, Inc., Beverly, MA). Radiolabeled Znt1 probe was generated in a similar fashion using 5'-TGCTGGAAGCA-GAATCATG-3' (forward) and 5'-TGCTAACTGCTGGGTCTTT-3' (reverse) primers.

Cellular viability. Cell viability was determined by using propidium iodide flow cytometric analysis. Cells from plateau phase cultures grown in T-25 flasks were harvested as described above, except that cells present in the growth medium and wash solution were isolated by centrifugation and included in the analysis. Cells were resuspended in 1 mL PBS, an aliquot of 3×10^6 cells transferred to a 4-mL tube, and the cells isolated by centrifugation. Cell pellets were resuspended in PBS supplemented with 2 $\mu\text{g/mL}$ propidium iodide (Sigma), incubated for 5 minutes at ambient temperature, and subjected to flow cytometric analysis. Flow cytometry was done on a FACSCalibur instrument and data were analyzed using the CellQuest Pro software package (BD Biosciences, San Jose, CA).

Cellular proliferation. The proliferation of exponential phase cultures of A549 and PC3 cells was assessed by formazan reduction (27). In brief, A549 (2,000 cells per well) or PC3 (4,000 cells per well) cells were seeded on 96-well microtiter plates and allowed to adhere overnight. Stock solutions of MGD or ZnOAc₂ in medium were added and plates were incubated at 37°C under a 5% CO₂/95% air atmosphere. After 24 hours, medium was replaced with fresh medium. After 2 additional days, medium was exchanged for fresh medium (150 $\mu\text{L}/\text{well}$) supplemented with the

tetrazolium dye, 3-(4,5-dimethylthiazol-2-yl)-2,5-diphenyltetrazolium bromide (MTT, Sigma Chemical, 0.5 mg/mL). Plates were incubated at 37°C and viable cells measured as described (21). Ramos cell cultures were seeded at an initial cell density of 2.5×10^5 cells/mL in 7 mL medium. T-25 flasks were sampled at indicated time intervals and counted using a Coulter counter.

Lipoate reduction. Thioredoxin reductase activity was assessed by measuring the rate of lipoate reduction (28). In brief, A549 or PC3 cells (10,000 cells per well) were plated on 96-well plates and allowed to adhere overnight and grow two additional days until confluent. Cells were treated with MGD, zinc, or 5% mannitol for 2 to 4 hours, as indicated. Medium was removed, cells were washed with HBSS, and a solution of 5 mmol/L lipoic acid and 1 mmol/L 5,5'-dithiobis(2-nitrobenzoic acid) in HBSS (100 μ L per well) was added. Plates were incubated at ambient temperature in the dark. At chosen time intervals, plate absorbance was measured at 405 minus 650 nm. Plate absorbances were normalized to wells containing neither exogenous zinc nor tetraphenyl complex to allow plate-to-plate comparison. In some experiments, buthionine sulfoximine (BSO, 100 μ M/L) was added 24 hours before MGD or zinc treatment to inhibit any contribution to lipoate reduction made by glutathione-dependent pathways (28). Actinomycin D (2.5 μ M/L) or cycloheximide (10 μ M/L), where present, was added 1 hour before tetraphenyl or zinc treatment. Viability was checked on parallel plates using the tetrazolium dye 3-(4,5-dimethylthiazol-2-yl)-5-(3-carboxymethoxyphenyl)-2-(4-sulphophenyl)-2H-tetrazolium (MTS) following the manufacturer's protocol (Promega Corp., Madison, WI). MTS signal was not altered by any treatment condition within the time frame of the lipoate reduction assay.

Intracellular free zinc. The concentration of intracellular free zinc was assessed using the ion-specific fluorescent probe, FluoZin-3-AM (FluoZin-3, Molecular Probes, Inc., Eugene, OR; ref. 29). Plateau phase cultures grown in T-25 flasks were treated with control 5% mannitol vehicle or zinc acetate in the presence or absence of MGD as described above, for 4 hours. After MGD

treatment, cells were washed with PBS, and treated with trypsin/EDTA for 5 minutes. Complete medium was then added and the cells isolated by centrifugation. Cell pellets were washed and resuspended in PBS. An aliquot of 10^6 cells (200 μ L) was removed, centrifuged, and resuspended in 100 μ L of 20 μ M/L FluoZin-3 and 0.2% pluronic acid F127 (Molecular Probes) in PBS. After a 25-minute incubation under ambient conditions, cells were washed twice with PBS, resuspended in 0.5 mL PBS, and again incubated for 20 minutes. An aliquot of the cell suspension was supplemented with 2 μ M/L propidium iodide (Sigma), incubated for 5 minutes, and subjected to two-parameter flow cytometric analysis. FluoZin-3 fluorescence was measured at 530 nm in live-gated cells. As controls, a portion of mannitol-treated cells was treated with 20 μ M/L pyridine (Sigma) and 50 μ M/L zinc acetate or with 20 μ M/L *N,N,N',N'*-tetrakis(2-pyridylmethyl)ethylenediamine (Sigma) for 15 minutes, then processed and analyzed as above. These cells displayed average fluorescence intensity at 530 nm of 2,600 and 29 units, respectively. In other experiments, A549 cultures were washed, incubated with zinc acetate and MGD in serum-free medium for 4 hours, then analyzed for intracellular zinc as above. Actinomycin D (2.5 μ M/L, Calbiochem, Inc., San Diego, CA) was added 1 hour before MGD and zinc acetate where indicated.

Results

Gene expression. To assess the effects of drug on gene expression profiles, total cellular RNA was isolated from plateau phase A549 cultures treated with 50 μ M/L MGD for 4, 12, and 24 hours in triplicate and analyzed on oligonucleotide microarrays (25). Eleven genes showed at least a 2-fold differential expression in response to MGD treatment (averaged across all time frames) that reached statistical significance by SAM analysis (Table 1). The most prominent consequence of MGD treatment was the up-regulation of various metallothionein isoform transcripts at all time points. In fact, 10 of the 11 transcripts listed in Table 1 are metallothionein related. The remaining transcript, hbc647, was also up-regulated by MGD treatment at all three time points. This cDNA (30) is located 5 kb downstream of the zinc transporter 1 (*ZnT1*) gene and is likely to make up part of the 3' UTR of this gene. Northern blot analysis confirmed the induction of metallothionein gene family members and *ZnT1* (Fig. 1B, top). These transcripts are under the control of metal-response element-binding transcription factor-1 (MTF-1; Fig. 1C; refs. 31–34).

Metallothionein induction by motexafin gadolinium compared with free gadolinium acetate. Metallothionein induction has been reported to occur in response to certain metal cations, including gadolinium(III), and oxidative stress (3–5, 35, 36). Therefore, we considered whether the metallothionein transcript up-regulation observed in the microarray analysis could be a consequence of free gadolinium(III) cation, released from MGD into the cell culture medium. High-performance liquid chromatography analysis of MGD stability in medium obtained from plateau phase cultures indicated that the drug seemed to be stable, with an apparent loss of only 4% after 24 hours (data not shown). Because the microarray analysis indicated strong transcript up-regulation after 4 hours of treatment with drug, we selected this time interval for further investigation of RNA transcript levels. RNA was harvested from plateau phase cultures treated with control vehicle, 50 μ M/L MGD, or 5 μ M/L gadolinium acetate for 4 hours. Northern blot analysis indicated metallothionein gene family members and *ZnT1* were induced only in cultures treated with MGD (Fig. 1B, bottom). Thus, even assuming a 10% loss of drug over the initial 4-hour incubation period, the resulting release of Gd(III) ion into the culture medium would be insufficient to induce the observed metallothionein and *ZnT1* transcript levels.

Table 1. Differential gene regulation in response to MGD treatment

GenBank ID*	4 h†	12 h†	24 h†	Average‡	Gene name
M10943	37.1	49.2	36.7	41.0	Metallothionein 1F
AF078844†	39.7	47.3	30.3	39.1	RNA helicase-related protein
NM_005951	29.8	32.0	9.5	23.8	Metallothionein 1H
AF333388	21.7	23.2	9.4	18.1	Metallothionein 1H-like
NM_002490	23.2	20.0	10.0	17.8	Metallothionein 1L
NM_005982	16.5	16.2	13.5	15.4	Metallothionein 1X
NM_005983	9.8	8.6	7.3	8.6	Metallothionein 2A
NM_005980	8.0	6.0	8.7	7.6	Metallothionein 1G
A1972416	6.8	4.7	3.5	5.0	Zinc transporter 1
A1031602	4.4	3.7	4.8	4.3	Similar to metallothionein 1E
BF217861	2.2	2.5	1.6	2.1	Metallothionein 1E

*Available at <http://www.ncbi.nlm.nih.gov/Entrez/index.html>.

†Ratio of gene expression scores for cultures treated and not treated with 50 μ M/L motexafin gadolinium for the indicated time frame.

‡Ratio of gene expression scores treated and not treated with 50 μ M/L motexafin gadolinium for all time frames. All genes that achieved significance using SAM criteria described in Materials and Methods are shown.

§Protein has a COOH-terminal domain similar to human metallothionein 1F.

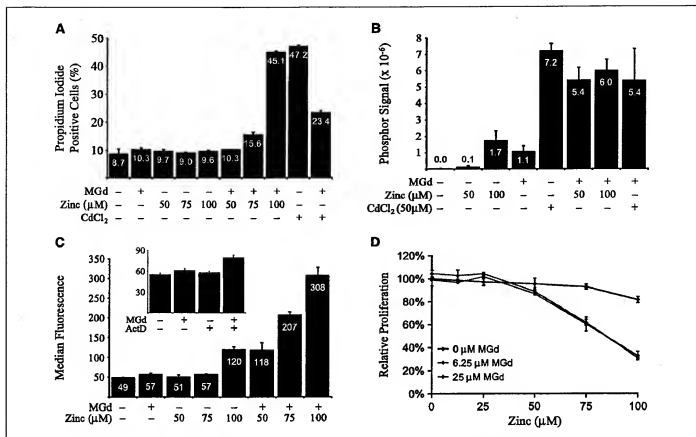


Figure 2. MGD treatment alters response of A549 cells to zinc or cadmium. **A**, cell viability as measured by propidium iodide exclusion. Plateau phase cultures were treated with zinc acetate (Zinc, 50–100 μmol/L), cadmium chloride (CdCl₂, 50 μmol/L), or MGD (50 μmol/L) for 24 hours in duplicate experiments. Bars, 1 SD. **B**, transcript levels of metallothionein family members in A549 cultures treated with MGD (50 μmol/L) and metal cations as determined by Northern blot analysis. Phosphorimager signals from metallothionein family members were normalized to those of internal β-actin controls. **C**, measurement of intracellular free zinc in A549 cells. Plateau phase cultures were treated with zinc acetate (50–100 μmol/L) or MGD (50 μmol/L) for 4 hours in duplicate experiments. Columns, median fluorescence at 530 nm of cells treated with FluoZin-3, as described in Materials and Methods. Bars, SD. Inset, median fluorescence of cells treated with MGD in serum-free medium in the absence and presence of 2.5 μg/mL actinomycin D (ActD). **D**, effect of MGD and zinc treatment on proliferation of A549 cells. Exponential growth phase cultures were treated with MGD (0, 6.25, and 25 μmol/L) and metal cation (0–100 μmol/L) for 24 hours, medium replaced, and proliferation relative to control assessed by colorimetric (MTT) assay after 72 hours. Cells treated with 12.5 and 18.75 μmol/L MGD behaved in a similar fashion to those treated with 25 μmol/L MGD (data not shown). Bars, SD.

Motexafin gadolinium increases sensitivity of cells to zinc acetate. The above findings indicated that MGD treatment might alter cellular response to metal cations. This could be relevant because the levels of zinc available to cultured cancer cells and to cancer cells *in vivo* may not directly coincide in all instances. To examine this possibility, A549 cultures were treated with zinc acetate (100 μmol/L) or cadmium chloride (50 μmol/L) for 24 hours in the presence or absence of 50 μmol/L MGD. Treatment with zinc acetate alone had no effect on cellular viability, as assessed by propidium iodide exclusion (Fig. 2A). By contrast, viability dropped from ~90% to ~55% after treatment with zinc acetate and MGD. This is dependent on treatment time because there are limited effects on cellular viability at 4 hours and only intermediate effects at 12 hours relative to 24-hour treatments (Supplementary Fig. 1). Conversely, viability after cadmium chloride treatment (~53%) was increased to ~76% by coinubation with MGD. It has been reported that metallothionein induction protects cells from cadmium chloride treatment (37, 38). The effects of zinc acetate and cadmium chloride were not altered by gadolinium acetate (50 μmol/L, data not shown).

Metallothionein induction by zinc and cadmium treatment in the presence and absence of motexafin gadolinium. RNA harvested from surviving A549 cells, treated as above, was analyzed for metallothionein transcript induction. Treatment with zinc acetate, cadmium chloride, or MGD resulted in significant increase in the levels of these RNA transcripts (Fig. 2B). Interestingly, cotreatment with zinc acetate and MGD led to a synergistic increase in the levels of metallothionein transcripts (Fig. 2B). Treatment with cadmium led to high levels of metallothionein transcription, in the presence or absence of MGD.

Intracellular free zinc is elevated in motexafin gadolinium-treated cells. The above findings indicated that MGD treatment might alter the cellular availability of zinc ion. Therefore, cultures of A549 cells were incubated with MGD and zinc for 4 hours, and cells were analyzed for free (chelatable) intracellular zinc using the ion-specific dye, FluoZin-3 (29). Treatment with 100 μmol/L zinc acetate significantly increased the cell-associated fluorescence of FluoZin-3 at 530 nm (Fig. 2C). Coinubation of cultures with 50 to 100 μmol/L zinc acetate and MGD led to synergistic increases in the corresponding fluorescent signals. Next, we attempted to

determine the mechanisms by which MGd treatment alters levels of free intracellular zinc. Cells were incubated in the complete absence of exogenous zinc (serum-free medium) to evaluate the role zinc uptake plays in this process. Cells were also treated with actinomycin D to minimize the expression of genes (i.e., metallothionein family members and *ZnT1*) that might mask drug-induced changes in free intracellular zinc levels. Interestingly, cotreatment of cells with MGd and actinomycin D led to a 1.5-fold increase in cellular fluorescence (Fig. 2C, inset). No increase in cellular fluorescence at 530 nm was observed in the absence of FluoZin-3 in these experiments.

Effect of motexafin gadolinium on the antiproliferative effects of zinc acetate. To determine whether MGd modulation of metal ion availability was restricted to quiescent cell cultures, exponential growth phase A549 cultures were treated with zinc in the presence or absence of MGd for 24 hours. After an additional 48 hour growth period, viable cells were measured using a tetrazole reduction assay. Zinc treatment modestly inhibited A549 cell proliferation at the highest (100 μM) concentration. Treatment with MGd alone had no effect on proliferation, but enhanced the antiproliferative activity of zinc at all MGd concentrations tested (Fig. 2D).

Motexafin gadolinium modulation of zinc activity in PC3 prostate cancer cells and Ramos lymphoma cells. Treatment of

plateau phase PC3 cultures with zinc had little effect on cell viability after 24 hours (data not shown), but increased cell death (2-fold at 100 μM /L zinc), as measured by propidium iodide exclusion, was apparent within 48 hours (Fig. 3A). MGd enhanced the cytotoxic effect of zinc (e.g., 5-fold at 100 μM /L zinc), similar to what was observed in the A549 line. Metallothionein and *ZnT1* levels were elevated after treatment with MGd and zinc (Fig. 3B). As before, treatment with MGd led to increased zinc-associated cellular fluorescence in the presence of exogenous zinc (Fig. 3C). Indeed, in this cell line, incubation with MGd alone led to a more marked increase in cellular fluorescence after 4 hours (~2-fold) than in A549. Interestingly, PC3 cell proliferation was also inhibited by zinc (Fig. 3D). As in the A549 line, treatment with MGd enhanced the effect of zinc. This effect was confirmed by colony-forming assay. A surviving fraction of 0.16 was measured in the presence of 10 μM /L MGd and 75 μM /L zinc, whereas zinc or MGd alone was without effect (data not shown).

Furthermore, we examined the effect of MGd and zinc treatment on viability, metallothionein and *ZnT1* gene expression, and intracellular levels of free zinc in Ramos B-cell lymphoma cells grown in suspension (Fig. 4A-C). Overall, the results were qualitatively similar to those obtained with A549 and PC3, with the difference that changes were generally observed at lower

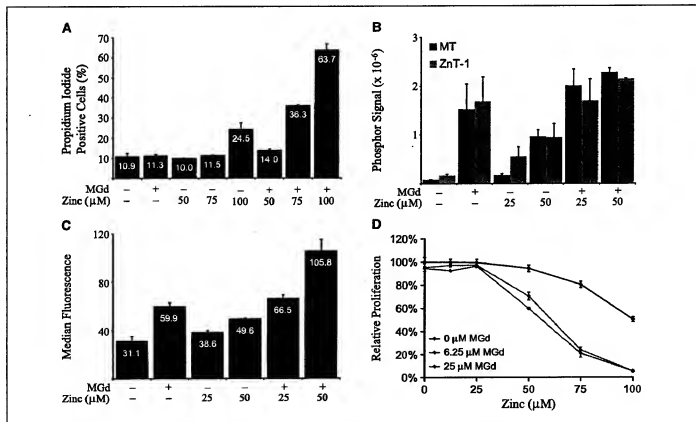


Figure 3. MGd treatment alters response of PC3 cells to zinc. **A**, cell viability as measured by propidium iodide exclusion. Plateau phase cultures were treated with zinc acetate (Zinc, 50–100 μM /L) or MGd (50 μM /L) for 48 hours in duplicate experiments. Bars, 1 SD. **B**, transcript levels of metallothionein family members and *ZnT1* in PC3 cultures treated with MGd (50 μM /L) and zinc acetate (25–50 μM /L) for 4 hours as determined by Northern blot analysis. Phosphorimager signals from metallothionein family members were normalized to those of internal β -actin controls. **C**, measurement of intracellular free zinc in PC3 cells. Plateau phase cultures were treated with zinc acetate (25–50 μM /L) or MGd (50 μM /L) for 4 hours in duplicate experiments. Median fluorescence at 530 nm of cells treated with FluoZin-3, as described in Materials and Methods. Bars, SD. **D**, effect of MGd and zinc treatment on proliferation of PC3 cells. Exponential growth phase cultures were treated with MGd (0, 6.25, and 25 μM /L) and zinc (0–100 μM /L) for 24 hours as described in the caption to Fig. 2. Cells treated with 12.5 and 18.75 μM /L MGd behaved in a similar fashion to those treated with 25 μM /L MGd (data not shown).

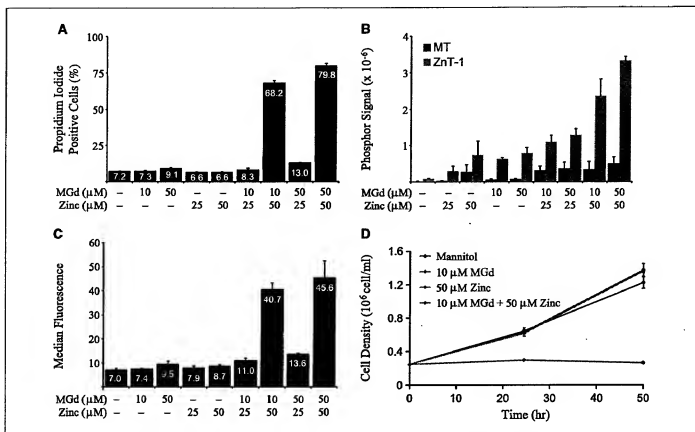


Figure 4. Effects of combined Mgd and zinc treatment in Ramos cells. Exponential growth phase Ramos cell cultures were treated with zinc acetate (25 or 50 μ M/L) or Mgd (10 μ M/L or 50 μ M/L) for 24 hours (A), 6 hours (B and C), or 48 hours (D) and assayed for (A) viability, (B) metallothionein family member and ZnT1 RNA transcript levels, (C) FluoZin-3 fluorescence, (D) proliferation. Cells, treatment with 25 μ M/L zinc with or without Mgd (25 or 50 μ M/L) had no effect on proliferation (data not shown). Also in (D), cotreatment with 50 μ M/L zinc and 50 μ M/L Mgd completely inhibited proliferation (data not shown). Bars, 1 SD.

(i.e., 25–50 μ M/L) concentrations of zinc. Cellular proliferation was strongly inhibited by 50 μ M/L zinc and Mgd, whereas either agent alone was without effect (Fig. 4D).

Inhibition of lipote reduction. We previously reported that Mgd caused an increase in radiation response in A549 cultures treated with BSO, an inhibitor of glutathione synthesis (21). This observation led us to investigate the effect of Mgd treatment on the complementary, glutathione-independent thioredoxin pathway. Thioredoxin reductase activity can be evaluated in intact cells by measuring the reduction of the oxidized form of the cell-permeable cofactor lipote to its reduced form, dihydrolipote (28). Using this method, we observed a modest (\sim 10%) inhibition of lipote reduction in plateau phase A549 cultures after a 2-hour treatment with Mgd alone (Fig. 5A). Moreover, up to a 30% inhibition of lipote reduction was observed after treatment of cultures with zinc alone, consistent with literature reports of thioredoxin reductase inhibition by this cation (39–41). Greater inhibition (up to 60%) was observed after treatment with both zinc and Mgd (Fig. 5A). This effect of Mgd was dose dependent, with an apparent inhibitory concentration of \sim 25 μ M/L. The inhibition of lipote reduction was less pronounced (\sim 30%) after 4 hours of incubation (Fig. 5B). Pretreatment with either actinomycin D (Fig. 5C) or cycloheximide (data not shown) restored the inhibitory effect of both Mgd and zinc on lipote reduction. These findings lead us to suggest that A549 cells compensate for increases in intracellular zinc levels by transcrip-

tion and translation-dependent processes. Lipote reduction was also inhibited in cells treated with zinc 1-hydroxypyridine-2-thiol, a zinc ionophore that increases the concentration of intracellular zinc (Fig. 5D). Preincubation of cultures with the glutathione synthesis inhibitor BSO increased the degree of inhibition by Mgd and zinc, demonstrating that both agents were targeting the glutathione-independent lipote reduction pathway (data not shown; ref. 28). Similar observations were obtained using plateau phase PC3 prostate cancer cell cultures (Fig. 5E–H). However, lipote reduction was inhibited at lower concentrations of zinc in PC3 cells as compared with A549. Lipote reduction was similarly inhibited by Mgd and zinc in exponential Ramos lymphoma cultures (data not shown).

Discussion

We examined the effect of Mgd treatment on mRNA levels in A549 lung cancer cell cultures at multiple exposure times and observed a highly specific response that consisted of a strong and sustained induction of metallothionein and ZnT1 transcripts (Table 1). Metallothioneins possess multiple cysteine-rich sites that can bind metal cations. They are expressed constitutively and may be further induced by toxic metal cations such as Cd(II) or by nontoxic cations such as Zn(II) (3–5). ZnT1 is a plasma membrane-bound protein that transports zinc to the outside of the cell (4, 11, 42, 43). The transcription of metallothionein genes

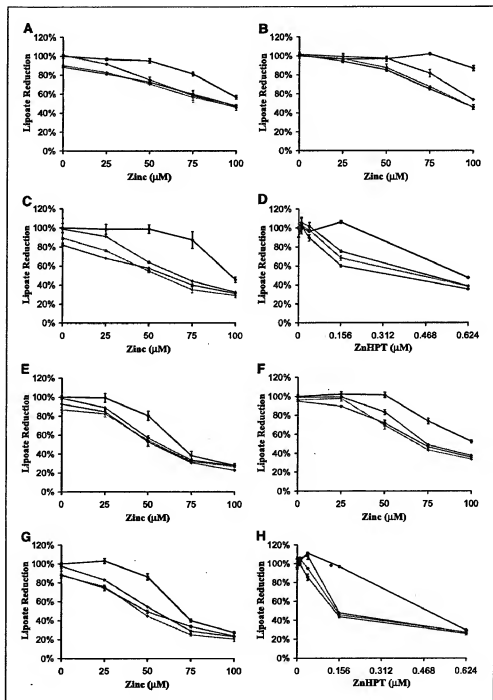
and *ZnT1* is induced by MTF-1 (31–34), a metal-dependent transactivator that binds to metal response elements located in the promoters of metallothionein and other genes (Fig. 1C; refs. 31–34).

Initially, displacement of zinc by free Gd(III) was considered as a possible explanation for the observed metallothionein induction (e.g., gadolinium chloride treatment has been reported to induce metallothionein expression in rat liver; ref. 35). However, the lack of metallothionein induction by free gadolinium as assessed by Northern blot analysis (Fig. 1B) is not consistent with this explanation. Moreover, stability studies indicate that release of free

Gd(III) from MGd is unlikely (data not shown). We therefore considered other pathways by which metallothionein induction could occur.

Zinc metallothioneins are believed to be a major site of intracellular zinc storage and transport (3–5, 31–34). As shown in Fig. 1C, oxidation of zinc metallothionein by hydrogen peroxide leads to the formation of thionein and the release of zinc (44–46). The disulfide bond in thionein must be reduced by thioredoxin reductase in order to recoordinate to zinc. The released zinc can bind and activate MTF-1, leading, in turn, to up-regulation of thionein expression (44–46). The binding of zinc by the newly

Figure 5. Lipidate reduction in A549 and PC3 cells. Plateau phase A549 (A–D) and PC3 (E–H) cultures were treated with zinc acetate (0–100 μM) or zinc 1-hydroxy-2-pyridinethione (ZnHPT, 0–0.624 μM) and MGd (0 (black line), 2.5 (blue line), 5 (green line), and 10 μM (red line)), medium exchanged, and relative lipidate reduction measured after 20–40 minutes) as described in Materials and Methods. A and E, 2-hour treatment; B and F, 4- or 3-hour treatment, respectively. C and G, as in (B) and (F), except actinomycin D (2.5 $\mu\text{g}/\text{mL}$) was added to cultures 1 hour before MGd or zinc. D and H, cultures coincubated with MGd and ZnHPT for 4 hours. Bars, 1 SD, although not readily visible due to the reproducibility of the data.



transcribed thioneins provides a negative feedback mechanism for metallothionein expression.

MgD is a redox active agent that has been shown to redox cycle and form reactive oxygen species in cells (20–23). Other redox cycling agents have been shown to induce metallothionein expression (36). Interestingly, recent data suggests that MgD oxidizes vicinal thiols such as dithiothreitol and can inhibit thioredoxin reductase (22). It is therefore possible that the generation of reactive oxygen species, the direct oxidation of zinc metallothionein by the complex, or thioredoxin reductase inhibition could be responsible for the observed metallothionein induction. However, MgD treatment affects only a subset of the genes reported to be induced or repressed by oxidative stress in cultured mammalian cells (47–52). This could be due to differences in the cell lines and growth conditions examined or the possible targeted nature of MgD action.

Treatment with MgD attenuated the cytotoxicity of cadmium chloride and potentiated that of zinc acetate in A549 cells (Fig. 2A). Metallothionein transcript levels were raised by treatment with MgD, zinc, cadmium, or combinations of these species (Fig. 2B). Attenuated cadmium toxicity is consistent with literature reports of protection from cadmium chloride toxicity by metallothionein induction (37, 38). Enhanced zinc toxicity, however, is inconsistent with a recent report of the protection of baby hamster kidney cells against zinc toxicity by metallothionein and zinc transporter 1 (43). In an effort to resolve this apparent contradiction, we examined intracellular levels of free zinc using the ion-specific probe, FluoZin-3 ($K_d = 15$ nmol/L; ref. 29), and observed significantly (at least 2.4-fold) increased cellular fluorescence signals after incubation with MgD and 50 to 100 μ M/L zinc for 4 hours (Fig. 2C). Synergistic increases in intracellular free zinc levels in response to incubation with MgD and zinc acetate could explain the cellular toxicity observed. Furthermore, the 1.5-fold increase in cellular fluorescence signal observed by incubating A549 cells with MgD and actinomycin D in zinc-free medium (Fig. 2C, inset) suggests that MgD treatment can mobilize bound intracellular zinc. This mobilization is normally quenched by cellular gene expression responses, most likely those of metallothionein gene family members and *ZnT1* because MgD treatment in the absence of actinomycin D only led to marginal increases in cellular fluorescence in both serum and serum-free media (1.2- and 1.1-fold, respectively, in A549).

Similar effects were observed in PC3 prostate cancer and Ramos B-cell lymphoma cell lines. Combined treatment with MgD and zinc led to increased cell death after 48 hours in PC3 cultures (Fig. 3A) and after 24 hours in Ramos cultures (Fig. 4A). Expression of metallothionein family members and *ZnT1* were increased by MgD in both lines (Figs. 3B and 4B). Larger changes in FluoZin-3 fluorescence (~2-fold) were observed in PC3 cultures treated with MgD alone than in the A549 or Ramos lines (Figs. 2C, 3C, and 4C). The difference could result from the lesser induction of gene expression of metallothionein gene family members or *ZnT1* in this line (4).

Increased intracellular zinc levels would also explain the effect of MgD and zinc on lipate reduction (Fig. 5). Lipate is mainly reduced by thioredoxin reductase in mammalian cells, accounting for approximately two thirds of this activity in A549 cultures, with the remainder due to glutaredoxin or other enzymes (28, 53). Inhibition of thioredoxin reductase by zinc in cell extracts was reported previously (40, 41). The data in Fig. 5 show that zinc

inhibition of thioredoxin reductase occurs in intact cells. MGd alone had a modest effect on the rate of lipate reduction under our conditions after 2 hours of treatment (Fig. 5A, y axis). Moreover, inhibition of lipate reduction by zinc was potentiated by MGd. The effect of MGd was dose dependent and saturated above a concentration of ~5 μ M/L. The inhibition of lipate reduction was less pronounced after 4 hours of incubation (Fig. 5B). However, pretreatment with either actinomycin D (Fig. 5C) or cycloheximide (data not shown) restored the inhibitory effect of both MGd and zinc. This is reminiscent of the effect of actinomycin D on the fluorescence measurements described above (Fig. 2C) and is consistent with compensatory cellular RNA and protein expression in response to MGd. Lipate reduction was also inhibited in cells treated with a zinc ionophore (Fig. 5D), demonstrating that the effect of MGd was independent of the mode of zinc uptake. Lipate reduction was similarly inhibited by zinc and MGd in PC3 and Ramos cultures (Fig. 5E–H and data not shown).

Thioredoxin reductase is an important component of the cellular antioxidant system and is involved in a variety of other processes including apoptotic signaling and DNA synthesis (54). It has recently been highlighted as an attractive target for anticancer agent activity (55). In the present study, combined treatment with MGd and zinc inhibited cell proliferation (Figs. 2D, 3D, and 4D) and led to cell death (Figs. 2A, 3A, and 4A). Similar observations were made using the HF-1 and DHL-4 B-lymphoma cell lines (data not shown). Thioredoxin reductase inhibition could contribute to the observed effects.

Of course, many other proteins require zinc for activity and may therefore be affected by changes in the intracellular concentration of available zinc. The observation of a sustained induction of *ZnT1* and metallothionein transcripts suggests a corresponding increase in the intracellular availability of zinc during drug treatment. MGd could therefore modulate a variety of downstream processes by mobilizing zinc. The importance of this would likely depend on the particular system under study but would be most likely to occur in tumors, where the drug seems to localize selectively (15–19).

Because zinc treatments were reported to inhibit tumor growth in animal models in 1969 (56), there has been considerable interest in the role of zinc in cancer development and progression (2, 57–59). MGd represents a novel class of compounds capable of altering the expression of MTF-1 responsive genes and altering zinc homeostasis in cancer cells. Therefore, MGd could be a valuable experimental tool to examine the role of zinc in the control of transcription and metabolic pathways. Furthermore, studies are under way to examine MTF-1 responsive genes as surrogate markers for the biological activity of MGd. Finally, the above findings provide support for the hypothesis that agents that increase intracellular zinc levels have potential applications as anticancer therapeutics.

Acknowledgments

Received 11/15/2004; revised 1/20/2005; accepted 2/8/2005.

Grant support: Donald K. and Delia B. Baxter Foundation (J.G. Hacia) and the V Foundation for Cancer Research (J.G. Hacia).

The costs of publication of this article were defrayed in part by the payment of page charges. This article must therefore be hereby marked advertisement in accordance with 18 U.S.C. Section 1734 solely to indicate this fact.

We thank Jaeger Reichardt at the University of Southern California for critical insights and discussion.

References

- Leonard SS, Bower JL, Shi X. Metal-induced toxicity, carcinogenesis, mechanisms and cellular responses. *Mol Cell Biochem* 2004;253:9-10.
- Leitman M, Stamper MJ, Wu K, Kolditz GA, Willett WC, Giovannucci EL. Zinc supplement use and risk of prostate cancer. *J Natl Cancer Inst* 2003;95:1004-7.
- Cherian MG, Jayaraj A, Bay BH. Metallothioneins in human tumors and potential roles in carcinogenesis. *Mutat Res* 2003;533:201-9.
- Hasumi M, Suzuki K, Matsui H, Koike H, Ito K, Yamanaoka H. Regulation of metallothionein and zinc transporter expression in human prostate cancer cells and tissues. *Cancer Lett* 2003;200:187-95.
- Jayaraj A, Bay BH, Yap WM, Tan NG, Tan RK. Proliferative potential in nasopharyngeal carcinoma: correlations with metallothionein expression and tissue zinc levels. *Carcinogenesis* 2002;23:1189-12.
- Kondoh M, Tanaka E, Araragi S, et al. Requirement of caspase and p38MAPK activation in zinc-induced apoptosis in human leukemia HL-60 cells. *Eur J Biochem* 2002;269:620-11.
- Kim CH, Kim JH, Moon SJ, et al. Pyritione, a zinc ionophore, inhibits NF- κ B activation. *Biochem Biophys Res Commun* 1999;259:502-9.
- Seo SR, Chong SA, Lee SI, et al. Zn²⁺-induced ERK activation mediated by reactive oxygen species causes cell death in differentiated PC12 cells. *J Neurochem* 2001;78:600-10.
- Forbes RJ, Zalewski PD, Gliniakowski C. Role for zinc in a cellular response mediated by protein kinase C in human B-lymphocytes. *Exp Cell Res* 1991;195:234-9.
- Uzzo RG, Leavis P, Hatch W, et al. Zinc inhibits nuclear factor- κ B activation and sensitizes prostate cancer cells to cytotoxic agents. *Clin Cancer Res* 2002;8:3579-83.
- Cousins RJ, Blanchard RK, Popp MP, et al. A global view of the selectivity of zinc deprivation and excess on genes expressed in human THP-1 monocytic cells. *Proc Natl Acad Sci U S A* 2003;100:6982-7.
- Hecht D, Jung D, Prabhu VV, Munson PJ, Hoffman MJ. Kleinman TSC Metallothionein promotes laminin-1-induced cancer differentiation *in vitro* and reduces tumor growth *in vivo*. *Cancer Res* 2002;62:5370-4.
- Zhang CX, Lippard SJ. New metal complexes as potential therapeutics. *Curr Opin Chem Biol* 2003;7:481-9.
- Renator D, Wang H. Protective mechanisms against the antitumor agent bleomycin: lessons from *Saccharomyces cerevisiae*. *Curr Genet* 2003;43:213-24.
- Rosenthal DJ, Nurenberg P, Bocerra CR, et al. A phase I single-dose trial of gadolinium tetrakis (Gd-Text), a tumor selective radiation sensitizer detectable by magnetic resonance imaging. *Clin Cancer Res* 1999;5:739-45.
- Carpe E, Timmerman R, Mehta MP, et al. Multicenter phase II/III trial of the radiation enhancer motexafin gadolinium in patients with brain metastases. *J Clin Oncol* 2001;19:5207-13.
- Mehta MP, Shapiro WR, Glantz MJ, et al. Lead-in phase to randomized trial of motexafin gadolinium and whole-brain radiation for patients with brain metastases: centralized assessment of magnetic resonance imaging, neurocognitive, and neurologic end points. *J Clin Oncol* 2002;20:45-53.
- Mehta MP, Rodriguez P, Terhaard CH, et al. Survival and neurologic outcomes in a randomized trial of motexafin gadolinium and whole-brain radiation therapy in brain metastases. *J Clin Oncol* 2003;21:2529-36.
- Rodriguez P. Motexafin gadolinium: a possible new radiosensitizer. *Expert Opin Invest Drugs* 2003;12:1205-10.
- Magda D, Gerasimchuk N, Lecane P, Miller RA, Biaglow JE, Sessler JL. Motexafin gadolinium reacts with ascorbate to produce reactive oxygen species. *Chem Commun (Camb)* 2002;22730-1.
- Magda D, Lepp C, Gerasimchuk N, et al. Redox cycling by motexafin gadolinium enhances cellular response to ionizing radiation by forming reactive oxygen species. *Int J Radiat Oncol Biol Phys* 2001;51:1025-34.
- Biaglow JE, Miller RA, Magda D, Lee I, Tuttle S. Inhibition of thioredoxin reductase by motexafin gadolinium: effects on PLDR. *Prog Abstr Radiat Res* 2002;2107.
- Rockwell S, Donnelly ET, Liu Y, Tang LQ. Preliminary studies of the effects of gadolinium tetrakis on the growth and radiosensitivity of EMT6 cells *in vitro*. *Int J Radiat Oncol Biol Phys* 2002;54:536-41.
- Varnes ME, Menegay HJ, McKenna DS. Inhibition of recovery from potentially lethal radiation damage in A549 cells by the K⁺/H⁺ ionophore nigericin. *Int J Radiat Oncol Biol Phys* 1991;20:291-5.
- Karaman MW, Houck ML, Chemnick LG, et al. Comparative analysis of gene-expression patterns in human and African great ape cultured fibroblasts. *Genome Res* 2003;13:1619-30.
- Tashir VG, Tibshirani R, Chu G. Significance analysis of microarrays applied to the ionizing radiation response. *Proc Natl Acad Sci U S A* 2001;98:5116-21.
- Mosmann T. Rapid colorimetric assay for cellular growth and survival: application to proliferation and cytotoxicity assays. *J Immunol Methods* 1983;65:55-63.
- Chen J, Tashir V, Tuttle S, Held K, Christensen C, Meyer J. A method for measuring disulfide reduction by cultured mammalian cells: relative contributions of glutathione-dependent and glutathione-independent mechanisms. *Anal Biochem* 2000;281:77-86.
- Gee KR, Zhou ZL, Ton-Thai D, Sensi SL, Weiss JH. Measuring zinc in living cells: A new generation of sensitive and selective fluorescent probes. *Cell Calcium* 2002;31:245-51.
- Takeda J, Yano H, Eng S, Zeng Y, Bell GI. A molecular inventory of human pancreatic islets: sequence analysis of 1000 cDNA clones. *Hum Mol Genet* 1992;1:793-8.
- Gindoff BP, Chen X, Apay JL. Metal response element (MRE)-binding transcription factor-1 (MTF-1) structure, function, and regulation. *Antioxid Redox Signal* 2001;3:77-96.
- Lichten P, Schaffner W. Putting its fingers on stressful situations: the heavy metal-regulatory transcription factor MTF-1. *Bioessays* 2001;23:1010-7.
- Lichten P, Wang Y, Belser T, et al. Target gene search for the metal-responsive transcription factor MTF-1. *Nucleic Acids Res* 2001;29:1514-23.
- Andrews GK. Cellular zinc sensors MTF-1: regulation of gene expression. *Biomol* 2001;14:223-37.
- Sauer JM, Waalkes MP, Hooser SB, Kuester RK, McQueen CA, Sipes IG. Suppression of Kupfer cell function prevents cadmium induced hepatocellular carcinoma in the male Sprague-Dawley rat. *Toxicology* 1997;121:155-64.
- Andrews GK. Regulation of metallothionein gene expression by oxidative stress and metal ions. *Biochem Pharmacol* 2000;59:95-104.
- Nordberg GF. Modulation of metal toxicity by metallothionein. *Biol Trace Elem Res* 1982;2:131-5.
- Acharar W, Acharar KB, Lewis JG, Waalkes MP. Cadmium induces c-myc, p53, and c-jun expression in normal human prostate epithelial cells as a prelude to apoptosis. *Toxicol Appl Pharmacol* 2000;164:291-300.
- Holmgren A. Thioredoxin. *Annu Rev Biochem* 1985;54:237-71.
- Lenartowicz E, Wudarczyk J. Enzymatic reduction of 5,5'-dithiobis(2-nitrobenzoic acid) by lysate of rat liver mitochondria. *Int J Biochem Cell Biol* 1995;27:831-7.
- Rigobello MR, Callegaro MT, Barzon E, Benetti M, Biondi A. Purification of mitochondrial thioredoxin reductase and its involvement in the redox regulation of membrane permeability. *Free Radic Biol Med* 1998;24:370-6.
- Langmade SJ, Ravindra R, Daniels PJ, Andrews GK. The transcription factor MTF-1 mediates metal regulation of the mouse Znt1 gene. *J Biol Chem* 2000;275:34803-9.
- Palmiter RD. Protection against zinc toxicity by metallothionein and zinc transporter 1. *Proc Natl Acad Sci U S A* 2004;101:4918-23.
- Zhang B, Georgiev O, Hagmann M, et al. Activity of metal-responsive transcription factor 1 by toxic heavy metals and H₂O₂ *in vitro* is modulated by metallothionein. *Mol Cell Biol* 2003;23:871-85.
- Maret W, Vallee BL. Thiolate ligands in metallothionein confer redox activity on zinc clusters. *Proc Natl Acad Sci U S A* 1998;95:3478-82.
- Jacob C, Maret W, Vallee BL. Control of zinc proteins between thionein, metallothionein, and zinc proteins. *Proc Natl Acad Sci U S A* 1998;95:3489-94.
- Murray JL, White SR, Trinklins NJ, Myers RM, Brown PG, Botstein D. Divergent and specific gene expression responses to stresses in cultured human cells. *Mol Biol Cell* 2004;15:2361-74.
- Yoneda K, Chang MM, Chmielek K, Chen Y, Wu R. Application of high-density DNA microarray to study smoke- and hydrogen peroxide-induced injury and repair in human bronchial epithelial cells. *J Am Soc Nephrol* 2003;14:5284-9.
- Weigel AL, Handa TJ, Hjelmeland LM. Microarray analysis of H₂O₂, HNE-, or LBH-treated ARPE-19 cells. *Free Radic Biol Med* 2002;33:1419-32.
- Chuang YC, Chen Y, Gadiseti, et al. Gene expression after treatment with hydrogen peroxide, menadione, or t-butyl hydroperoxide in breast cancer cells. *Cancer Res* 2002;62:46-54.
- Morgan KT, Ni H, Brown RH, et al. Application of cDNA microarray technology to *in vitro* toxicology and the selection of genes for a real-time RT-PCR-based screen for oxidative stress in Hep-G2 cells. *Toxicol Pathol* 2002;30:435-51.
- Suzuki T, Spitz DR, Gandhi P, Lin HY, Crawford RB. Mammalian resistance to oxidative stress: a comparative analysis. *Gene Expr* 2002;10:179-91.
- Arner ES, Nordberg J, Holmgren A. Efficient reduction of liposome and lipoleic acid by mammalian thioredoxin reductase. *Biochem Biophys Res Commun* 1996;225:568-74.
- Arner ES, Holmgren A. Physiological functions of thioredoxin and thioredoxin reductase. *Eur J Biochem* 2000;267:102-9.
- Smart DK, Ortiz LC, Mattson D, et al. Thioredoxin reductase as a potential molecular target for anticancer agents that induce oxidative stress. *Cancer Res* 2004;64:6716-24.
- Cherkasova EV. The effect of zinc on oxygen consumption, phagocytosis and the development of *Plasmodium* sporozoites. *Vopr Onkol* 1969;15:81-5.
- Liang JY, Liu Y, Zou J, Franklin RB, Costello LC, Feng P. Inhibitory effect of zinc on human prostatic carcinoma cell growth. *Prostate* 1999;40:200-7.
- Feng P, Li J, Guan ZX, Franklin RB, Costello LC. Effect of zinc on prostatic tumorigenicity in nude mice. *Ann N Y Acad Sci* 2003;1003:16-20.
- Yin H, Smith M, Glas J. Stable expression of C/EBP α in prostate cancer cells down-regulates metallothionein and increases zinc-induced toxicity. *Prostate* 2005;62:209-16.